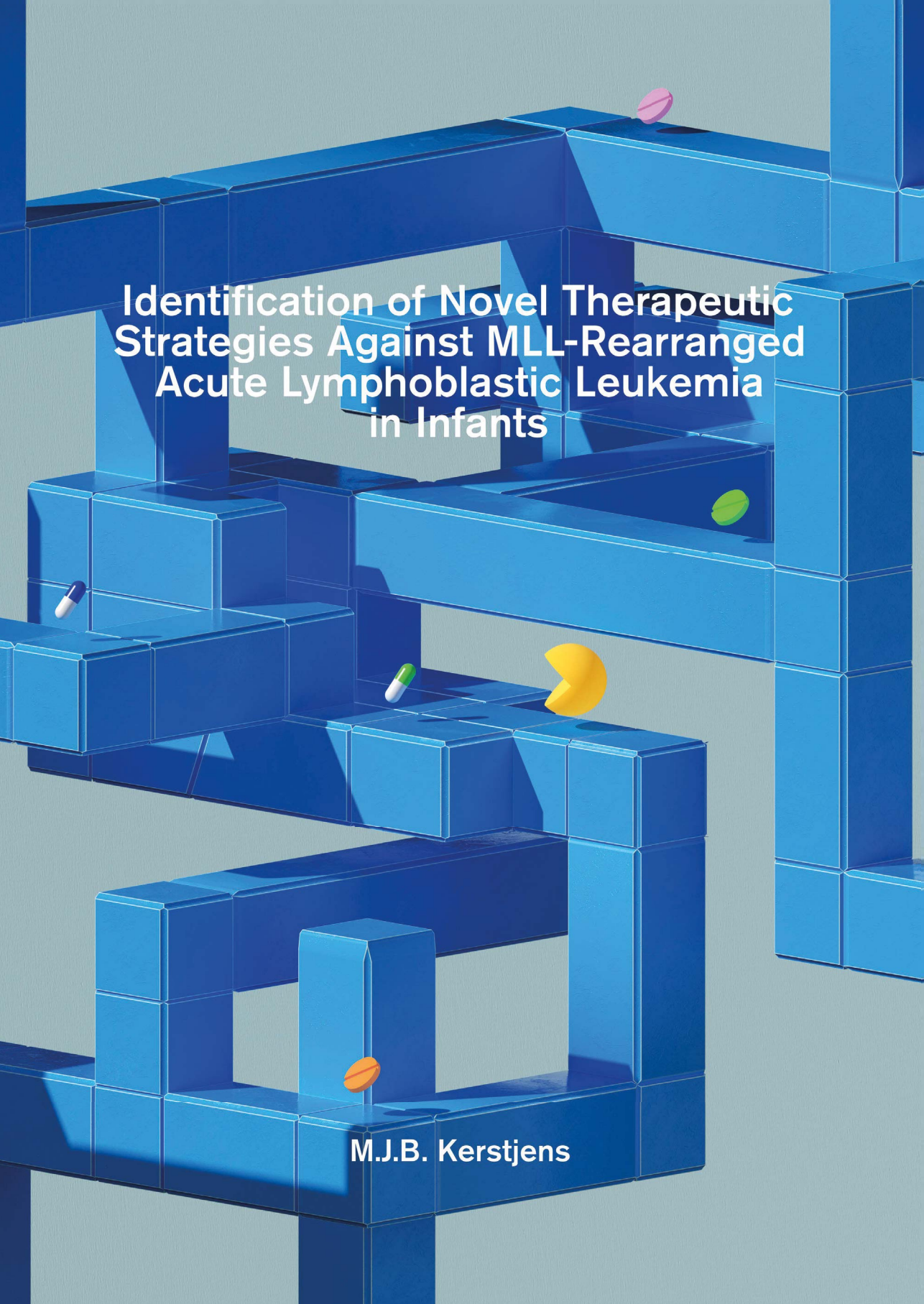

Identification of Novel Therapeutic Strategies Against MLL-Rearranged Acute Lymphoblastic Leukemia in Infants

M.J.B. Kerstjens

Identification of Novel Therapeutic Strategies Against *MLL*-rearranged Acute Lymphoblastic Leukemia in Infants

Mark Johannes Bernardus Kerstjens

ISBN: 978-94-6380-406-6

Layout: Mark Kerstjens and Niels Moolenaar

Cover design: Niels Moolenaar

Printed by: Proefschriftmaken.nl

The research described in this thesis was financially supported by Stichting Kinderen Kankervrij (KiKa).

Identification of Novel Therapeutic Strategies Against *MLL*-rearranged Acute Lymphoblastic Leukemia in Infants

Identificatie van nieuwe therapeutische strategieën tegen *MLL*-herschikte acute lymfatische leukemie bij zuigelingen

Proefschrift

ter verkrijging van de graad van doctor aan de
Erasmus Universiteit Rotterdam
op gezag van de
rector magnificus
Prof. dr. R.C.M.E. Engels

en volgens besluit van het College voor Promoties.

De openbare verdediging zal plaatsvinden op
dinsdag 3 september 2019 om 13:30 uur

door

Mark Johannes Bernardus Kerstjens
geboren te Beverwijk.

Erasmus University Rotterdam

Promotiecommissie

Promotor:	Prof. dr. R. Pieters
Co-promotor:	Dr. R.W. Stam
Overige leden:	Prof. dr. M.L. den Boer
	Prof. dr. R. Bernards
	Prof. dr. H.J. Vormoor
	Prof. dr. C.M. Zwaan
	Prof. dr. H.R. Delwel
	Dr. I.M. van der Sluis

Table of contents

Chapter 1

General Introduction

Hematopoiesis and leukemia

Our body is made up of over thirty trillion (3×10^{13}) cells, all contributing to the homeostastic mechanisms that are in place to ensure our health.[1] To allow the different cells to function, we have five liters of blood in our body, containing different cell types that fulfill several important roles, namely: oxygen and carbon dioxide transport (erythrocytes/red blood cells), thrombosis (thrombocytes/platelets) and protection against pathogens (leukocytes/white blood cells). All blood cells are derived from a multipotent progenitor cell, known as the hematopoietic stem cell (HSC). HSCs have long-term self-renewal capacity, and through several differentiation steps these cells give rise to the various blood cell lineages. Early in HSC differentiation, two branches can be identified, with the myeloid progenitor and lymphoid progenitor at the top of the respective lineages. Hematopoiesis during embryonic development mainly takes place in the fetal liver and spleen, before the bone marrow becomes the permanent site of blood cell production, approximately 2 months before birth.[2]
Leukemia is the abnormal proliferation of immature (and therefore non-functional) white blood cells. Leukemia progression can be rapid and aggressive, in which case it is referred to as *acute leukemia*. Cell proliferation and disease progression can also be more protracted, in which case it is known as *chronic leukemia*. As leukemia progresses, the immature blood cells suppress normal haematopoiesis, resulting in anemia, thrombocytopenia, and impairment of the immune system. Two general acute leukemia subtypes are differentiated, depending on the lineage, namely *acute myeloid leukemia* and *acute lymphoblastic leukemia*. The majority of childhood leukemias are of the acute lymphoblastic type (ALL), with approximately 125 newly diagnosed cases each year in the Netherlands. While lymphoblastic leukemias can be subdivided in B-cell derived and T-cell derived leukemia, the majority of childhood ALL patients are diagnosed with B-cell precursor (BCP) acute lymphoblastic leukemia or B-ALL. Over the past decades the treatment of childhood B-ALL has vastly improved through use of general chemotherapeutics, better scientific understanding of the disease, and stratification of patient risk groups, going from <10% survival chance in the 1960s to ~90% survival nowadays.[3] However, this tremendous bettering has not led to similar prognoses for the youngest childhood ALL patients: i.e. infants or children < 1 year of age.

MLL-rearranged infant ALL

In the Netherlands, around 5 infants are diagnosed with ALL each year. The majority (~80%) of infant ALL cases are characterized by chromosomal rearrangements involving the *Mixed Lineage Leukemia* (*MLL*) gene, also known as *Lysine-Specific Methyltransferase 2A* (*KMT2A*), which fuse part of the *MLL* gene to part of one of its translocation partner genes.[4] Although as many as 80 different fusion partner genes have been identified, most *MLL*-rearranged infant ALL cases involve *MLL*

being fused to *AF4* (~50%), *AF9* (~20%) or *ENL* (~10%), also referred to as t(4;11), t(9;11) and t(11;19) translocations, respectively.[5] Interestingly, the long-term event free survival (EFS) of infants with germline *MLL* (i.e. without an *MLL* translocation) is approximately 75%, just below the EFS for ALL in older children.[4] However, infants with ALL involving an *MLL*-rearrangement fare significantly worse, with EFS rates of approximately 35-45%, independent of *MLL* fusion partner.[4,6-8]

The wildtype MLL protein functions as a histone methyl transferase, catalyzing the trimethylation of lysine 4 on histone H3, which in turn initiates the formation of the transcriptional elongation complex in preparation of active transcription.[9,10] MLL fulfills a key role in normal haematopoiesis, through regulation of the homeobox A (*HOXA*) gene cluster.[11,12] While in healthy cells additional stimuli are required to activate RNA polymerase, an MLL fusion protein can circumvent this. Although the MLL fusion protein has lost its methyltransferase domain, it has gained the capacity to recruit the methyltransferase DOT1L, which in turn dimethylates lysine 79 at histone H3, activating transcriptional elongation.[13-15] Hence, MLL fusions induce disturbed histone methylation and associated enhanced expression of specific genes. Interestingly, besides abnormal histone methylation, *MLL*-rearranged infant ALL is also characterized by increased DNA methylation at specific promoter regions, thereby suppressing gene expression.[16] Together, these perturbations in epigenetic machinery result in aberrant gene expression profiles that distinguish *MLL*-rearranged ALL from *MLL* germline infant ALL and BCP-ALL in older children.[17]

Leukemia-inducing *MLL*-rearrangements arise *in utero*, and while these lesions are the common denominator in the majority of infant ALL cases, and predictive of poor prognosis, the short latency of the disease has instigated investigation of potential secondary oncogenic hits or cooperative drivers.[18,19] A recent study into the mutational landscape of *MLL*-rearranged infant ALL revealed an extremely low frequency of additional mutations.[20] Still, this study confirmed earlier identified (sub-clonal) mutations in *NRAS* and *KRAS*.[21,22] Previously, the presence of (sub-clonal) *RAS* mutations had been associated with therapy resistance and an extremely dismal prognosis for the *MLL-AF4* infant ALL subgroup, with hardly any chance of survival.[21] The discovery of *RAS* mutations is especially intriguing, considering the frequent increase in *FMS-like receptor tyrosine kinase-3* (*FLT3*) expression in *MLL*-rearranged infant ALL, which is coupled to downstream RAS pathway activation as well as an inferior prognosis.[23,24]

Clinical presentation and current therapy

MLL-rearranged ALL cells are characterized by a highly immature pro-B immunophenotype, corresponding to the expression of the cell surface markers CD34 and CD19, and absence or diminished expression of CD10, and are further typically characterized by the expression of certain myeloid markers.[25,26] Several

clinical features have been identified as predictors for a poor prognosis, including age at diagnosis (<6 months), high white blood cell counts, poor glucocorticoid response (determined after 8 days of prednisone mono-therapy, prior to induction therapy), CD10 negativity, and central nervous system infiltration.[4,6,27-29] Additionally, low expression of *HOXA* genes is associated with a poor prognosis.[28] Although the majority of *MLL*-rearranged infant ALL patients (~95%) go into remission, ~50% of the patients have a relapse (typically within 1 year from diagnosis, while still on treatment), resulting in overall survival chances of approximately 50%.[4] Present international 2-year treatment protocols consist of combination chemotherapy, including glucocorticoids (prednisone, dexamethasone), antimetabolites (cytarabine, 6-mercaptopurine, methotrexate), L-asparaginase, daunorubicin and vincristine. A minority of patients at very high risk of relapse undergoes allogeneic stem cell transplantation. Given the exceedingly high relapse rate in *MLL*-rearranged infant ALL, current treatment regimes clearly are not sufficient. Therefore, the recent research focus has been on the discovery of novel, more targeted therapies to improve prognosis.

Development of targeted therapeutic strategies against *MLL*-rearranged infant ALL

The disturbed epigenetic landscape that characterizes *MLL*-rearranged infant ALL has provided clues into new therapeutic strategies. With DOT1L as one of the key components in MLL fusion protein mediated aberrant regulation of gene expression,[30,31] it is no surprise that inhibitors (EPZ004777 and EPZ-5676) against this histone methyltransferase have been developed.[32,33] Using connectivity mapping, Stumpel *et al.* discovered that inhibitors of histone deacetylase (HDAC) enzymes could reverse aberrant gene expression profiles that define *MLL*-rearranged infant ALL.[34] This has led to the identification and characterization of the HDAC inhibitor LBH-589 (or panobinostat), which has shown high potency and efficacy against *MLL*-rearranged infant ALL cells *in vitro*, as well as *in vivo* in xenograft mouse models.[35] Additionally, the Bromodomain and Extra-Terminal (BET) family of proteins has proven an interesting target for *MLL*-rearranged infant ALL, as BET proteins function as epigenetic "readers" of histone acetylation, and facilitate transcription through chromatin remodeling as part of multi-protein complexes.[15,36] Therefore, different BET inhibitors have been investigated as drug candidates, with especially I-BET151 showing promising results in *MLL*-rearranged leukemia cell lines, as well as in mouse models.[37] The observed increased DNA methylation, and promoter hypermethylation more specifically, have further instigated the research into demethylating agents, with decitabine and zebularine as effective drugs against *MLL*-rearranged ALL cells.[16,38] While these drugs have shown promise as therapeutic strategies for *MLL*-rearranged infant ALL, the transition from the laboratory to the

patient is still a time-consuming process, especially considering the fact that these drugs need to be safe and efficacious in adults before the transition can be made to pediatric application. Awaiting results from clinical investigation of these previously identified therapeutics, this thesis describes the investigation of new therapeutic candidates, predominately FDA-approved and off-patent drugs, in order to expedite the implementation of potent agents into current therapeutic regimens for *MLL*-rearranged infant ALL.

Outline of this thesis

Chapter 2 describes a drug repurposing approach through screening of mainly FDA-approved and off-patent drugs on different *MLL*-rearranged infant ALL and BCP-ALL cell line models. This led to the identification of topoisomerase I inhibitors, especially 7-ethyl-10-hydroxycampthotecin (SN-38), as potent inhibitors of *MLL*-rearranged infant ALL cells *in vitro*. Additionally, the efficacy of the SN-38 pro-drug irinotecan was investigated *in vivo* using xenograft mouse models of *MLL*-rearranged infant ALL.

In **chapter 3**, we report the investigation of inhibitors against *MLL*-rearranged ALL cells harboring additional *RAS* mutations. Hereto, different (approved) inhibitors of RAS-pathway components were tested on *MLL*-rearranged cell line models, as well as primary patient material. Among all inhibitors tested in this study, MEK inhibitors showed the most promising results. Moreover, since *RAS* mutations are associated with glucocorticoid resistance, we investigated the effect of MEK inhibition on the response of *MLL*-rearranged ALL cells to the glucocorticoid prednisolone, and observed glucocorticoid-sensitizing effects. Furthermore, **chapter 4** reports the *in vivo* evaluation of trametinib, the most potent MEK inhibitor as found in **chapter 3**, in a xenograft mouse model of *RAS* mutant *MLL*-rearranged infant ALL.

Since *MLL*-rearranged infant ALL is characterized by aberrant histone methylation and DNA methylation, we performed drug screens using two drug libraries consisting of epigenetic drugs in **chapter 5**. S-adenosylhomocysteine hydrolase inhibitors potently inhibited *MLL*-rearranged infant ALL *in vitro*. Additionally, we investigated the mechanism of action of these inhibitors, while also assessing efficacy in an *MLL*-rearranged infant ALL xenograft mouse model.

Finally, the results described in this thesis are discussed and summarized in **chapter 6,** and **chapter 7** provides a layman's summary in Dutch.

Chapter 2

Irinotecan induces remission in human *MLL*-rearranged acute lymphoblastic leukemia xenotransplanted mice

Mark J.B. Kerstjens*, Patricia Garrido Castro*, Sandra Mimoso Pinhanços, Pauline Schneider, Priscilla Wander, Rob Pieters and Ronald W. Stam

* These authors contributed equally to this work.

Submitted

Abstract

Acute Lymphoblastic Leukemia (ALL) in infants (<1 year of age) remains one of the most aggressive types of childhood hematologic malignancies. The majority (~80%) of infant ALL cases is characterized by chromosomal translocations involving the *MLL* (or *KMT2A*) gene, which confer highly dismal prognoses with current combination chemotherapeutic regimens. Hence, more adequate therapeutic strategies are urgently needed. To expedite clinical transition of potentially effective therapeutics, we implemented a drug repurposing approach by performing *in vitro* screens of clinically approved drug libraries for agents killing *MLL*-rearranged ALL cells. Out of 3685 compounds tested, topoisomerase I inhibitor camptothecin and its derivatives 10-HCPT and SN-38 appeared most effective at low nanomolar concentrations; and molecular analyses *in vitro* showed rapid induction of DNA damage accompanied by cell death after SN-38 exposure. Using *MLL*-rearranged ALL xenograft mouse models we demonstrate that the SN-38 pro-drug irinotecan completely blocks leukemia expansion and induces profound remission in mice with advanced leukemia. Taken together our data show that irinotecan exerts highly potent anti-leukemia effects against *MLL*-rearranged ALL.

Introduction

Acute Lymphoblastic Leukemia (ALL) in infants (children <1 year of age) is an aggressive hematologic malignancy characterized by a very poor prognosis, with overall 5-year event-free survival (EFS) rates of 40-50%.[4,6-8]
In contrast, over the past decades the 5-year EFS for older children diagnosed with ALL has improved toward 85%, due to better risk stratification and accordingly adjusted treatment protocols. Approximately 80% of infant ALL cases are characterized by chromosomal rearrangements of the *Mixed Lineage Leukemia* (*MLL*, or *KMT2A*) gene, and this patient group in particular fares significantly worse, with an EFS of only 30-40%.[4] Evidently, there is a dire need for improved therapeutic strategies to ameliorate clinical outcome for these patients.
MLL translocations give rise to chimeric MLL fusion proteins, which induce inappropriate histone modifications by recruiting the histone methyl transferase DOT1L.[13,20,39] This induces a perturbed epigenetic landscape resulting in severely altered gene expression signatures and DNA methylation patterns, giving rise to a leukemia type which differs biologically and clinically from ALL in older children.[5,16,17]
We and others have been investigating therapeutic approaches targeting components of the epigenetic machinery important in *MLL*-rearranged ALL. So far, this has led to the discovery of inhibitors against DOT1L (e.g. EPZ004777), DNA methyltransferases (e.g. 5-azacytidine, zebularine), BET family proteins (e.g. I-BET151) and histone deacetylases (HDACs) (e.g. vorinostat, panobinostat) as potential candidates.[16,33,34,37,38]
Although these epigenetic-based drugs are very promising, the transition from preclinical studies towards clinical application is an elaborate and time-consuming process. Awaiting clinical evaluation of these inhibitors, we decided to adopt a drug repurposing approach, using drug library screening of FDA-approved and off-patent drugs. Using this strategy, we aimed to identify effective therapeutics against *MLL*-rearranged ALL, which have been characterized and approved in other diseases, thus expediting their transition into clinics.[40]
In this study we identified the camptothecin-derivative 7-ethyl-10-hydroxycamptothecin (SN-38), and in particular its pro-drug irinotecan (Camptosar), as highly effective agents against *MLL*-rearranged ALL. In fact, we here demonstrate that irinotecan mono-therapy successfully induces remission in xenograft mouse models of *MLL*-rearranged ALL.

Materials & Methods

Cell culture

Cell lines (see supplemental methods) were cultured in RPMI-1640 with GlutaMAX, 10% Fetal Calf Serum, 100 IU/mL penicillin, 100 IU/mL streptomycin and 0.125 µg/mL amphotericin B (Invitrogen Life Technologies, Waltham, MA, USA) at 37°C under 5% CO_2 atmosphere. Regular DNA fingerprinting and mycoplasma testing were performed.

Primary *MLL*-rearranged infant ALL samples were obtained at the Sophia Children's Hospital (Rotterdam, the Netherlands) as part of the international INTERFANT treatment protocol. The Erasmus MC Institutional Review Board approved these studies, and informed consent was obtained according to the Declaration of Helsinki. Processing of samples occurred as described previously.[23] Leukemic blast percentage was at least 90%, as confirmed by May-Grünwald-Giemsa counterstained cytospins.

Drug screening

For the Spectrum Collection (MicroSource, Gaylordsville, USA), Prestwick library (Prestwick Chemical, Illkirch, France) and anti-neoplastic Sequoia library (Sequoia Research Products, Pangbourne, United Kingdom), DMSO dissolved stocks were diluted in non-supplemented RPMI and cytotoxicity was assessed using MTS assays (DMSO concentration <0,5%). Data was normalized to vehicle control. Heatmaps were generated using Gene-E software (Broad Institute, Cambridge, USA).

In vitro drug exposures

Cell proliferation and apoptisis were tracked by flow cytometry (MACSQuant, Miltenyi) using propidium iodide exclusion and the PE Annexin-V Apoptosis Detection Kit (BD Pharmingen), respectively. Data was analyzed using FlowJo software.

Cell lysates were made on ice in RIPA supplemented with protease and phosphatase inhibitors.

MTS and MTT dose-response data were acquired in duplicate and presented as mean +/- s.e.m. (cell lines) or mean +/- sd (patient samples).

Western blot

Lysates were resolved on pre-cast SDS-polyacrylamide gels (TGX, Bio-Rad, Veenendaal, The Netherlands) and transferred to nitrocellulose membranes using the Transblot Turbo Transfer System (BioRad, Veenendaal, The Netherlands). Membranes were blocked with 5% BSA or skim milk in TBS and probed with primary antibodies against PARP, (phospho-)CHK2, (phospho-)H2AX (Cell Signalling Technologies) or β-actin (Abcam), and fluorophore-conjugated secondary antibodies. Images were acquired using the Odyssey imaging system (LI-COR, Leusden,

The Netherlands).

Animal experiments

Animal experiments were performed according to Dutch legislation and approved by the Erasmus MC Animal Ethical Committee, Rotterdam, The Netherlands (EMC3389).

Briefly, NSG mice were transplanted with SEM-SLIEW or patient-derived leukemic cells and leukemia progression was assessed through intra-vital imaging or human CD45+ cell counts in blood samples. Vehicle or irinotecan (40 mg/kg) treatment was administered intraperitoneally 3 times per week. Mice were humanely euthanized and tissue samples were acquired for further analysis. See supplemental methods for more details.

Statistical tests were performed in GraphPad Prism using non-parametric (Kruskal-Wallis, Mann-Whitney) or parametric tests (one-way ANOVA and unpaired t-test), as indicated. Significance was defined as $p<0.05$.

Results

Drug library screening identifies camptothecin derivatives as promising leads

We performed drug library screening using the Spectrum and Prestwick drug libraries (consisting of 2320 and 1200 therapeutically diverse FDA-approved compounds, respectively) at 1 μM drug concentration on *MLL*-rearranged ALL cell lines to identify therapeutic agents against *MLL*-rearranged ALL, and also included B-cell precursor (BCP) ALL cell lines. While the majority of drugs did not affect the leukemia cell lines tested, approximately 12% of the compounds inhibited *MLL*-rearranged ALL cell viability by at least 20%, for both the Spectrum (Fig.1A) and Prestwick (Fig.1B) libraries. Among the most effective drugs we found vincristine, cytarabine and vorinostat, which are being used in current treatment protocols or have been identified previously as therapeutic options for *MLL*-rearranged ALL, confirming the validity of the screening approach.[4,34,41]

Similarly, we found various corticosteroid drugs to be effective in the *MLL*-rearranged ALL cell lines; however, we found none to be more potent or effective than prednisolone (Sup.Fig.1A,B). Therefore this drug class was excluded from further studies.

Since a number of drugs abolished ALL cell viability, we wondered whether lower drug concentrations could reveal any leukemia subtype specificity missed at 1 μM concentration. Therefore, 54 potential leads were selected based on their inhibitory effect on *MLL*-rearranged ALL cells, and further validated at concentrations of

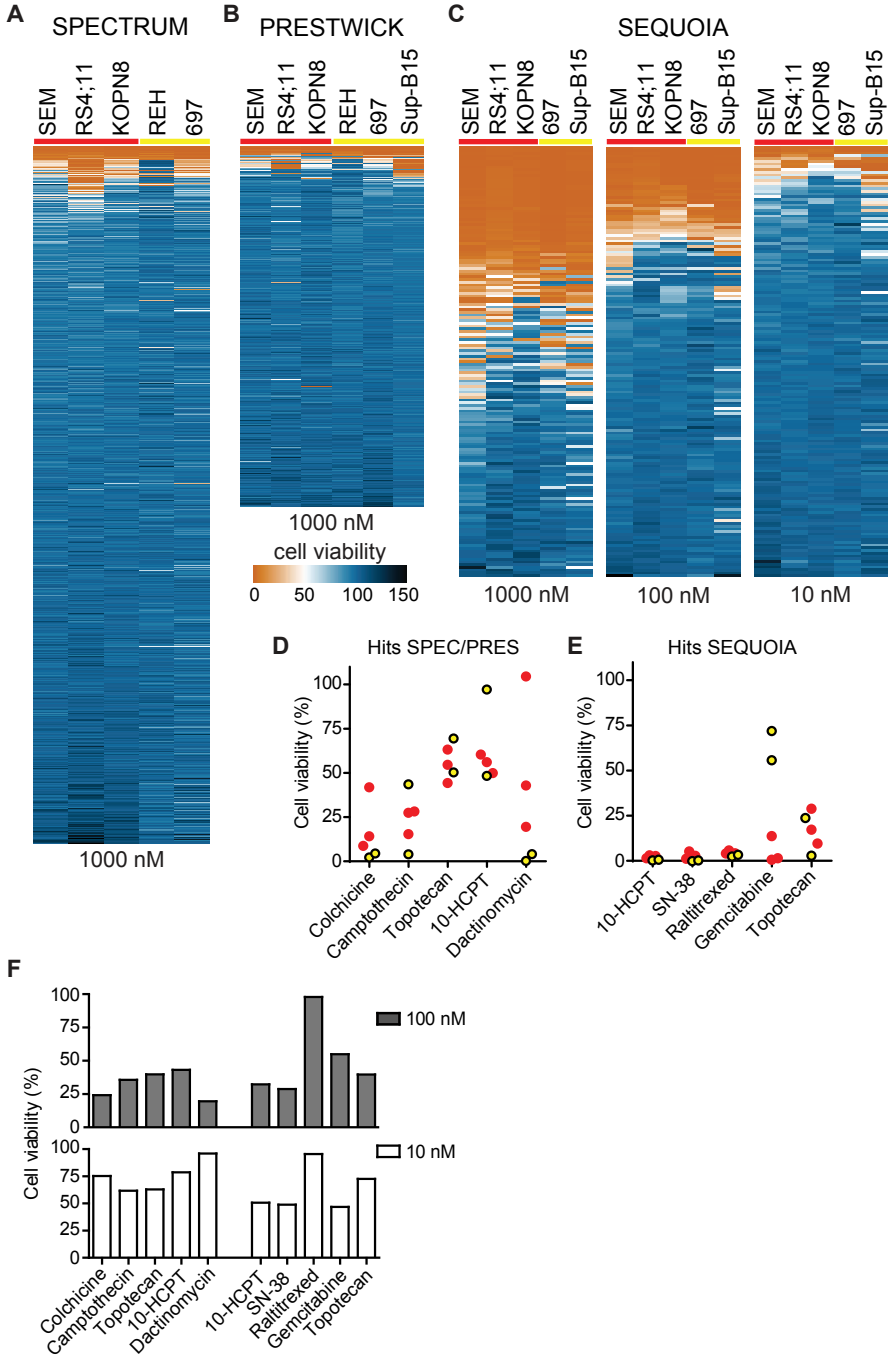
A
SPECTRUM
SEM
RS4;11
KOPN8
REH
697
1000 nM
B
PRESTWICK
SEM
RS4;11
KOPN8
REH
697
Sup-B15
1000 nM
cell viability
0
50
100
150
C
SEQUOIA
SEM
RS4;11
KOPN8
697
Sup-B15
1000 nM
100 nM
10 nM
D
Hits SPEC/PRES
Cell viability (%)
100
75
50
25
0
Colchicine
Camptothecin
Topotecan
10-HCPT
Dactinomycin
E
Hits SEQUOIA
Cell viability (%)
10-HCPT
SN-38
Raltitrexed
Gemcitabine
Topotecan
F
Cell viability (%)
100 nM
10 nM
Colchicine
Camptothecin
Topotecan
10-HCPT
Dactinomycin
10-HCPT
SN-38
Raltitrexed
Gemcitabine
Topotecan

Figure 1. Drug library screening yields no *MLL*-rearranged ALL specific drugs, but identifies camptothecin derivatives as potent candidates. (A,B) Heatmaps of ALL cell viability after exposure to the Spectrum and Prestwick drug libraries (1 μM, 96h), respectively. n=1 **(C)** Heat maps showing the effect of the anti-neoplastic Sequoia library against ALL cell viability (1 μM, 100 nM and 10 nM; left, middle and right, respectively; 96h). n=1 **(D,E)** Cell viability data for the 5 most effective Spectrum and Prestwick library derived hits and the most effective Sequoia library hits, respectively (10nM, 96h). *MLL*-rearranged ALL cell lines are shown in red, BCP-ALL cell lines are shown in yellow. **(F)** Cell viability of a primary *MLL*-rearranged infant ALL sample exposed to the top hits at 100 nM (top; grey bars) and 10 nM (bottom; white bars). n=1.

100 nM and 10 nM, yielding a narrow selection of very potent compounds (Sup. Fig.1C,D,E). None of these drugs appeared to display leukemia subtype specificity. In addition, the anti-neoplastic Sequoia drug library (consisting of 165 anti-neoplastic chemotherapeutics commonly used in the treatment of human cancers) was screened in the same set-up at 1 μM drug concentration. This drug screen yielded a substantial number of effective compounds; 52 compounds with >75% inhibition of *MLL*-rearranged ALL cell viability. Efficacy testing at 100 nM and 10 nM concentrations allowed further selection of a panel of highly potent agents (Fig.1C).

Figures 1D and E show the effects on viability of *MLL*-rearranged ALL and BCP-ALL cell lines for the top 5 drugs from the Spectrum and Prestwick libraries, and the top 5 drugs from the Sequoia library, respectively, at 10 nM drug concentration. The top compounds in all three drug libraries appeared to be camptothecin and its derivatives 10-hydroxycamptothecin (10-HCPT), 7-ethyl-10-hydroxycamptothecin (SN-38) and topotecan (Fig.1D,E). For additional validation, we tested whether the 54 selected Spectrum/Prestwick drugs and the Sequoia library inhibited an *MLL*-rearranged ALL patient sample to a similar extent as observed for the cell lines. While some of the drugs performed differently on the primary patient sample compared to the cell line models, camptothecin and its derivatives were highly effective against the patient cells (Fig.1F).

Camptothecin derivative SN-38 most potently inhibits ALL cell viability

To validate the results from our drug library screens, we tested camptothecin and its derivatives SN-38 and 10-HCPT using dose-response curves on the *MLL*-rearranged and BCP-ALL cell lines used in the original drug library screens, and additionally included the T-ALL cell line Jurkat. All three agents strongly inhibited leukemic cell viability in each cell line tested, with IC_{50} values in low nanomolar ranges (Fig.2A,B,C); the efficacy of the most potent agent, SN-38, was further validated in multiple primary *MLL*-rearranged infant ALL patient samples (Fig.2D). Notably, the IC_{50} of SN-38 in the cell lines was lower than in the primary patient samples (1,4-5,6 nM vs. 13,9-434,1 nM, respectively), possibly due to the fact that SN-38 activity requires cell proliferation, and patient-derived leukemic cells hardly divide *in vitro*.

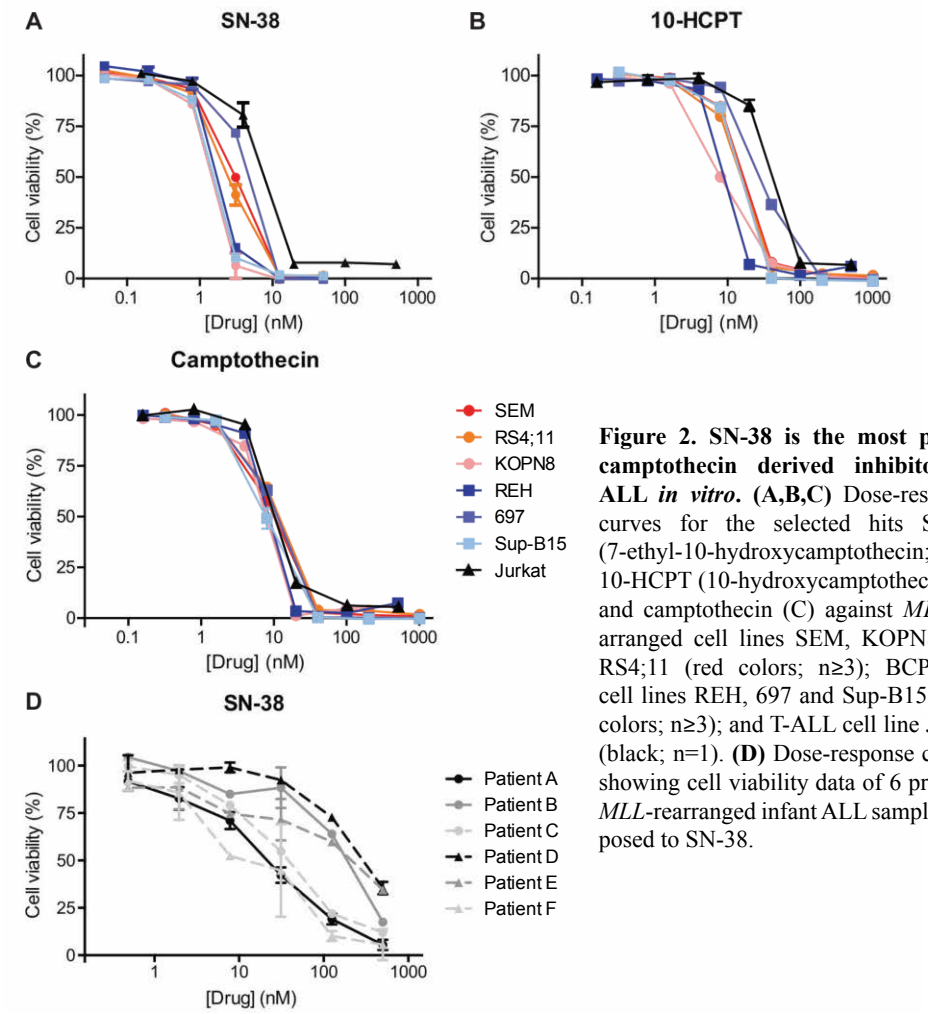

Figure 2. SN-38 is the most potent camptothecin derived inhibitor of ALL *in vitro*. (A,B,C) Dose-response curves for the selected hits SN-38 (7-ethyl-10-hydroxycamptothecin; A), 10-HCPT (10-hydroxycamptothecin; B) and camptothecin (C) against *MLL*-rearranged cell lines SEM, KOPN8 and RS4;11 (red colors; n≥3); BCP-ALL cell lines REH, 697 and Sup-B15 (blue colors; n≥3); and T-ALL cell line Jurkat (black; n=1). **(D)** Dose-response curves showing cell viability data of 6 primary *MLL*-rearranged infant ALL samples exposed to SN-38.

SN-38 induces DNA damage and apoptotic cell death in ALL

To elucidate the mechanism underlying SN-38 mediated inhibition of cell viability, we exposed both *MLL*-rearranged (SEM) and non-*MLL*-rearranged (697) ALL cell lines to 5 nM or 25 nM SN-38 and assessed changes in proliferation over time. We observed reduced cell numbers for both cell lines at both concentrations already after 24 hours, which progressively decreased at 48 and 72 hours (Fig.3A and Sup. Fig.2A). Cell death determination by flow cytometry after 8, 24 and 48 hours showed that apoptosis was initiated already after 8 hours of exposure with 25 nM of SN-38, and progressed dramatically in both SEM and 697 cells for either concentration after

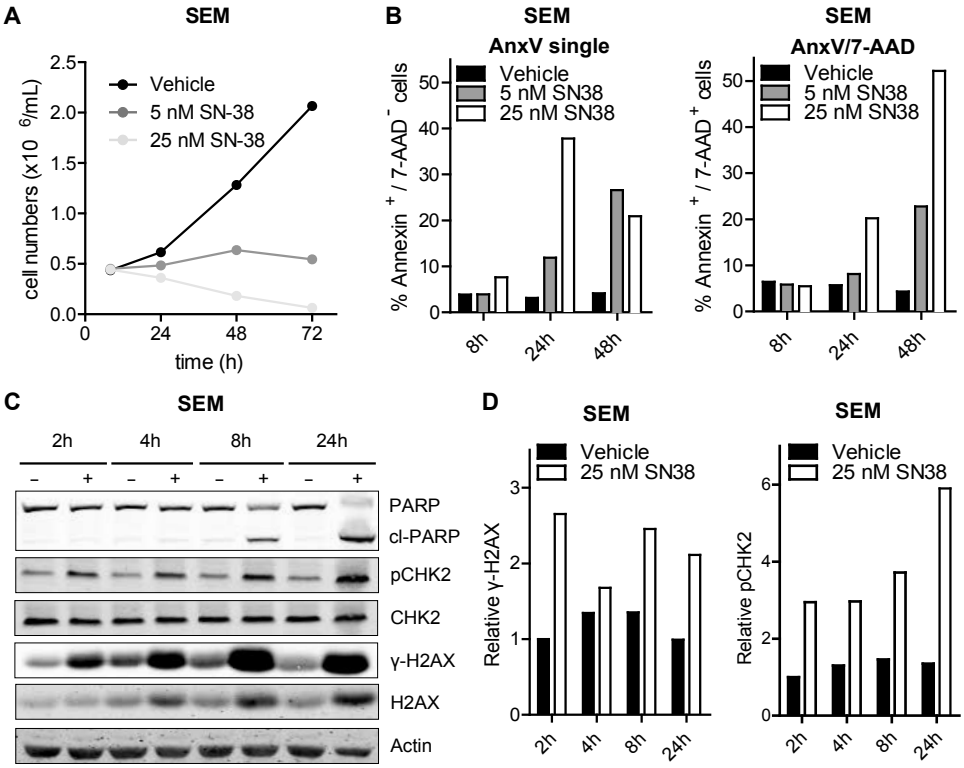

Figure 3. SN-38 induces DNA damage and apoptosis in ALL cells. (A) SEM cell counts over time (8h, 24h, 48h and 72h) after exposure to vehicle (DMSO), 5 nM or 25 nM SN-38 (black, dark grey and light grey lines; respectively; n=3). **(B)** Percentages of (early and late) apoptotic SEM cells exposed to SN-38. Representative of 3 separate experiments. **(C)** Western blots of SEM lysates after exposure to vehicle (-) or 25 nM SN-38 (+) for the indicated time-points. **(D)** Quantification of the phosphorylated H2AX (γ-H2AX) level relative to total H2AX and relative CHK2 phosphorylation in the SEM samples is shown in the left and right graphs, respectively.

48 hours, reaching 70-80% (Fig.3B and Sup.Fig.2B). Apoptosis induction was further confirmed by detection of PARP cleavage, already present after 8 hours of 25 nM SN-38 exposure (Fig.3C; and Sup.Fig.2C).

During chromatin replication or transcription, topoisomerase I (TOP1) induces DNA single strand breaks to release DNA supercoiling-induced torsional stress.[42] SN-38 binds to TOP1 to prevent DNA-religation, thereby locking TOP1 onto the DNA. The resulting DNA/TOP1/SN-38 complexes can lead to accumulation of replication fork collision-induced DNA breaks, especially in fast-dividing cells. Important hallmarks of camptothecin-derivative mediated DNA breaks are enhanced phosphorylation of the DNA damage response (DDR) proteins CHK2 and H2AX (γ-H2AX).[43-45] We ob-

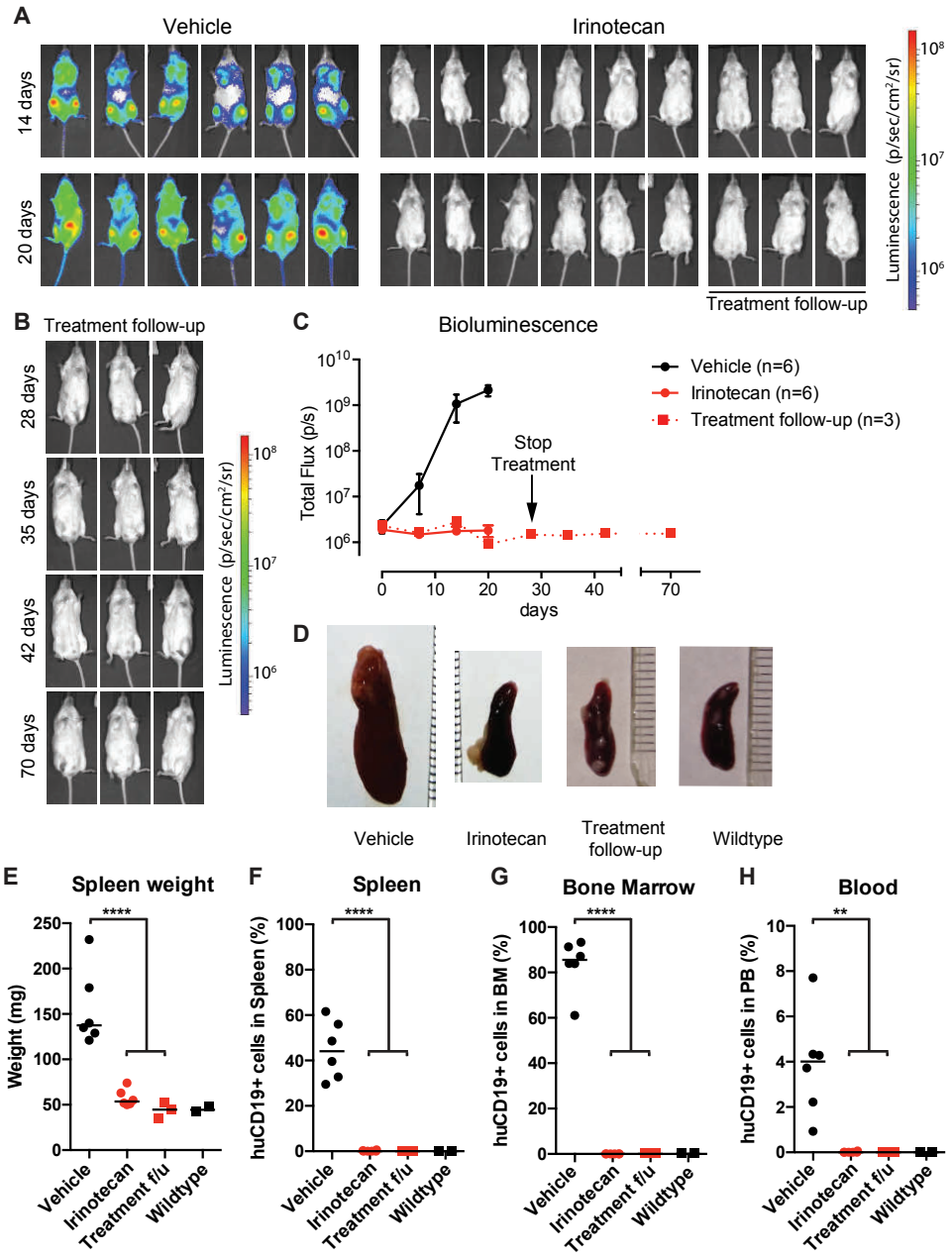
A
Vehicle
Irinotecan
14 days
20 days
Treatment follow-up
Luminescence (p/sec/cm²/sr)
B
Treatment follow-up
28 days
35 days
42 days
70 days
C
Bioluminescence
Vehicle (n=6)
Irinotecan (n=6)
Treatment follow-up (n=3)
Stop Treatment
Total Flux (p/s)
days
D
Vehicle
Irinotecan
Treatment follow-up
Wildtype
E
Spleen weight
Weight (mg)
F
Spleen
huCD19+ cells in Spleen (%)
G
Bone Marrow
huCD19+ cells in BM (%)
H
Blood
huCD19+ cells in PB (%)

served increased phosphorylation of CHK2 and H2AX, as well as slightly increased total H2AX protein levels, after exposing SEM and 697 cells to 25 nM SN-38, as determined by immunoblotting (Fig.3C,D and Sup.Fig.2C,D).

The SN-38 pro-drug irinotecan effectively inhibits *MLL*-rearranged ALL *in vivo*

To assess the efficacy of SN-38 *in vivo*, we used a previously established *MLL*-rearranged ALL xenograft mouse model.[35] However, since SN-38 is notorious for its poor bioavailability, we decided to treat our mice with irinotecan (CPT-11, or Camptosar), which is a pro-drug metabolised into SN-38 *in vivo* by native carboxylesterases.[46,47] NSG mice (n=19) were xenotransplanted with our *MLL*-rearranged ALL luciferase reporter cell line SEM-SLIEW and equally allocated over the vehicle (n=10) and irinotecan (n=9; 40 mg/kg) treatment groups, ensuring comparable leukemia burden before treatment (Sup.Fig.3A). Irinotecan or vehicle treatment was administered 3 times per week via intraperitoneal injections. Weekly assessment of leukemia progression through bioluminescent imaging revealed no detectable signs of leukemic cells in irinotecan-treated mice after 14 and 20 days (Fig.4A; top and bottom, respectively). As relapses in *MLL*-rearranged ALL patients occur early during treatment, suggesting that small subsets of leukemic cells evade therapy,[4,48] we studied whether the observed ablation of leukemia by irinotecan would be maintained after cessation of irinotecan treatment. Therefore, a subset (n=6) of the irinotecan-treated mice were sacrificed at day 28 and used to investigate leukemic infiltration of tissues, while the remaining n=3 irinotecan-treated mice were kept alive without any further treatment (from here on referred to as the treatment follow-up group) (Fig.4A; right), while disease monitoring continued by weekly bioluminescent imaging. Interestingly, the intra-vital images showed no outgrowth of leukemia for up to 42 days off treatment

Figure 4. SN-38 pro-drug irinotecan can impede *MLL*-rearranged leukemia outgrowth *in vivo*. (A) Intra-vital imaging of SEM-SLIEW transplanted mice treated with either vehicle (n=6; left) or 40 mg/kg irinotecan (n=9; right) after 14 or 20 days (top and bottom, respectively). All images were generated with the same luminescent scale (legend on far right side). **(B)** Intra-vital imaging of 3 irinotecan treated mice after cessation of treatment on day 28 (treatment follow-up group), tracked until day 70. Luminescent scale is the same as in A. **(C)** Quantification of bioluminescent signal from the vehicle (black), irinotecan (red circles, solid line) and treatment follow-up (red squares, dashed line) mice. Black arrow indicates cessation of irinotecan treatment (treatment follow-up group; day 28). Data presented as median total flux (emitted photons/second) +/- sd. **(D)** Representative images of mouse spleens from the vehicle, irinotecan and treatment follow-up groups, as well as a wildtype mouse spleen. **(E)** Individual spleen weights for vehicle (black circles), irinotecan (red circles) treatment groups, treatment follow-up (red squares) and wildtype (black squares) mice. Horizontal bars indicate median. **(F,G,H)** Percentage live human CD19+ cells derived from homogenized spleen, bone marrow and peripheral blood of vehicle (black circles), irinotecan (red circles), treatment follow-up (red squares) and wildtype (black squares) mice. Horizontal bars indicate median. *$0.01<p<0.05$; **$0.001<p<0.01$; ***$0.0001<p<0.001$; ****$p<0.0001$.

(day 70) in this group (Fig.4B), indicating no signs of leukemia relapse since cessation of irinotecan administrations**.** Quantification of the total flux (emitted photons/second) confirmed a lack of signal for mice on the irinotecan treatment arm, and this lack of bioluminescence signal persisted also after end of treatment, in the follow-up group. In contrast, a rapid increase in bioluminescence was observed in the vehicle-treated mice, marking progressive leukemia (Fig.4C).
After sacrificing mice from the vehicle (n=6), irinotecan (n=6) and follow-up (n=3) groups, relevant tissues were extracted and further analyzed. In addition, we included two healthy, untransplanted and untreated NSG mice as basal controls. As expected, vehicle-treated control mice characteristically presented with splenomegaly, while irinotecan-treated mice, both in the initial treatment and the follow-up group, had significantly lower spleen weights ($p<0.0001$), resembling spleens of healthy control mice (Fig.4D,E). Next, we processed the spleens, bone marrows and peripheral blood and determined leukemic cell burden in these tissues using multicolor flow cytometry, as outlined in Sup.Fig.3B-D. In the homogenized spleens from the vehicle group, approximately 45% CD19+ human leukemia cells were observed, whereas no leukemic cells were detected in spleens derived from irinotecan-treated mice, nor in the spleens from the treatment follow-up group (Fig.4F). Similarly, bone marrow and peripheral blood samples of vehicle-treated mice contained on average ~85% and ~4% of human leukemic cells, respectively, whereas no leukemic cells were detected in the bone marrow and peripheral blood of the irinotecan-treated mice, nor in the mice after stop of irinotecan treatment (Fig.4G,H).

Irinotecan cures mice with advanced *MLL*-rearranged ALL

While irinotecan mono-therapy was able to completely block human *MLL*-rearranged ALL expansion in mice when treatment was initiated shortly after xenotransplantation, this may not represent a clinically relevant model, as patients present with full-blown leukemia at diagnosis. Therefore, we tested whether irinotecan could cure advanced leukemia in xenotransplanted mice. Four mice from the vehicle-treated group (as presented in Fig.4A) with advanced leukemia were selected for subsequent treatment with irinotecan (40 mg/kg) (from hereon referred to as curative group), which was initiated at 16 days after transplantation. Remarkably, already after 2 injections of irinotecan (in the first week of treatment), intra-vital bioluminescent imaging showed the systemic leukemia starting to regress, which was clearly visible in all mice (Fig.5A; 20 days). Moreover, successive treatment further diminished the leukemia considerably, and although 1 of these mice was found dead (day 26; unknown cause), quantification of the bioluminescence from the other 3 mice confirmed the rapid decline in leukemic burden (Fig.5B). At the end of this curative study (day 36), the mice were sacrificed and tissues were harvested and processed as previously described. Interestingly, the spleens from the curative group were sig-

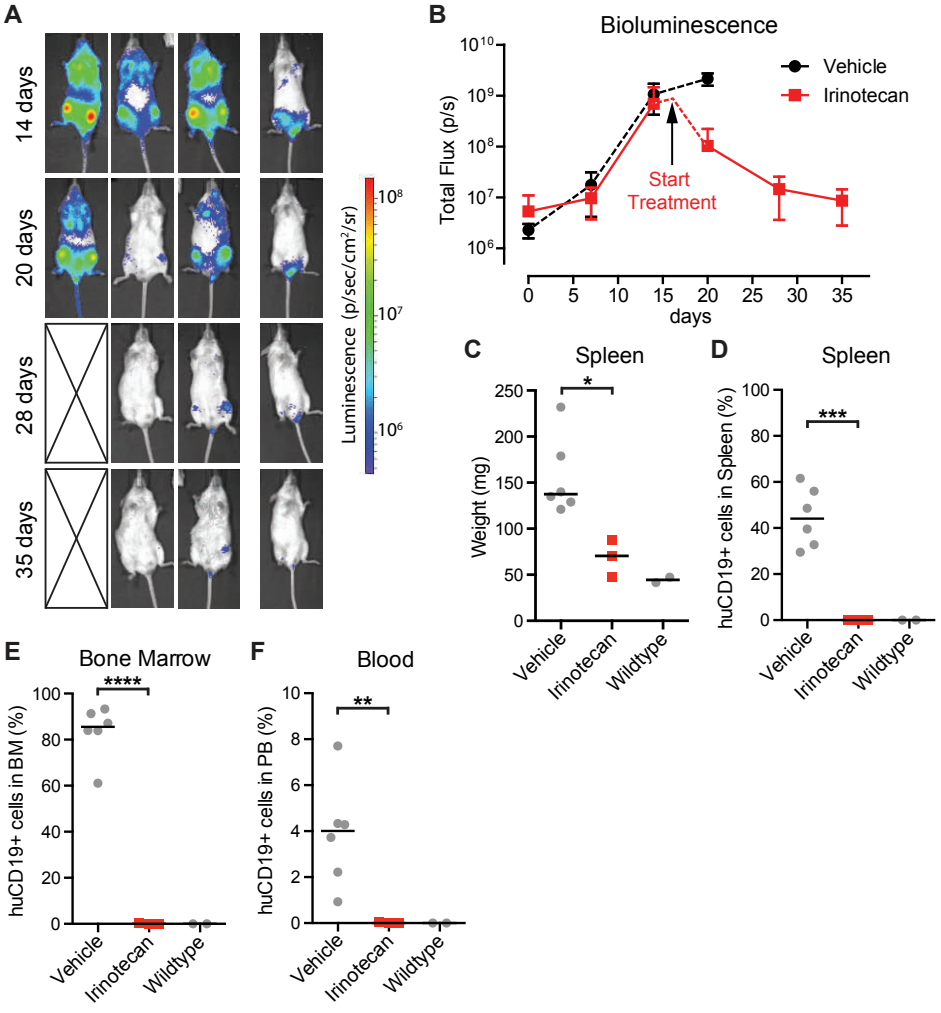

Figure 5. Irinotecan treatment cures mice with advanced leukemia. (A) Intra-vital imaging of SEM-SLIEW transplanted mice with advanced leukemia (14 days; top row) and when started on curative irinotecan treatment (20, 28 and 34 days). Deceased mouse is indicated by cross. Luminescent scale is identical to Fig.4A and B. **(B)** Quantification of bioluminescence from the curative group (n=3; deceased mouse excluded). Vehicle bioluminescent signal (black dotted line) from Fig.4 included for reference. The black arrow indicates initiation of curative irinotecan treatment (day 16). **(C)** Spleen weight of the curative irinotecan treated mice (red squares). Vehicle (left grey circles) and wildtype (right grey circles) data from Fig.4 included for comparison. Horizontal bars represent median values. **(D,E,F)** Percentage live human CD19+ cells in spleen, bone marrow and peripheral blood (respectively) of curative group (red squares). Again, vehicle (left grey circles) and wildtype (right grey circles) data from Fig.4 is included. Horizontal bars represent group medians. *0.01<p<0.05; **0.001<p<0.01; ***0.0001<p<0.001; ****p<0.0001.

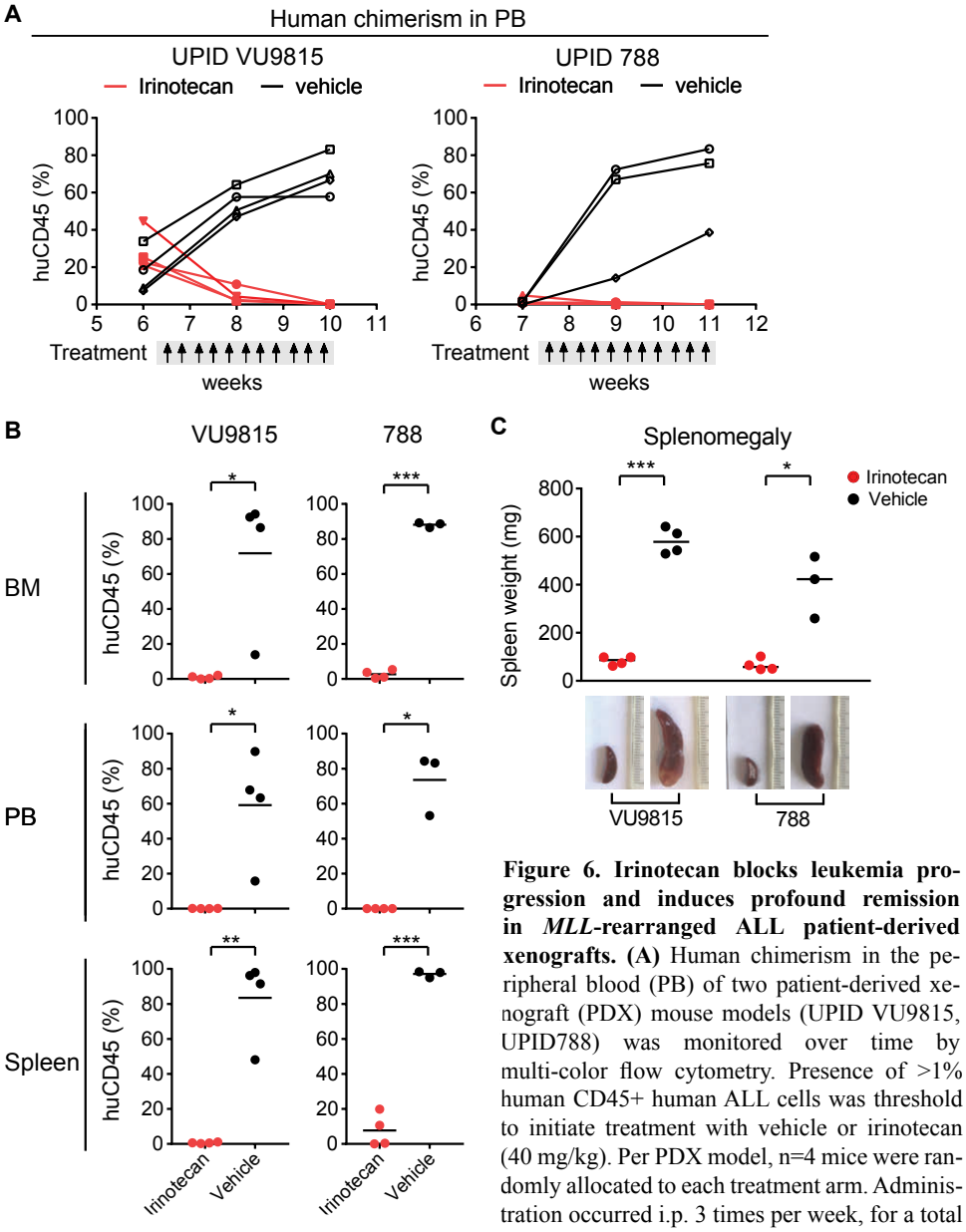

Figure 6. Irinotecan blocks leukemia progression and induces profound remission in *MLL*-rearranged ALL patient-derived xenografts. (A) Human chimerism in the peripheral blood (PB) of two patient-derived xenograft (PDX) mouse models (UPID VU9815, UPID788) was monitored over time by multi-color flow cytometry. Presence of >1% human CD45+ human ALL cells was threshold to initiate treatment with vehicle or irinotecan (40 mg/kg). Per PDX model, n=4 mice were randomly allocated to each treatment arm. Administration occurred i.p. 3 times per week, for a total of 10 dosages. Changes in human leukemic cell burden was monitored every other week. N=1 mouse in the UPID VU9815 was excluded due to technical reasons (*i.e.* died during bleeding procedure). **(B)** At the end of treatment, mice were euthanized and human leukemic cell infiltration in bone marrow (BM), PB and spleen measured by multi-color flow cytometry. Statistical differences were determined using Student's t-test with Welch correction; *p<0.05; **p<0.01; ***p<0.001. **(C)** Splenomegaly was

nificantly smaller than those from the vehicle-treated group (Fig.5C). Furthermore, no human leukemic cells were detected in the spleens, bone marrows or peripheral blood of the curatively treated mice (Fig.5D,E,F; respectively).
Similarly, histological staining revealed lack of leukemic cell infiltration in irinotecan-treated xenograft-derived tissues, which resembled those of healthy control mice (Sup.Fig.4). Of great interest is the observation that brain tissues of all the irinotecan-treated mice, and particularly the mice in the curative group, were devoid of leukemic cells, while there was infiltration in to leptomeningeal space in mice of the vehicle group (Sup.Fig.5). This is of great clinical relevance, as it indicates the ability of irinotecan to eradicate central nervous system (CNS) infiltration; CNS leukemia involvement is common in *MLL*-rearranged infant ALL and represents an adverse prognostic factor.

Irinotecan shows potent anti-leukemic effects in *MLL*-rearranged ALL patient-derived xenograft mouse models

To exclude the possibility that the observed results of the irinotecan treatment are only valid in cell line models, we investigated the anti-leukemic efficacy of irinotecan also in patient-derived xenograft (PDX) models with leukemic cells of two *MLL*-rearranged ALL patients (UPID VU9815; UPID 788). After transplantation, disease development was monitored by tail vein bleeding, to determine presence of human CD45+ leukemic cells in peripheral blood. Treatment was initiated after an engraftment of >1% was confirmed by multi-color flow cytometry; one PDX model (UPID VU9815) already displayed more substantial engraftment levels, with human chimerism of 7-44% human CD45+ leukemic cells, representing a curative model close to what is observed in the clinic. In this curative treatment set-up, mice were randomly allocated to either the vehicle control group (n=4 UPID VU9815, n=4 UPID 788) or the irinotecan treatment group (n=4 UPID VU9815, n=4 UPID 788); the treatment regimen was comparable to the cell line xenografts. Disease progression in the mice was monitored every other week by determining human chimerism in peripheral blood. Regardless of the PDX model, already less than two weeks after treatment initiation there was a substantial decrease in human chimerism in the irinotecan treatment groups, while there was an exponentially increased accumulation of human CD45+ cells in the vehicle groups, as is characteristic for progressive leukemia. After 10 doses of irinotecan, mice were in complete remission (<0.2%), while the leukemic burden in control mice was 38%-83% CD45+ human leukemic

illustrated by differences in spleen weights and sizes between irinotecan- and vehicle-treated xenograft mice. Statistically significant differences were analyzed using Mann-Whitney U testing; *p<0.05; ***p<0.001.

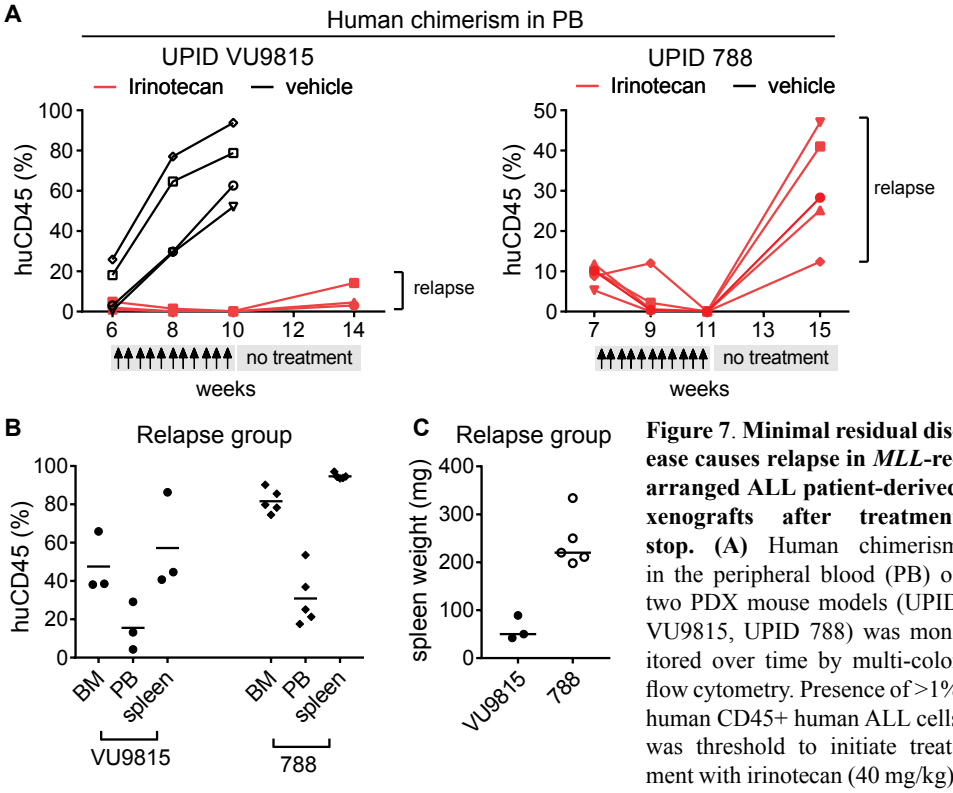

Figure 7. Minimal residual disease causes relapse in *MLL*-rearranged ALL patient-derived xenografts after treatment stop. (A) Human chimerism in the peripheral blood (PB) of two PDX mouse models (UPID VU9815, UPID 788) was monitored over time by multi-color flow cytometry. Presence of >1% human CD45+ human ALL cells was threshold to initiate treatment with irinotecan (40 mg/kg). Mice were randomly allocated to the different treatment arms: For the VU9815 PDX model there was a vehicle control (n=4) and irinotecan remission/relapse group (n=3). The UPID 788 PDX model only had an irinotecan remission/relapse group (n=5). Initial irinotecan group sizes were bigger (VU9815: n=4 irinotecan; UPID788: n=8 irinotecan), however, n=4 mice with high blast burden in the peripheral blood died shortly after treatment initiation, possibly due to acute tumor lysis syndrome, and have been excluded from the analysis. Administration occurred i.p. 3 times per week, for a total of 10 dosages, followed by a 4-week treatment stop. Changes in human leukemic cell burden were monitored every other week. **(B)** At the end of treatment, mice were euthanized and human leukemic cell infiltration in bone marrow (BM), PB and spleen measured by multi-color flow cytometry. **(C)** Splenomegaly was illustrated by spleen weights.

cells (Fig.6A). Both vehicle and irinotecan-treated mice were sacrificed, and tissues were harvested and analyzed. As observed in the cell line xenografts, human leukemic cells were nearly completely eradicated in irinotecan-treated PDX mice in the bone marrow, peripheral blood and spleen, or could only be sporadically detected at low levels in one PDX model (Fig.6B). In line with this, spleens of irinotecan-treated mice were significantly smaller than spleens from the vehicle group (Fig.6C).
In parallel to the curative set-up, we also established a separate follow-up treatment arm from both PDX models (VU9815, UPID788) in order to monitor for relapse of

the disease, similar to the treatment arms in the cell line model. As with the curative PDX treatment arm, administration of irinotecan was initiated after detection of human leukemic cells in the peripheral blood. Strikingly, a few mice with high leukemic blast burden died shortly after treatment initiation. A possible explanation might be acute tumor lysis syndrome, which can occur during treatment in disseminated leukemias.[49] As the vast majority of mice showed no adverse effects, we proceeded with the remaining mice. Irinotecan treatment was stopped after 10 dosages, and the irinotecan-treated mice were kept alive in the treatment follow-up group, whereas the control mice were sacrificed. Here, in contrast to the cell line model, the irinotecan-treated mice of the follow-up group relapsed after 4 weeks following the last treatment (Fig.7A). The mice were sacrificed and the tissues analyzed, showing systemic dissemination of human leukemic cells (Fig.7B,C). A possible explanation for the relapse is the presence of leukemic cells at minimal residual disease levels. Whereas at treatment stop there were hardly any leukemic cells detectable in the peripheral blood, analyses of the comparable treatment groups in the curative treatment setting (Fig.6) showed sporadic presence of human CD45+ leukemic cells in the bone marrow and spleen, which could act as a cell reservoir inducing leukemia relapse.

Discussion

MLL-rearranged infant ALL is an aggressive hematologic malignancy with a poor prognosis, which urgently requires improved therapeutic strategies.[4] In this study we employed a drug repurposing approach by screening different drug libraries consisting of 3685 mostly FDA-approved drugs, adopting the rationale that such therapeutics could be expeditiously transitioned to clinical practice. We successfully identified the camptothecin derivative SN-38, and its pro-drug irinotecan, as a very promising therapeutic option for *MLL*-rearranged ALL. Our data, combined with the fact that irinotecan is a well-characterized anti-neoplastic drug, strongly advocate for clinical investigation of irinotecan for the treatment of *MLL*-rearranged infant ALL. Although the rationale behind drug repurposing through screening of FDA-approved drug libraries in itself is not innovative,[40] it has not previously been reported for *MLL*-rearranged ALL with drug libraries of this magnitude. However, earlier drug discovery attempts involving FDA-approved drug screens have resulted in the identification of leukemia-subtype specific inhibitors against for example *AML1-ETO*-positive acute myeloid leukemia (AML) and *NOTCH1*-mutated T-cell ALL.[50,51]

Our drug library screens resulted in the identification of the camptothecin-derived drug class of TOP1 inhibitors, which effectively inhibited *MLL*-rearranged ALL cell lines, with SN-38 as the most potent inhibitor of ALL cell viability. The mechanism

of action for this drug class involves the generation of DNA/TOP1/drug complexes, which lead to collisions with either DNA synthesis- or transcriptional elongation-related replication forks, thereby inducing double-strand DNA breaks.[43,52] We observed higher SN-38 IC_{50} values for infant ALL patient samples compared to the ALL cell line models, which might be explained by the limited division capacity of patient-derived leukemic cells *in vitro* and the high proliferation rate of immortalized cell lines. Still, nanomolar SN-38 concentrations could effectively inhibit primary leukemia cells *in vitro*, even in absence of leukemic cell proliferation. The DNA breaks induced by SN-38 result in activation of DNA damage response pathways, including the cell cycle regulating ATM-CHK2 pathway, and this is accompanied by the formation of phosphorylated H2AX (γ-H2AX) foci.[44,45] We confirmed that low nanomolar concentrations of SN-38 induced the DNA-damage response pathway in leukemic cells via enhanced phosphorylation of CHK2 and H2AX, followed by rapid induction of apoptosis.

The anti-leukemic effect of SN-38 could be validated in *MLL*-rearranged ALL xenograft models, where the SN-38 pro-drug irinotecan effectively inhibited leukemia development. Moreover, since the leukemia is usually fully disseminated in patients at diagnosis, we started administering irinotecan to mice with advanced leukemia to mimic the start of treatment in a clinical setting. In all mice, progressive leukemia drastically regressed within days, with no detectable residual leukemic cells at the endpoint of the experiment in cell line xenografts, and minimal residual disease levels in PDX mice. These very low levels of residual human leukemic cells most likely represented the relapse-initiating cells in the PDX follow-up treatment arm. Prolonging the treatment should help to eradicate this, as it has been previously described that dosage regimen and duration is pivotal for the efficacy of camptothecin-derivatives,[53] and the initial irinotecan treatment duration of the PDX mice was shorter than the treatment of the cell line xenografts due to the exponential disease kinetics of the vehicle control group. Nevertheless, it is important to emphasize that while numerous studies show inhibition of leukemic expansion in xenograft mouse models when treatment commences shortly after xenotransplantation, complete regression of advanced leukemia in mice, especially by single agent therapy, has only been reported sporadically.[54-59] Interestingly, Jones *et al*. recently reviewed results from a pediatric ALL xenograft platform, including one *MLL*-rearranged acute leukemia sample, and reported TOP1 inhibitor topotecan effectively inhibited seven out of eight PDX ALL models.[60] Moreover, clinical trials investigating TOP1 inhibitors for acute leukemia have been reported, showing promising results.[61-64] For example, Prébet *et al*. reported improved survival and lower cumulative incidence of relapse in adult AML patients receiving combination therapy with topotecan replacing anthracycline therapy.[65] This could raise the question why these inhibitors have not progressed into clinical application. Possibly, the improved outcome with conventional

chemotherapy for pediatric ALL in the past decades, has favored implementation of targeted therapies over chemotherapeutics like TOP1 inhibitors. In contrast, outcome in *MLL*-rearranged infant ALL has stagnated over the last decade and novel treatment rationales are urgently required; the results from present study, particularly in the context of the clinical data on irinotecan treatment in literature, suggest that TOP1 inhibitors may indeed be a valuable addition to infant ALL treatment protocols, warranting further clinical investigation.

Advantageously, irinotecan has been on the market for two decades already, and the amount of available information and clinical data is substantial. Besides the extensive use in adult patients for the treatment of several solid tumors, irinotecan has been an important component of pediatric sarcoma therapy for the past 15 years, and earlier clinical experiences and challenges have recently been reviewed, including important considerations for dosage regimens.[66] Additionally, Thompson *et al*. previously established a pharmacokinetics model for irinotecan in non-infant pediatric cancer patients and concluded metabolism and SN-38 plasma levels were dependent on age.[67] These studies should aid and expedite the transition of irinotecan/SN-38 towards clinical application for infants with *MLL*-rearranged ALL, and possibly other high-risk types of childhood leukemia. Interestingly, in a Phase II trial for pediatric ALL patients at first relapse, upfront 5-day topotecan administration as part of dexamethasone/vincristine/asparaginase induction therapy resulted in similar response rates as anthracycline-containing regimens, while avoiding anthracycline-associated cardiac toxicity, and there was the expectation that prolonged topotecan treatment might further improve response.[68,69] Moreover, whereas irinotecan/SN-38 monotherapy already shows promise, combination therapy with HDAC inhibitors has been shown to synergistically inhibit other malignancies.[70-74] Together with our previous work, demonstrating that HDAC inhibition effectively and specifically targets *MLL*-rearranged ALL both *in vitro* and *in vivo*,[34] this opens up further treatment possibilities for infant ALL, such as irinotecan and HDAC inhibitor combination therapy, potentially reducing dosages and/or alleviating treatment regimens.

In summary, the here presented data convincingly advocates for the implementation of irinotecan (or comparable compounds) in the treatment of *MLL*-rearranged infant ALL.

Acknowledgements

This work was supported through use of imaging equipment of the Applied Molecular Imaging Erasmus MC facility. We thank Prof. Dr. Hans Clevers for reading the manuscript and scientific input.

Supplemental Methods

Cell lines

The leukemia cell lines SEM, KOPN8, REH, 697, Sup-B15, and Jurkat were obtained from the German Collection of Microorganisms and Cell Cultures (DSMZ, Braunschweig, Germany). The cell line RS4;11 was obtained from The Global Biosource Center (ATCC, Middlesex, UK).

Animal experiments (extensive)

Immunodeficient NOD.Cg-*Prkdc*^{scid}*Il2rg*^{tm1Wjl}/SzJ (NSG) mice from in-house breeding were transplanted with the previously generated SEM-SLIEW luciferase reporter cell line through tail-vein injection (10^6 cells/mouse). The SLIEW reporter construct encoding eGFP (enhanced green fluorescent protein) and luciferase was a generous gift from Dr. O. Heidenreich (North of England Stem Cell Institute, Newcastle and Durham Universities, Newcastle upon Tyne, UK). After 2 days, mice received an intraperitoneal injection with luciferin (RediJect D-Luciferin Bioluminescent Substrate, Perkin Elmer) and intra-vital bioimaging (IVIS Spectrum Imaging System, Perkin Elmer) was performed. Subsequently, mice were equally divided (based on total photon flux) over the respective treatment groups, and received vehicle (10% DMSO in PEG300) or Irinotecan (40 mg/kg) intraperitoneally 3 times per week. Leukemia progression was monitored through weekly intra-vital imaging until the end of the study and acquired images were analyzed using Living Image software (Perkin Elmer), with equal exposure setting for all mice per time point.
Additionally, patient-derived xenografts (PDX) were established using intrafemural injection of primary *MLL*-rearranged ALL cells of two infant patients (UPID 788; UPID VU9815) into NSG mice. Treatment was initiated after confirmation of engraftment using bioluminescence imaging (SEM-SLIEW xenografts), or presence of >1% human leukemic cells in the blood was detected by multi-color flow cytometry (PDX); mice were randomly allocated to different treatment arms, and administered with either vehicle (controls) or irinotecan (40 mg/kg) intraperitoneally 3 times per week.
If signs of overt leukemia were present, or when the end of the study was reached, mice were humanely euthanized and peripheral blood (PB) and tissues were harvested for further analyses. Leukemic burden in PB and infiltration into bone marrow (BM) and spleen were determined using a multicolor immunotyping flow cytometry approach. Briefly, erythrocytes in the PB were removed by red blood cell lysis (155 mM NH_4Cl, 12 mM NH_4CO_3, 0.1 mM EDTA, pH 7.3-7.5). BM cells were obtained by flushing the femur and tibia with PBS and resuspending to single cell suspension. Spleens were mechanically homogenized into PBS through a cell strainer (EASYstrainer, 70 μM, Greiner Bio-one), present erythrocytes were removed using

the previously described buffer and splenocytes were resuspended in PBS. Subsequent immunotyping flow cytometry was performed using 7-AAD exclusion as cell viability marker and using an antibody mix against human and mouse cell surface markers, containing human CD19-APC, human CD45-PE, mouse Cd45-PE-Cy7 and the mouse erythrocyte marker Ter119-PE-Cy7 (all BD Biosystems). Samples were measured on a MACSQuant flow cytometer (Miltenyi) and analyzed with the FlowJo software. Gating strategy is shown in Sup.Fig.3, for pure SEM-SLIEW (B), and representative examples of homogenized spleen from a vehicle (C) and irinotecan (D) treated mouse.

Isolated tissues were fixated in 4% formaldehyde, embedded in paraffin and tissue slides were stained with hematoxylin and eosin (H&E). Images were acquired with a Leica digital microscope.

Supplemental Figures

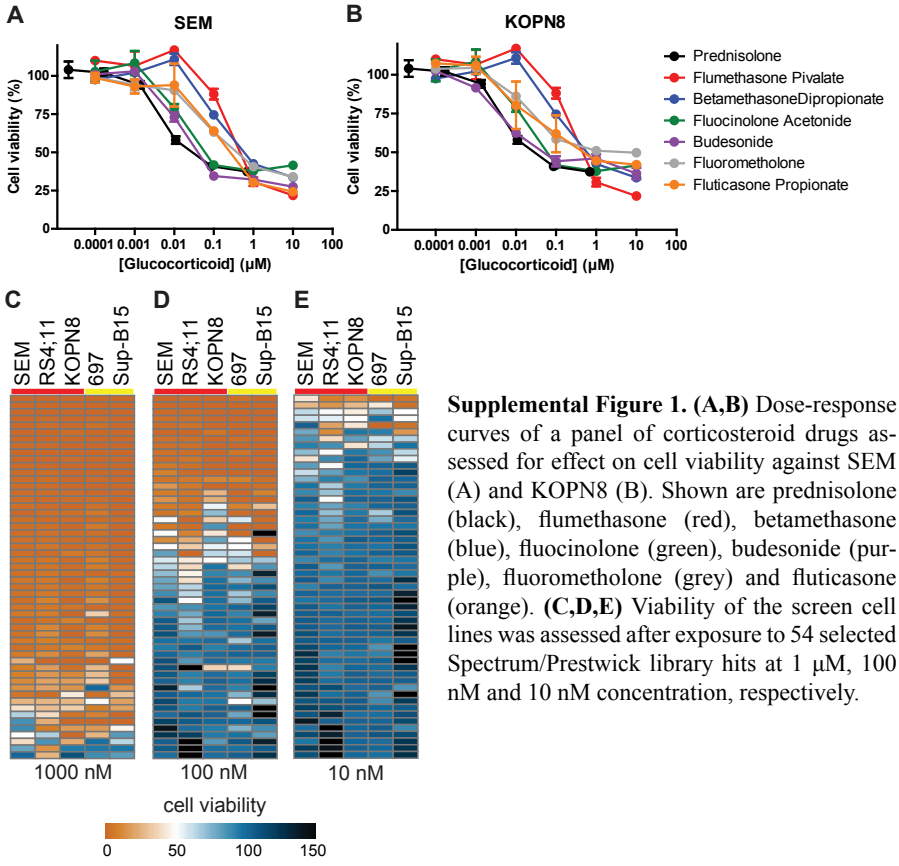

Supplemental Figure 1. (A,B) Dose-response curves of a panel of corticosteroid drugs assessed for effect on cell viability against SEM (A) and KOPN8 (B). Shown are prednisolone (black), flumethasone (red), betamethasone (blue), fluocinolone (green), budesonide (purple), fluorometholone (grey) and fluticasone (orange). **(C,D,E)** Viability of the screen cell lines was assessed after exposure to 54 selected Spectrum/Prestwick library hits at 1 μM, 100 nM and 10 nM concentration, respectively.

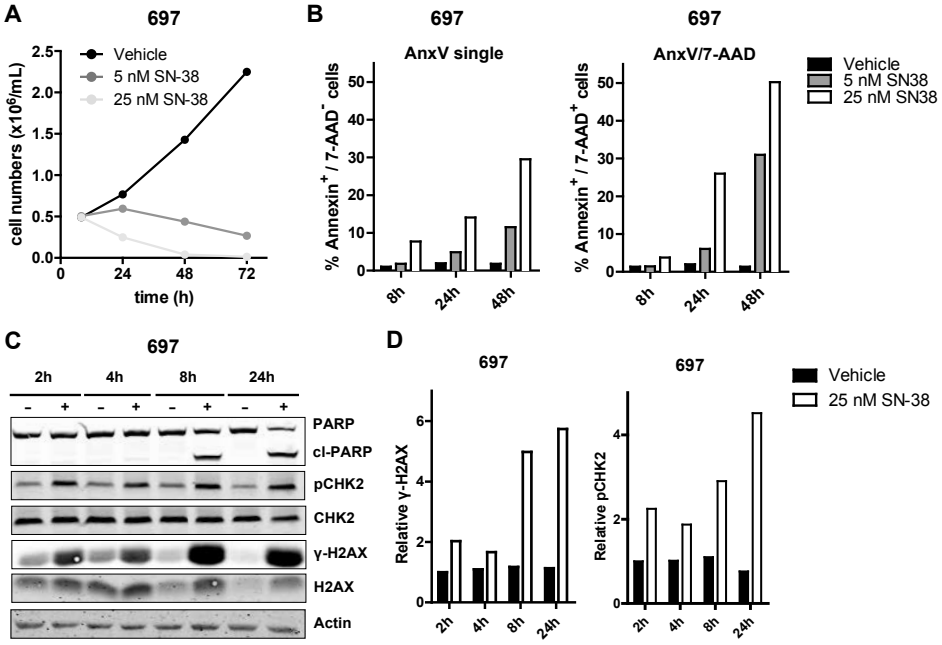

Supplemental Figure 2. (A) 697 cell counts over time (8h, 24h, 48h and 72h) after exposure to vehicle (DMSO), 5 nM or 25 nM SN-38 (black, dark grey and light grey lines, respectively; n=3). **(B)** Percentages of (early and late) apoptotic 697 cells exposed to SN-38. Representative of 3 separate experiments. **(C)** Western blots of 697 lysates after exposure to vehicle (-) or 25 nM SN-38 (+) for the indicated timepoints. **(D)** Quantification of the phosphorylated H2AX (γ-H2AX) level relative to total H2AX (left) and quantification of phosphorylated CHK2 relative to total CHK2 (right).

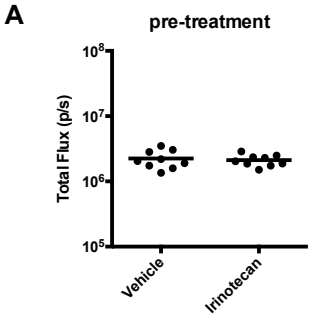

Supplemental Figure 3. (A) Quantification of the pre-treatment intra-vital imaging of the mice divided according to treatment group (vehicle or irinotecan) shows equal total flux. **(B,C,D)** Example gating for flow cytometry detection of leukemic cells in (homogenized) mouse tissues. Shown are gating of cellular events (removing debris; left), gating of live cells (7-AAD negative; center) and detection of human CD19+ (APC channel) and mouse Cd45-/mouse Ter119- (PE-Cy7 channel) cells (right) of pure SEM-SLIEW cells (B), and homogenized spleen samples of a vehicle treated mouse (C) and an irinotecan treated mouse (D).

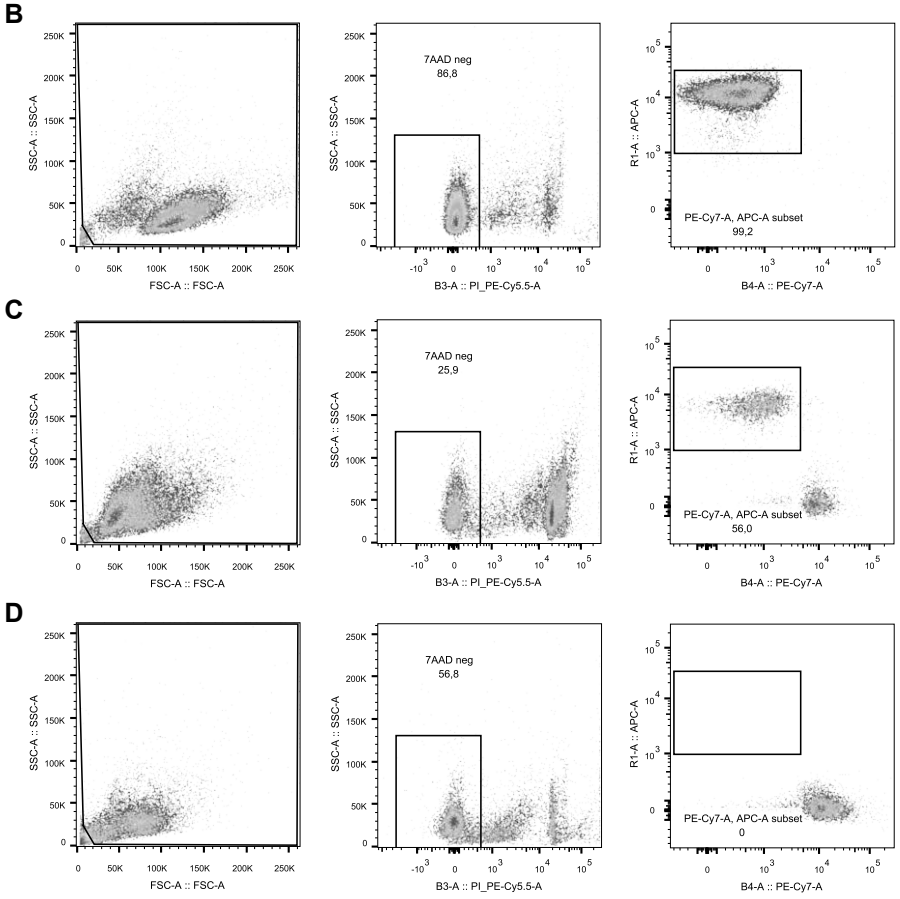

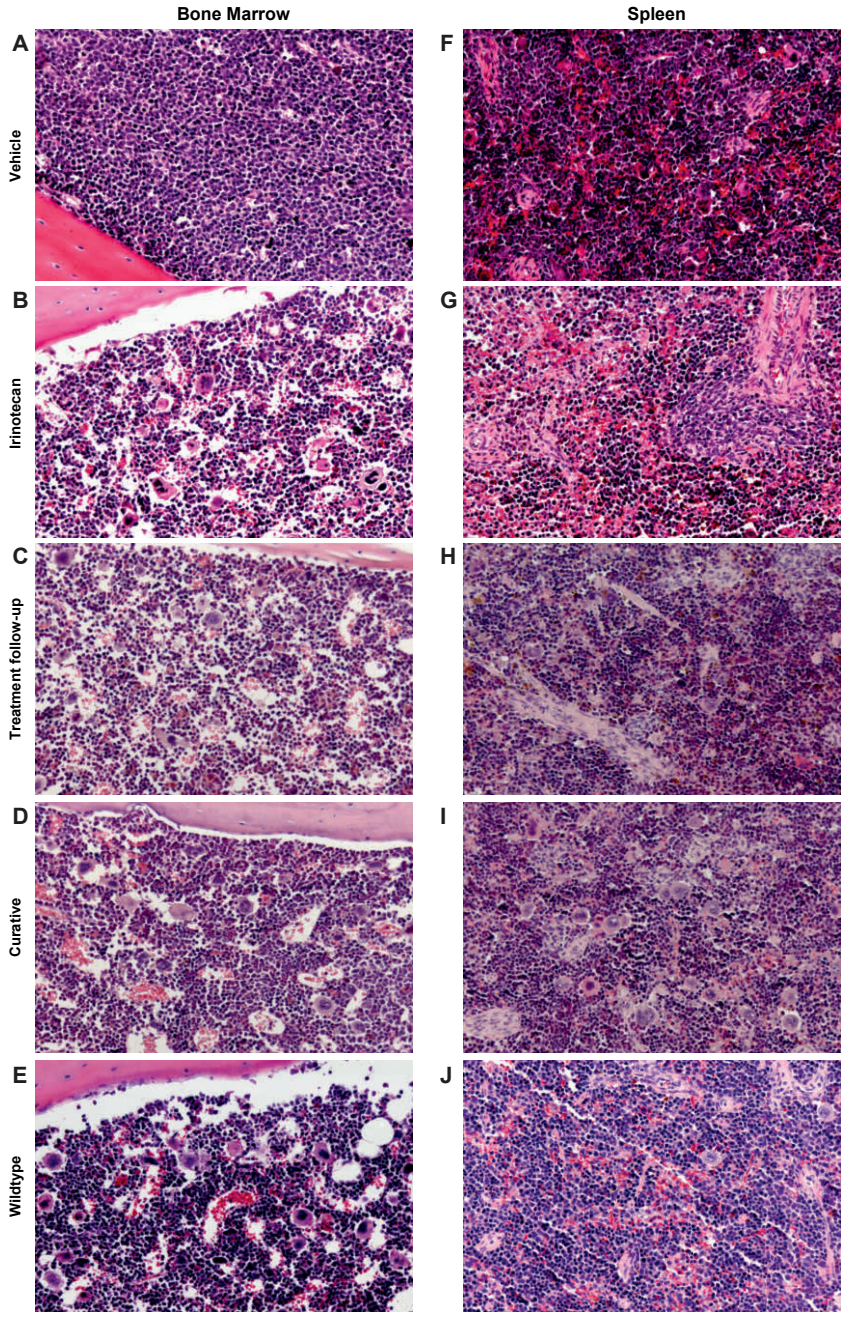

Supplemental Figure 4. (A-E) Hematoxylin and eosin (H&E) stained bone marrow tissue-sections of vehicle, irinotecan, treatment follow-up, curative and wildtype mice, respectively. **(F-J)** H&E stained spleen sections of vehicle, irinotecan, treatment follow-up, curative and wildtype mice, respectively.

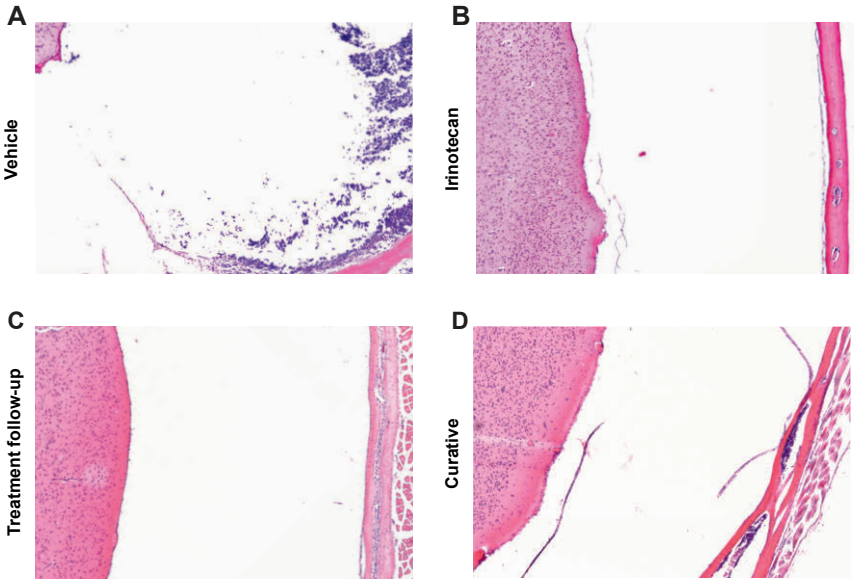

Supplemental Figure 5. (A-D) Representative H&E stained skull sections of mice from the vehicle, irinotecan, treatment follow-up and curative treatment groups, respectively.

Chapter 3

MEK inhibition is a promising therapeutic strategy for *MLL*-rearranged infant acute lymphoblastic leukemia patients carrying *RAS* mutations

Mark J.B. Kerstjens*, Emma M.C. Driessen*, Merel Willekes, Sandra Mimoso Pinhanços, Pauline Schneider, Rob Pieters and Ronald W. Stam

* These authors contributed equally to this work.

Oncotarget. 2017. Feb 28;8(9):14835-14846.

Abstract

Acute lymphoblastic leukemia (ALL) in infants is an aggressive malignancy with a poor clinical outcome, and is characterized by translocations of the *Mixed Lineage Leukemia (MLL)* gene. Previously, we identified *RAS* mutations in 14-24% of infant ALL patients, and showed that the presence of a *RAS* mutation decreased the survival chances even further. We hypothesized that targeting the RAS signaling pathway could be a therapeutic strategy for *RAS*-mutant infant ALL patients. Here we show that the MEK inhibitors trametinib, selumetinib and MEK162 severely impair primary *RAS*-mutant *MLL*-rearranged infant ALL cells *in vitro*. While all *RAS*-mutant samples were sensitive to MEK inhibitors, we found both sensitive and resistant samples among *RAS*-wildtype cases. We confirmed enhanced RAS pathway signaling in *RAS*-mutant samples, but found no apparent downstream over-activation in the wildtype samples. However, we did confirm that MEK inhibitors reduced pERK levels, and induced apoptosis in the *RAS*-mutant *MLL*-rearranged ALL cells. Finally, we show that MEK inhibition synergistically enhances prednisolone sensitivity, both in *RAS*-mutant and *RAS*-wildtype cells. In conclusion, MEK inhibition represents a promising therapeutic strategy for *MLL*-rearranged ALL patients harboring *RAS* mutations, while patients without *RAS* mutations may benefit through prednisolone sensitization.

Introduction

Acute lymphoblastic leukemia (ALL) in infants (<1 year of age) represents an aggressive malignancy, associated with high relapse rates and a poor clinical outcome.[75] The majority (~80%) of these patients carry a leukemia-specific chromosomal translocations involving the *Mixed Lineage Leukemia* (*MLL*) gene.[75] *MLL*-rearranged infant ALL patients fare significantly worse than infant ALL patients who do not carry *MLL* translocations, with event-free survival rates of 30-40% vs. ~80%, respectively.[4] Recently, we demonstrated that 24% of the infant ALL patients carrying *MLL* translocation t(4;11), the most frequently observed translocation of *MLL* among these patients, also carry a *RAS* mutation. Mutations in *NRAS* were found in 11% and *KRAS* mutations in 13% of cases.[21] Moreover, we showed that the presence of a *RAS* mutation in *MLL*-rearranged patients represented an independent predictive factor for an even worse clinical outcome in this high-risk group. Nearly all *RAS*-mutant t(4;11)$^{+}$ infant ALL patients relapsed within the first year from diagnosis, while still on treatment, and all died within 4 years from diagnosis.[21]

Despite this strong association with an exceedingly poor prognosis, a recent study by Emerenciano *et al*. suggested that *RAS* mutations in *MLL*-rearranged infant ALL may not act as driver mutations and are not required for disease progression, but rather act only at disease onset.[22] Yet, our previous data clearly showed that *RAS*-mutant *MLL*-rearranged infant ALL patients are at extremely high-risk of therapy failure and early death. Moreover, RAS pathway inhibition, including MEK inhibition, was previously shown to effectively inhibit *RAS*-mutant *MLL*-rearranged AML *in vitro*.[76,77] Therefore, we decided to investigate the potential of *RAS* pathway inhibition and found that *RAS*-mutant *MLL*-rearranged ALL cells are remarkably sensitive to MEK inhibitors.

Materials & Methods

Patient samples and cell lines

Bone marrow and peripheral blood samples from untreated infant ALL patients were collected at the Sophia Children's Hospital (Rotterdam, The Netherlands) as part of the international collaborative INTERFANT treatment protocol.[4] Approval for these studies was obtained from the Erasmus MC Institutional Review Board. Informed consent was obtained according to the Declaration of Helsinki. All samples were processed within 24 hours after sampling as described before, with optional removal of contaminating non-leukemic cells by immunomagnetic beads, to ensure leukemic blast content for all samples was >90%.[23] The t(4;11)-rearranged ALL cell line SEM and t(11;19)-rearranged ALL cell line KOPN8 were purchased from the German

Collection of Microorganisms and Cell Cultures (DSMZ, Braunschweig, Germany), while the t(4;11)-rearranged ALL cell line RS4;11 was purchased from The Global Biosource Center (ATCC, Middlesex, UK). All cell lines were cultured in suspension in RPMI-1640 with GlutaMAX (Invitrogen Life Technologies, Waltham, MA, USA) supplemented with 10% Fetal Calf Serum, 100 IU/mL penicillin, 100 IU/mL streptomycin and 0.125 µg/mL amphotericin B (Invitrogen Life Technologies) at 37°C under 5% CO_2 atmosphere.

In vitro cytotoxicity assay and small molecule inhibitors

The *in vitro* cytotoxicity of MEK162, selumetinib and Trametinib (MedChem Express, Stockholm, Sweden) was tested by MTS and MTT assays. All inhibitors were weighed, dissolved in dimethyl sulfoxide (DMSO) and stored at -20°C until use. Cytotoxicity assay dilutions were prepared in cell culture medium, keeping final DMSO concentration <0.5%. Final concentrations of the small molecule inhibitors ranged from 50 µM to 0.15 nM, indicated in the respective figures. The *in vitro* sensitivity of cell lines was assessed by using 4-day MTS conversion assays, as described previously.[78] *In vitro* cytotoxicity of patient cells was assessed by using a 4-day MTT conversion assay, as described before.[23] Data was normalized to vehicle (DMSO) controls.

Western blot

Protein extracts (25 µg) were electrophoretically resolved on pre-cast SDS-polyacrylamide gels (anyKD, TGX, Bio-Rad, Veenendaal, The Netherlands) and transferred to nitrocellulose membranes. Membranes were blocked with 5% bovine serum albumin and subsequently probed with antibodies directed against total or phosphorylated ERK, MEK, ELK-1, Akt, or p70S6K (Cell Signaling, Danvers, MA, USA). Membranes were counterstained with IRDye® 680/800 conjugated secondary antibodies (Li/COR, Leusden, The Netherlands) and were scanned by an Odyssey imaging system (Li/COR). Membranes were re-probed with mouse monoclonal anti-β-actin antibodies (Sigma-Aldrich, St. Louis, MO, USA) as loading control. Fluorescence was quantified using the Odyssey 3.0 application software.

RAS activation

RAS activation was analyzed using the RAS Activation Assay Kit (17-218, Merck-Millipore, Amsterdam, The Netherlands). Briefly, $1x10^7$ cells were isolated and lysed with Mg^{2+} Lysis Buffer (MLB), and stored at -80°C until use. GST-fused RAF-1 RAS-binding domain (RBD) bead slurry was added to the lysate and incubated for 1 hour at 4°C while agitating. Beads were isolated by centrifugation and washed with MLB, and precipitated protein was denatured with Laemmli buffer at 95°C before immunoblotting. As a positive control, total cell lysate was included in the

immunoblotting procedure. The provided RAS antibody (05-516, Merck-Millipore) was used, and GST (Cell Signaling) and β-actin (Sigma-Aldrich) antibodies were used as loading controls for the beads and total protein, respectively. Fluorescence was quantified using the Odyssey 3.0 application software.

Annexin-V/7-AAD apoptosis and cell cycle assays

For assessment of early and late apoptosis, the PE Annexin-V Apoptosis Detection Kit (BD Pharmingen, Breda, The Netherlands) was used according to the manufacturer's protocol. Briefly, drug-exposed cells were isolated, washed with PBS and re-suspended in binding buffer. Cells were stained with PE Annexin V and/or 7-AAD for 15 minutes, and sorted using fluorescence activated cell sorting (FACS). Cell cycle progression was assessed by permeabilization of isolated cells through hypotonic lysis. Subsequently, RNAse treatment was performed, and DNA was stained using propidium iodide, after which FACS determined DNA content. Data was analyzed using FlowJo software (FlowJo, Ashland, OR, USA).

Gene expression data

Recently published gene expression data (Affymetrix HU133plus2.0) for part of the $t(4;11)^{+}$ patient samples was available (i.e. for 6 of 9 MEK inhibitor resistant *RAS*-wildtype samples, 4 of 5 sensitive *RAS*-wildtype samples and 3 of 6 *RAS*-mutant samples).[28] This data is available in GEO database19 (accession number GSE19475) and was acquired as previously described.[28] Tyrosine kinase receptor expression was derived from this dataset, using the following probe sets: 206674_at (FLT3), 204406_at (VEGFR-1), 203934_at (VEGFR-2), 234379_at (VEGFR-3), 210973_s_at (FGFR-1), 208225_at (FGFR-2), 204380_s_at (FGFR-3), 204579_at (FGFR-4), 211551_at (EGFR), 210930_s_at (ERBB2), 226213_at (ERBB3), 214053_at (ERBB4), 205463_s_at (PDGFR-A), 217112_at (PDGFR-B), 204891_s_at (Lck) and 213324_at (Src).

Statistical analysis

Statistical analyses were performed with SPSS Statistics version 17.0 (SPSS Inc. Chicago, IL, USA). All tests were two-tailed and *p*-values < 0.05 were considered significant. The effect of combining drugs (i.e. synergy, additivity or antagonism) was assessed using Berenbaums criteria, as previously described.[79,80] Briefly, we calculated the Synergy Factor (F_{Syn}) with the formula F_{Syn} = ([Drug $X_{\text{in combination with Y}}$]/[Drug X]) + ([Drug $Y_{\text{in combination with X}}$] / [Drug Y]) for a particular fractional effect. If the drug combination results in $F_{Syn} < 1$, this is considered synergy.

Results

RAS-mutant *MLL*-rearranged ALL cells are sensitive to MEK inhibition

Since the previously identified *RAS* aberrations are all activating mutations (at residues G12, G13 or Q61), we wondered whether small molecule inhibitors targeting RAS pathway components could suppress *RAS*-mutant leukemic cells.[21,81] Therefore, 7 RAS pathway inhibitors, already approved for therapeutical use or under clinical investigation for other malignancies with RAS pathway mutations, were selected as therapeutic strategies for the *RAS*-mutant infant ALL patients. Using 4-day MTS cell viability assays we tested the *in vitro* anti-leukemic potential of salirasib (RAS localization inhibitor), vemurafenib (BRAF inhibitor), sorafenib (pan-kinase inhibitor), trametinib, selumetinib and MEK162 (MEK inhibitors) and temsirolimus (mTOR inhibitor) against *RAS*-mutant *MLL*-rearranged ALL cell line KOPN8, and the *RAS*-wildtype *MLL*-rearranged cell lines SEM and RS4;11. Interestingly, the *RAS*-mutant cell line KOPN8 was more sensitive to the MEK inhibitors MEK162, selumetinib and trametinib (Fig.1). Temsirolimus and sorafenib potently reduced cell viability of both *RAS*-mutant and *RAS*-wildtype cell lines. Additionally, salirasib and vemurafenib did not substantially reduce cell viability, even at high concentrations (>10μM). To confirm the efficacy of these inhibitors, we performed 4-day MTT cell viability assays on primary diagnostic *RAS*-mutant (n=6) and *RAS*-wildtype (n=14) t(4;11)$^{+}$ infant ALL samples. Interestingly, compared to *RAS*-wildtype t(4;11)$^{+}$ ALL cases, the *RAS*-mutant t(4;11)$^{+}$ infant ALL cases were significantly more sensitive to all MEK inhibitors (Fig.2A) with median IC_{50} values of <0.1 μM for MEK162 and selumetinib and <0.01 μM for trametinib (Fig.2B). Additionally, all other tested inhibitors (salirasib, temsirolimus, sorafenib and vemurafenib) reached only IC_{50} values of >10μM (Sup.Fig.1).

Also, we included one matched pair of diagnostic/relapse t(4;11)$^{+}$ samples. For this particular patient, no *RAS* mutation was present at diagnosis, but a *RAS* mutation could be identified at relapse. Indeed, the *RAS*-mutant relapse sample of this patient was more sensitive to all three MEK inhibitors tested than the *RAS*-wildtype diagnostic sample (Fig.2B).

Enhanced RAS activation in t(4;11)$^{+}$ infant ALL cells carrying *RAS* mutations

The MEK inhibitors MEK162, selumetinib and trametinib significantly reduce viability of *RAS*-mutant *MLL*-rearranged ALL cells. Notably, a subset of the *RAS*-wildtype primary t(4;11)$^{+}$ infant ALL samples also responded favorably to the MEK inhibitors (Fig.2B). We wondered whether other biomarkers, besides *RAS* mutation status, could predict MEK inhibitor sensitivity in *MLL*-rearranged ALL. Wildtype RAS proteins are under regulation of upstream signaling events, often involving ty-

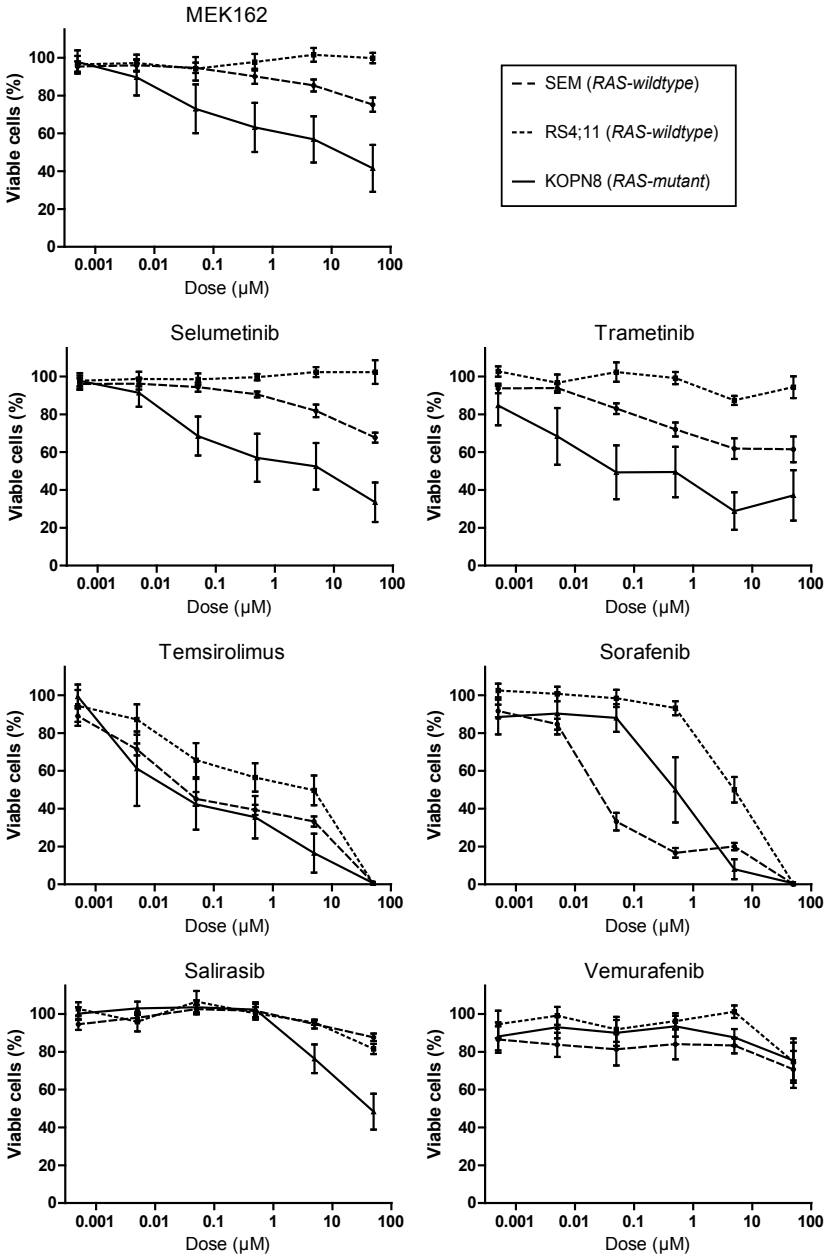

Figure 1. MEK inhibitors specifically impede *RAS*-mutant *MLL*-rearranged ALL cell line KOPN8. Cell viability of *MLL*-rearranged cell lines exposed to MEK162, selumetinib, trametinib, temsirolimus, sorafenib, salirasib and vemurafenib. All cell lines respond to sorafenib and temsirolimus, while *RAS*-mutant KOPN8 (solid line) is more sensitive than *RAS*-wildtype SEM (large dashed line) or RS4;11 (small dashed line). Data are represented as mean +/- sem. n≥3.

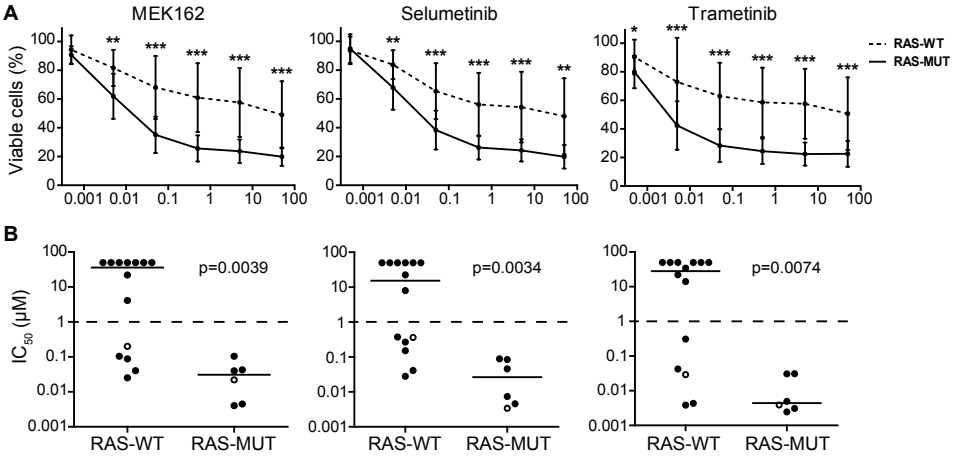

Figure 2. Primary *RAS*-mutant *MLL*-rearranged ALL cells are sensitive to MEK inhibitors. (A) Patient derived t(4;11)+ infant ALL cells exposed to MEK inhibitors indicate *RAS*-mutant samples (solid line, n=6) are more sensitive compared to *RAS*-wildtype samples (dashed line, n=14). Data are represented as median +/- sd. *0.01<p<0.05; **0.001<p<0.01; ***p<0.001. **(B)** The IC50 (concentration needed to inhibit 50% of the leukemic cell viability) of the individual t(4;11)+ infant ALL patient samples shown in (A). Median IC50 values, represented by horizontal bars, confirm strong sensitivity of *RAS*-mutant patient samples compared to the majority of *RAS*-wildtype samples. Open circles indicate matched diagnosis (wildtype) and relapse (mutant) samples. The tick lines indicate separation between MEK inhibitor sensitive and resistant patient samples (IC50<1μM and IC50>1μM, respectively).

rosine kinase receptors, while mutant RAS proteins are less dependent on upstream activation due to reduced GTPase activity, rendering a surplus of activated GTP-bound RAS. Therefore, we determined the RAS protein levels and RAS activity in our primary t(4;11)$^+$ infant ALL cells. No significant difference in RAS protein levels was observed between the *RAS*-mutant and *RAS*-wildtype t(4;11)$^+$ infant ALL samples using Western blot analysis (Fig.3A). Next, we investigated the level of active (GTP-bound) RAS in these samples by precipitation with RAF-1 RAS interaction protein, followed by immunoblotting. As expected, the *RAS*-mutant t(4;11)$^+$ infant ALL samples showed significant (p=0.013) higher levels of RAS activation as compared to *RAS*-wildtype samples (Fig.3B). No differences in RAS activation were observed between *RAS*-wildtype samples that were sensitive or resistant to MEK inhibition.

Subsequently, we determined phosphorylation levels of MEK (pMEK) and ERK (pERK) by immunoblotting (Sup.Fig.2A and B, respectively). Quantification of the blots indicated a significantly higher level of pMEK in our *RAS*-mutant samples, compared to *RAS*-wildtype samples (p=0.0312, Fig.3C), although there was no difference in pMEK levels between the MEK inhibitor resistant and sensitive *RAS*-wildtype subgroups. Still, we did find a higher pMEK level in the mutated relapse sample

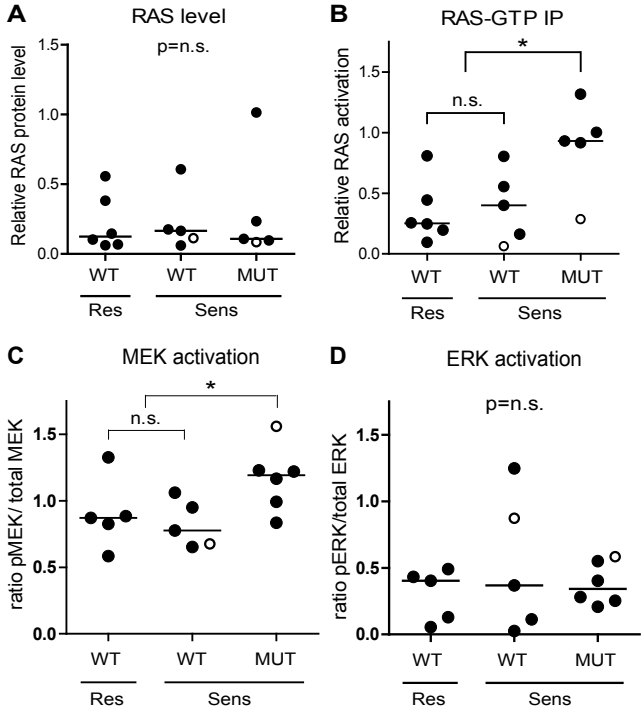

Figure 3. *RAS*-mutant t(4;11)+ ALL cells have enhanced downstream activation. (A) RAS protein level, relative to β-actin, determined by western blotting in t(4;11)+ infant ALL samples, subdivided according to *RAS* mutation status (WT or MUT) and MEK inhibitor sensitivity (resistant (Res) and sensitive (Sens)). No differences in median protein level (horizontal bars) are observed between the different subgroups. **(B)** Relative RAS activation is enhanced in *RAS*-mutant t(4;11)+ patient samples, though no difference is observed between the MEK inhibitor resistant and sensitive *RAS*-wildtype subgroups. **(C)** Ratio phosphorylated MEK (pMEK)/total MEK in *RAS*-mutant (MUT) and *RAS*-wildtype (WT) t(4;11)+ infant ALL samples shows increased MEK activation in *RAS*-mutant samples, while the MEK inhibitor resistant and sensitive *RAS*-wildtype samples have comparable MEK activation. **(D)** Ratio phosphorylated ERK (pERK)/total ERK in *RAS*-mutant and *RAS*-wildtype t(4;11)+ infant ALL samples shows no significant differences in ERK activation between subgroups. Horizontal bars present group medians. Open circles indicate matched diagnosis (wildtype) and relapse (mutant) samples. *$p<0.05$.

compared to its matched wildtype diagnosis sample. Additionally, no differences in pERK levels were found between *RAS*-wildtype and *RAS*-mutant samples (Fig.3D), nor between *RAS*-wildtype cells that were sensitive or resistant to MEK inhibition.
In *MLL*-rearranged AML, MEK inhibitor resistance can occur through activation of tyrosine kinase receptor (TKR) signaling (i.e. involving VEGFR-2).[76] Furthermore, we previously found *MLL*-rearranged ALL is characterized by high expression of Fms-like tyrosine kinase 3 (*FLT3*).[23] Therefore, we interrogated available gene expression profiles of primary samples for possible differences in TKR expression levels between the MEK inhibitor sensitive and resistant subgroups (Sup.Fig.3). Interestingly, apart from *FLT3*, expression of TKRs is relatively low in the different patient samples. Surprisingly, *FGFR-1* expression is significantly lower in MEK inhibitor resistant *RAS*-wildtype samples (p=0.02), while there are no significant differences in expression of *FLT3*, *VEGFR* (1-3), *FGFR* (2-4), *EGFR* and *ERBB* (2-4), *PDGFR* (A-B) or *Lck* and *Src*.

MEK inhibition results in reduced ERK phosphorylation

Next, we exposed *MLL*-rearranged ALL cell lines SEM and KOPN8 to the MEK inhibitors (selumetinib, MEK162 and trametinib) and determined pERK and pMEK levels by immunoblotting (Fig.4). Interestingly, pERK levels were drastically reduced in both SEM and KOPN8, already after 6 hours of exposure, and this effect was sustained for at least 48 hours, regardless of the inhibitor used (Fig.4A). Furthermore, prolonged exposure (24 and 48 hours) to the MEK inhibitors selumetinib and MEK162 resulted in an increase of pMEK in SEM and KOPN8 (Fig.4B). Additionally, we determined phosphorylation of ERKs downstream effector ELK-1, but ELK-1 activation was not influenced by MEK inhibition (Sup.Fig.4A).

Since SEM cells responded modestly to MEK inhibition but did show a significant loss of pERK levels, we investigated whether these cells could circumvent loss of ERK activation by upregulating RAS-mediated PI3K-Akt-mTOR signaling. There-

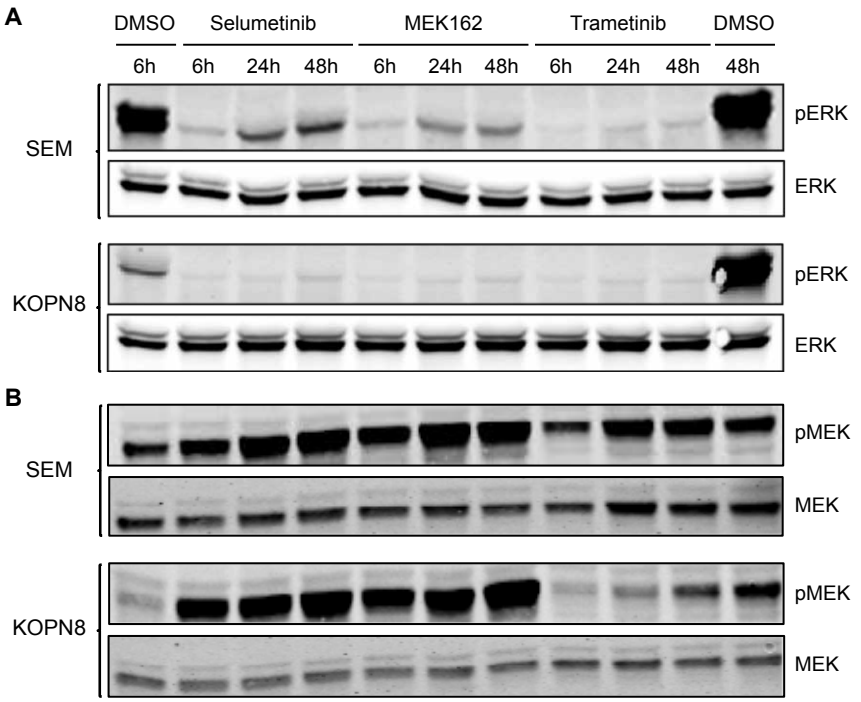

Figure 4. MEK inhibition results in reduced ERK phosphorylation. (A) Western blot analysis of SEM and KOPN8 (upper and lower panels, respectively) exposed to 500 nM of MEK inhibitor or vehicle control (DMSO) for 6, 24 and 48 hours. Both cell lines almost completely lose ERK phosphorylation (pERK), while total ERK (ERK) levels remain unaffected. **(B)** Analysis of MEK phosphorylation (pMEK) suggests exposure to MEK162 and selumetinib results in enhanced MEK phosphorylation in both cell lines, whereas total MEK (MEK) levels remain constant.

fore, the downstream phosphorylation of Akt (Ser437) and p70S6K (Thr389) was assessed by immunoblotting. However, no differences in Akt and p70S6K phosphor-

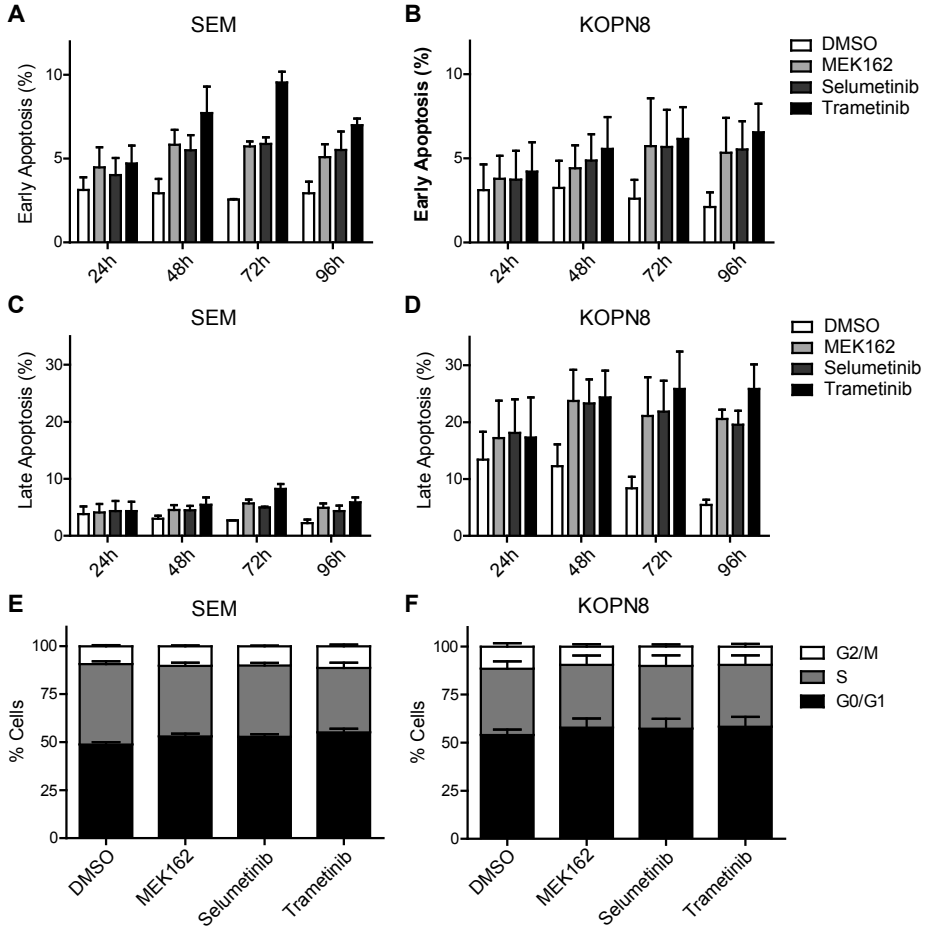

Figure 5. MEK inhibitors induce apoptosis. (A,B) Early apoptosis (percentage AnnexinV single positive of total) of SEM and KOPN8 cells (respectively) after exposure to DMSO vehicle (white bars) or 500 nM MEK162, selumetinib or trametinib (light grey, dark grey and black bars, respectively), indicates MEK inhibition slightly induces early apoptosis. Data are represented as mean +/- sem. n=3. **(C,D)** Late apoptosis (percentage AnnexinV and 7-AAD double positive cells of total) of SEM and KOPN8 (respectively) show that while SEM cells have no induction of late apoptosis in response to MEK inhibition, compared to the DMSO controls, KOPN8 clearly undergoes apoptosis, especially after prolonged exposure (>48 hours). Data are represented as mean +/- sem. n=3. **(E,F)** Cell cycle analysis of SEM and KOPN8 (respectively) after 96 hours exposure to vehicle (DMSO) or 500 nM MEK162, selumetinib or trametinib indicates MEK inhibition does not impinge on the cell cycle progression. Stacked bar graph indicates percentage of cells in G0/G1 (black), S (grey) and G2/M (white) cell cycle stages. Data are represented as mean +/- sem. n=3.

ylation were observed in response to MEK inhibitor exposure (Sup.Fig.4B and C, respectively).

MEK inhibitors induce apoptosis

Subsequently, we investigated the phenotypic effects of the MEK inhibitors on SEM and KOPN8 through analysis of early and late apoptosis markers (Annexin-V and 7-AAD, respectively), using flow-cytometry. Interestingly, both *RAS*-wildtype SEM and *RAS*-mutant KOPN8 undergo early apoptosis, after treatment with MEK inhibitor (Fig.5A and B, respectively). However, while late apoptosis is barely observed for SEM (Fig.5C), late apoptosis in MEK inhibitor exposed KOPN8 cells is enhanced substantially, especially after prolonged exposure (Fig.5D), suggesting the response to MEK inhibition is characterized by increased apoptosis. Furthermore, MEK inhibitor exposure induced protein levels of pro-apoptotic BIM, most evidently for KOPN8, while p53 levels remained unaffected (Sup.Fig.5). Additionally, we investigated cell cycle progression under influence of MEK inhibition. Interestingly, no considerable differences in SEM or KOPN8 cell cycle progression are observed after 96 hours exposure to MEK162, selumetinib or trametinib (Fig.5E and F, respectively), nor after exposure for 24, 48 and 72 hours (Sup.Fig.6A-B, C-D and E-F, respectively).

MEK inhibition enhances prednisolone sensitivity

In our previous study, we found that *MLL*-rearranged infant ALL patient samples harboring *RAS* mutations are more resistant to prednisolone.[21] Therefore, we examined whether inhibition of MEK could enhance prednisolone sensitivity of *RAS*-mutant cells. As shown in Figure 6A, prednisolone alone decreases cell viability of SEM cells to only ~50%. Interestingly, while trametinib by itself induces only minor cell viability decrease in SEM cells (Fig.6B), the combination of trametinib and prednisolone greatly enhanced the efficacy of prednisolone, especially at higher concentrations (Fig.6A). The combination of prednisolone and trametinib also strongly decreased cell viability in KOPN8 more potently than either drug alone; low concentrations of trametinib nearly eradicated all KOPN8 cells that did not respond to prednisolone treatment (Fig.6C). A similar sensitizing effect was observed when exposing SEM and KOPN8 to MEK162 or selumetinib in combination with prednisolone (Sup.Fig.7A-D and F-I, respectively). Since trametinib alone already effectively decreases viability of KOPN8 cells (Fig.6D), we quantified the combinatorial effect of MEK inhibitors and prednisolone using the synergy factor (F_{Syn}) calculation, as previously described.[79,80] The plot in Figure 6E shows the fractional effect (i.e. the relative decrease of cell viability) induced by the combination of trametinib with prednisolone, and the corresponding Synergy Factor. Interestingly, in both SEM and KOPN8 cells we observed F_{Syn} values < 0.5, indicating strong synergy

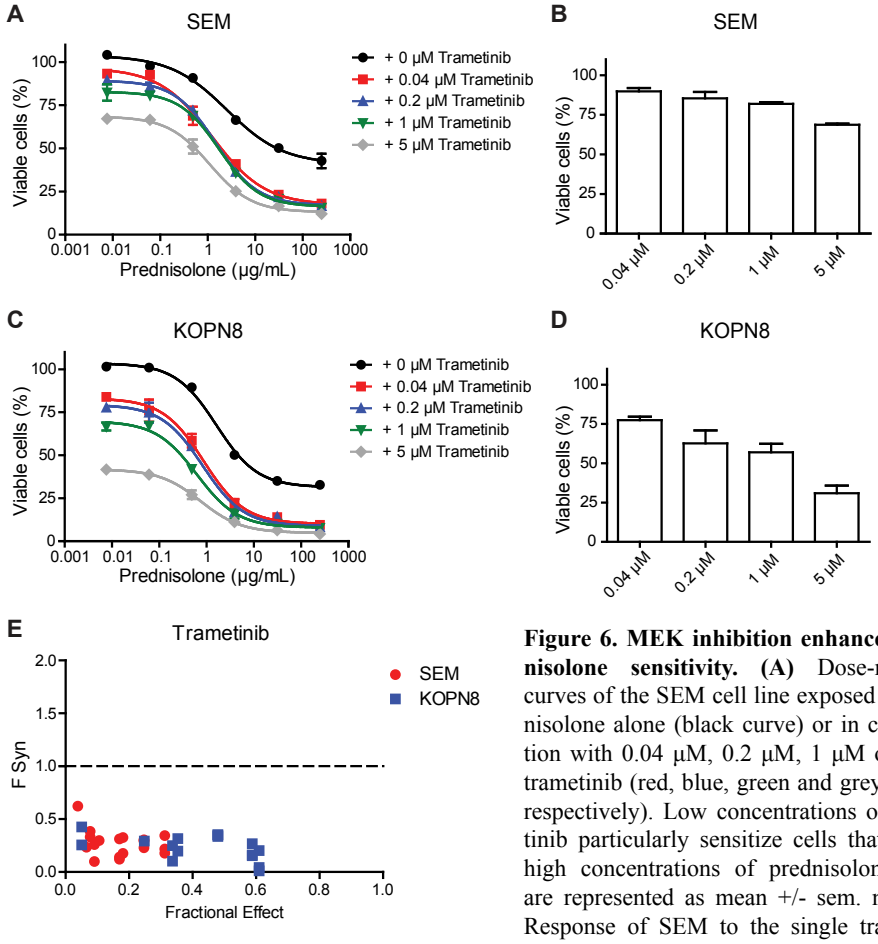

Figure 6. MEK inhibition enhances prednisolone sensitivity. (A) Dose-response curves of the SEM cell line exposed to prednisolone alone (black curve) or in combination with 0.04 µM, 0.2 µM, 1 µM or 5 µM trametinib (red, blue, green and grey curves, respectively). Low concentrations of trametinib particularly sensitize cells that escape high concentrations of prednisolone. Data are represented as mean +/- sem. n=3. **(B)** Response of SEM to the single trametinib concentrations used in A. n=3. **(C)** Dose-response curves of KOPN8 treated with prednisolone (black curve), or in combination with the aforementioned trametinib concentrations (shown in red, blue, green and grey, respectively). KOPN8 cells are also sensitized towards prednisolone by co-exposure with low concentrations of trametinib. Data are represented as mean +/- sem. n=3 **(D)** KOPN8 exposed to single trametinib concentrations. Data are represented as mean +/- sem. n=3. **(E)** Combined exposure to prednisolone and trametinib (merged data from 3 separate experiments) was quantified using FSyn calculations (FSyn<1 indicates synergy) and plotted against fractional effect (i.e. inhibition of cell viability). In SEM (red) moderate to strong synergy was observed, while all combinations of trametinib and prednisolone resulted in strong to very strong synergy in KOPN8 (blue).

between trametinib and prednisolone. Also combining MEK162 or selumetinib with prednisolone resulted in moderate to strong synergistic effects (Sup.Fig.7E and J, respectively). Additionally, we investigated whether this enhanced effect was related to differential expression of the glucocorticoid receptor (GR), the target of prednis-

olone. However, MEK inhibitor exposure did not alter GR protein levels in either SEM or KOPN8 cells (Sup.Fig.7K).

Discussion

MLL-rearranged ALL in infants is a high-risk hematologic malignancy, characterized by a high incidence of relapse and high mortality rate.[82] Recently, we showed that 14-24% of these patients carry a *RAS* mutation, as an independent predictor of extremely poor outcome.[21] In the present study, we demonstrate that the MEK inhibitors trametinib, selumetinib and MEK162 display strong anti-leukemic effects against *RAS*-mutant *MLL*-rearranged ALL cells. Considering the dismal prognosis for infants suffering from *MLL*-rearranged ALL with additional *RAS* mutations, our data supports application of these inhibitors in the treatment of this patient group. Recently, Irving *et al.* already showed that selumetinib effectively inhibits leukemia progression in an *in vivo* model of *RAS*-mutant BCP-ALL, and Burgess *et al*. found trametinib to prolong the survival of mice transplanted with $NRAS^{G12D}$ AML cells.[83,84] Moreover, trametinib has recently been approved for the treatment of adult *BRAF*-mutated melanoma, while different clinical trials show promising results in adult patients with *RAS*/*RAF* mutation positive melanoma and non-small-cell lung cancer for selumetinib and MEK162.[85-89] Even though most clinical trials focused on solid tumors in adult patients, pediatric clinical trials are underway for neurofibromas and gliomas, and could expedite clinical application of these MEK inhibitors in *MLL*-rearranged infant ALL. Interestingly, while all *RAS*-mutant *MLL*-rearranged ALL patient samples are susceptible to MEK inhibition, patients without *RAS* mutations also might benefit from MEK inhibitor treatment, since a subgroup of *RAS*-wildtype patient samples appears sensitive to MEK inhibition. While in our previous study, we identified *RAS* mutations and found no *BRAF* aberrations, mutations of other upstream regulators, i.e. tyrosine kinase receptors, can occur in other malignancies.[21] Andersson *et al.* recently showed that additional somatic mutations in *MLL*-rearranged infant ALL, like (sub-)clonal RAS/PI3K pathway aberrations, occur in up to 50% of the cases, supporting our previous observation that *RAS* mutations in *MLL*-rearranged infant ALL frequently occur at a sub-clonal level.[20,21] These findings do not support the hypothesis that other (upstream) mutations are driving RAS-MEK-ERK signaling, but also do not explain observed extensive MEK inhibitor sensitivity of all (subclonal) *RAS*-mutant and specified *RAS*-wildtype patient samples. While we found enhanced RAS and MEK activation in *RAS*-mutant samples, these biomarkers could not differentiate MEK inhibitor sensitive and resistant *RAS*-wildtype samples. Interestingly, Kampen *et al.* recently proposed a MEK inhibitor escape mechanism in *MLL*-rearranged AML, which was mediated by VEGFR-2

and PI3K-signaling, and we wondered whether this could play a role in the MEK inhibitor resistance of our wildtype patient cells.[76] However, we observed no difference in downstream PI3K-signalling (i.e. Akt or p70S6 phosphorylation) in response to MEK inhibitor exposure. Additionally, we discovered no significant tyrosine kinase receptor expression differences in *MLL*-rearranged infant ALL patient samples that could explain the MEK inhibitor response of *RAS*-wildtype samples. Surprisingly, *FGFR-1* expression was lower in MEK inhibitor resistant samples, but it is unclear how this would explain MEK inhibitor resistance. Alternatively, Minjgee *et al.* report that *RAS*-mutant transfected cells can induce downstream RAS signaling in a paracrine manner, through excretion of cytokines.[90] Interestingly, Nakanishi *et al.* previously demonstrated that *MLL*-fusion proteins can induce ERK phosphorylation through regulating EphA7 receptor tyrosine kinase expression, but this was not accompanied by increased RAF or MEK phosphorylation.[91] Still, their data shows that leukemic cells carrying the t(4;11) translocation are sensitive to small molecule inhibitors of ERK phosphorylation. These findings indicate alternative regulatory mechanisms for ERK signaling in *MLL*-rearranged leukemia could explain the MEK inhibitor sensitivity we observe in *RAS*-wildtype cells.

Loss of ERK phosphorylation in response to MEK162, selumetinib or trametinib exposure confirmed the effect of MEK inhibition. Interestingly, prolonged exposure of cells to MEK162 or selumetinib resulted in increased MEK phosphorylation. Previously, Hatzivassiliou *et al.* showed that the aromatic fluorine of allosteric MEK inhibitor GDC-0973 interacts with MEK residue S212.[92] Their data indicate this interaction results in exposure of the phosphorylation sites S218/S222, which are then susceptible to RAF mediated phosphorylation. Since MEK162 and selumetinib both have this aromatic fluorine, the mechanism of interaction with MEK is probably similar to GDC-0973. Hence, although MEK activation in presence of GDC-0973, MEK162 or selumetinib can still occur, the transduction of the signal by MEK-mediated phosphorylation of ERK is no longer possible, as we show in Figure 4.

Recently, we found the presence of *RAS* mutations in *MLL*-rearranged infant ALL cells correlated with prednisolone resistance, an obstacle in the treatment of infant ALL.[4,21] Remarkably, our present data shows that MEK inhibition strongly enhances the sensitivity of both *RAS*-wildtype and *RAS*-mutant *MLL*-rearranged ALL cells to prednisolone, also further exemplifying the possible value of MEK inhibitors for *RAS*-mutant, as well as *RAS*-wildtype, *MLL*-rearranged infant ALL patients. The prednisolone-sensitizing effect of MEK inhibitors proposes a possible role for RAS-MEK-ERK signaling in the response to glucocorticoids. Recent work by Jones *et al.* shows that MEK plays a key role in drug resistance in relapsed pediatric ALL, and that MEK inhibition can sensitize ALL relapse samples to chemotherapeutics, including methylprednisolone.[93] Moreover, Ariës *et al.* found trametinib could restore prednisolone sensitivity in *RAS*-mutant BCP-ALL patient samples, whereas Rambal

et al. showed that MEK activation reduces dexamethasone sensitivity, and the MEK inhibitor PD183452 enhanced dexamethasone responses in ALL cells in a BIM-dependent manner. [94,95] Activated ERK can phosphorylate BIM, targeting it for proteasomal degradation, and thereby diminishing apoptosis induced by dexamethasone.[96] Moreover, we established that, while glucocorticoid receptor expression remains constant, MEK inhibition upregulates pro-apoptotic BIM, which implies that inhibiting MEK, resulting in abrogation of ERK phosphorylation, may result in prolonged maintenance of pro-apoptotic BIM activity upon prednisolone exposure, leading to enhanced prednisolone sensitivity. This is further supported by our previous study showing that in *MLL*-rearranged ALL, prednisolone sensitization mediated by pan-BCL-2 family inhibitors was largely driven by the upregulation of pro-apoptotic BID and BIM.[97]

In summary, our data shows that *RAS*-mutant *MLL*-rearranged infant ALL patients may benefit from therapeutic strategies administering small-molecule MEK inhibitors. Furthermore, since MEK inhibition sensitizes *MLL*-rearranged ALL cells to prednisolone regardless of the *RAS* mutations status, *RAS*-wildtype *MLL*-rearranged infant ALL patients may also benefit from MEK inhibitor treatment through enhanced sensitivity to prednisolone.

Acknowledgements

The authors would like to thank the members and participating institutes of the INTERFANT-99 study for generously providing leukemic samples.

Members of the INTERFANT-99 study are as follows: M. Campbell (Programa Infantil Nacional de Drogas Atineoplasicas (PINDA)), M. Felice (Argentina), A. Ferster (Children's Leukemia Group (CLCG)), I. Hann and A.Vora (UK Children's Cancer Study Group (UKCCSG)), L. Hovi (Nordic Society of Paediatric Haematology and Oncology (NOPHO)), G. Janka-Schaub (Cooperative Study Group for Treatment of ALL (COALL)), C.K. Li (Hong Kong), G. Mann (Berlin-Frankfurt-Munster Group-Austria (BFM-A)), T. LeBlanc (French ALL Group (FRALLE)), R. Pieters (Dutch Childhood Oncology Group (DCOG)), G. de Rossi and A. Biondi (Associazione Italiana Ematologia Oncologia Pediatrica (AIEOP)), J. Rubnitz (St Jude Children's Research Hospital (SJCRH)), M. Schrappe (Berlin-Frankfurt-Munster Group-Germany (BFM-G)), L. Silverman (Dana-Farber Cancer Institute (DFCI)), J.Stary (Czech Paediatric Haematology (CPH)), R. Suppiah (Australian and New Zealand Children's Haematology/Oncology Group (ANZCHOG)), T. Szczepanski (Polish Paediatric Leukemia and Lymphoma Study Group (PPLLSG)), and M. Valsecchi and P. de Lorenzo (Trial Operating Center (CORS)).

We thank P. Garrido Castro and D. Geerts for scientific input and reading the manuscript.

Supplemental Figures

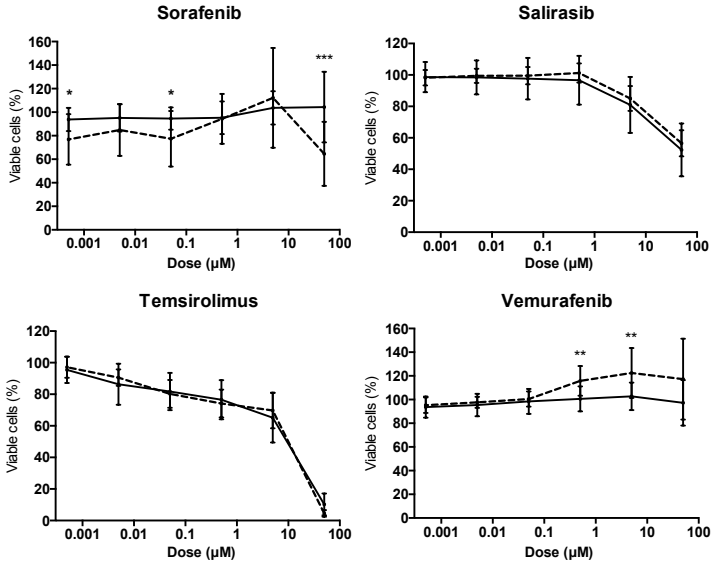

Supplemental Figure 1. MTT assays of patient derived *RAS*-mutant (solid line, n=6) and *RAS*-wild-type (dashed line, n=14) t(4;11)+ infant ALL cells exposed to sorafenib, salirasib, temsirolimus and vemurafenib. Data is presented as median +/- sd. *0.01<p<0.05; **0.001<p<0.01; ***p<0.001.

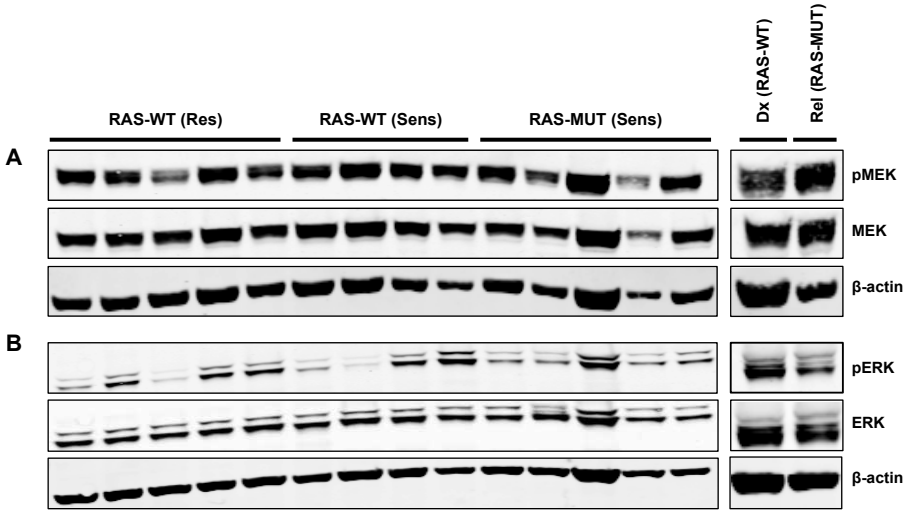

Supplemental Figure 2. (A) Western blots of MEK inhibitor resistant (Res) and sensitive (Sens) *RAS*-wildtype and *RAS*-mutant t(4;11)+ patient samples (left) and the matched diagnosis/relapse (Dx/Rel) samples (right) for phosphorylated MEK (upper), total MEK (middle) and β-actin (lower). **(B)** Western blots of t(4;11)+ patient samples for phosphorylated ERK (upper), total ERK (middle) and β-actin (lower).

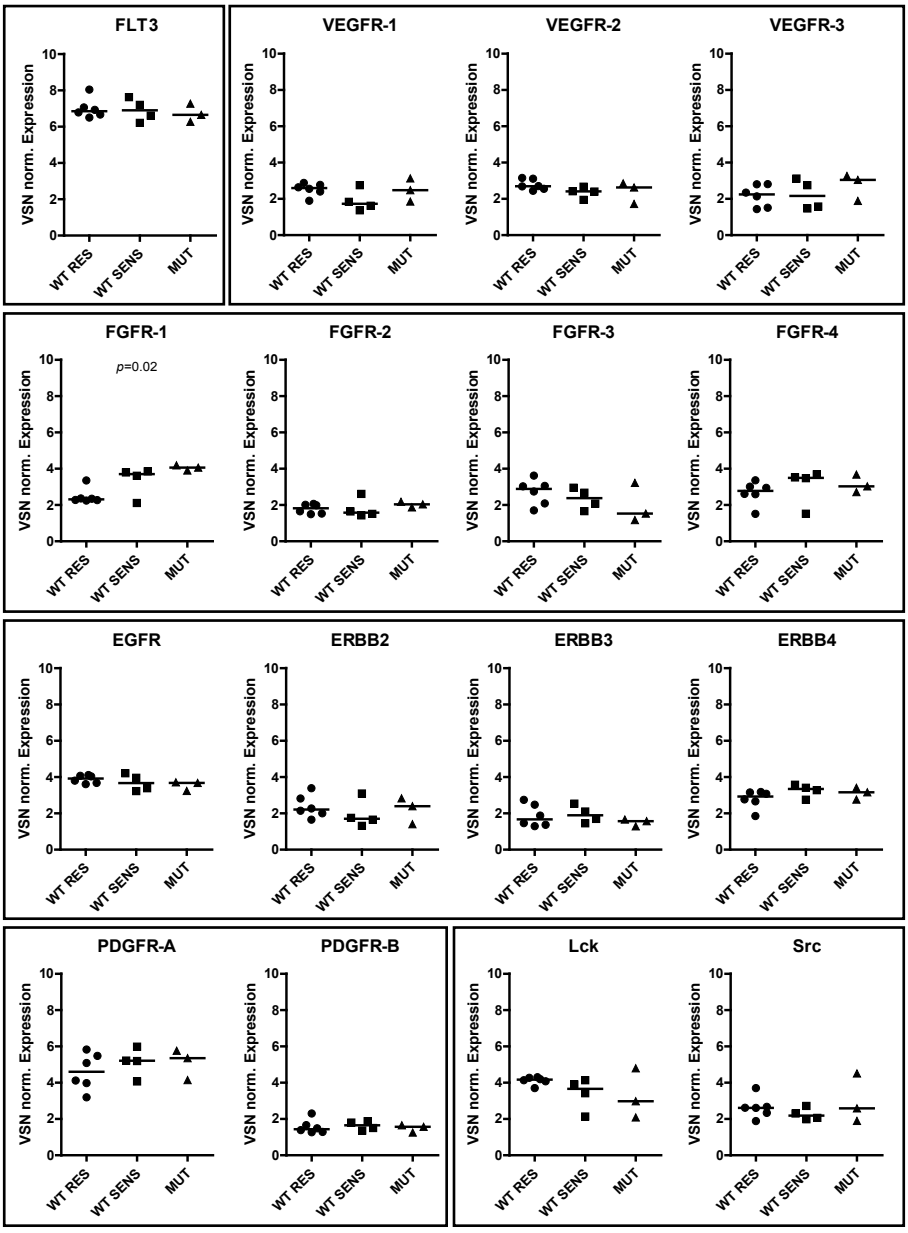

Supplemental Figure 3. Tyrosine kinase receptor mRNA expression (Affymetrix HU133plus2.0 microarray data) for FLT3, VEGFR-1, VEGFR-2, VEGFR-3, FGFR-1, FGFR-2, FGFR-3, FGFR-4, EGFR, ERBB2, ERBB3, ERBB4, PDGFR-A, PDGFR-B, Lck and Src in MEK inhibitor resistant *RAS*-wildtype (WT RES), MEK inhibitor sensitive *RAS*-wildtype (WT SENS) and *RAS*-mutant (MUT) primary samples.

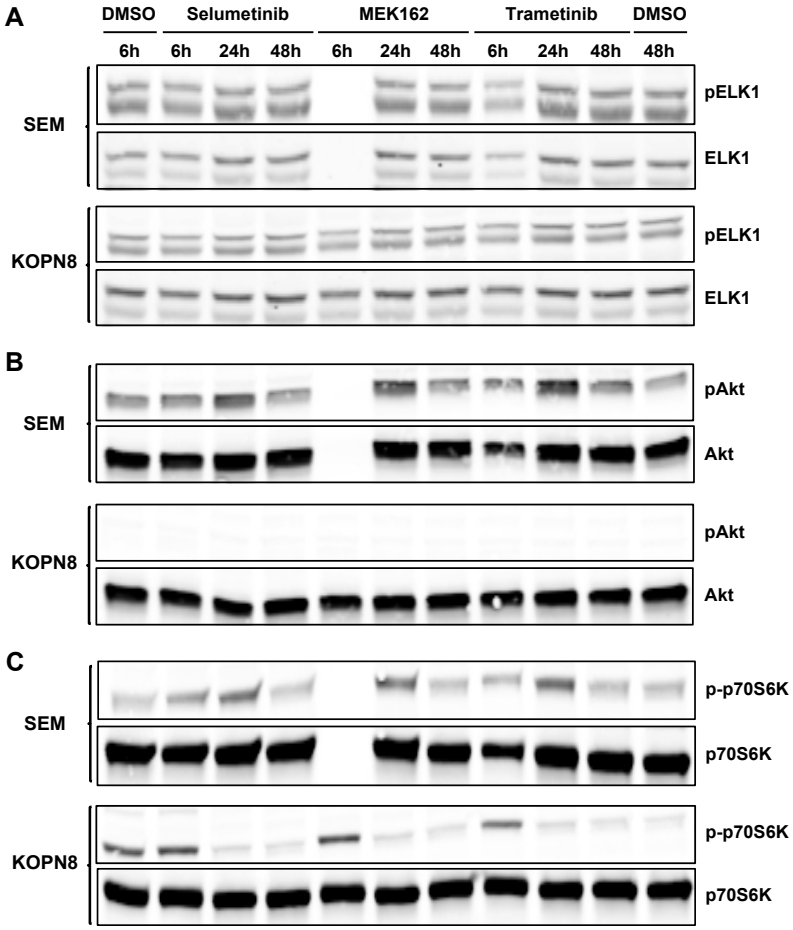

Supplemental Figure 4. (A) Western blots of SEM (two upper panels) and KOPN8 (two lower panels), exposed for 6, 24 and 48 hours to either vehicle (DMSO) or selumetinib, MEK162 or trametinib, detecting phosphorylated ELK-1 and total ELK-1. (**B)** Western blots of SEM and KOPN8, exposed to aforementioned MEK inhibitor conditions, for phosphorylated and total Akt. (**C)** Western blots of SEM and KOPN8, exposed to aforementioned MEK inhibitor conditions, for phosphorylated and total p70S6K.

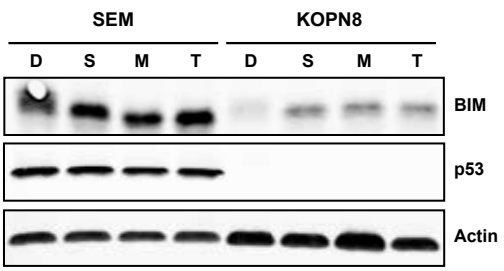

Supplemental Figure 5. Western blots of SEM and KOPN8 exposed for 48 hours to DMSO (D), selumetinib (S), MEK162 (M) or trametinib (T), for determination of BIM and p53 protein levels. Actin was used as loading control.

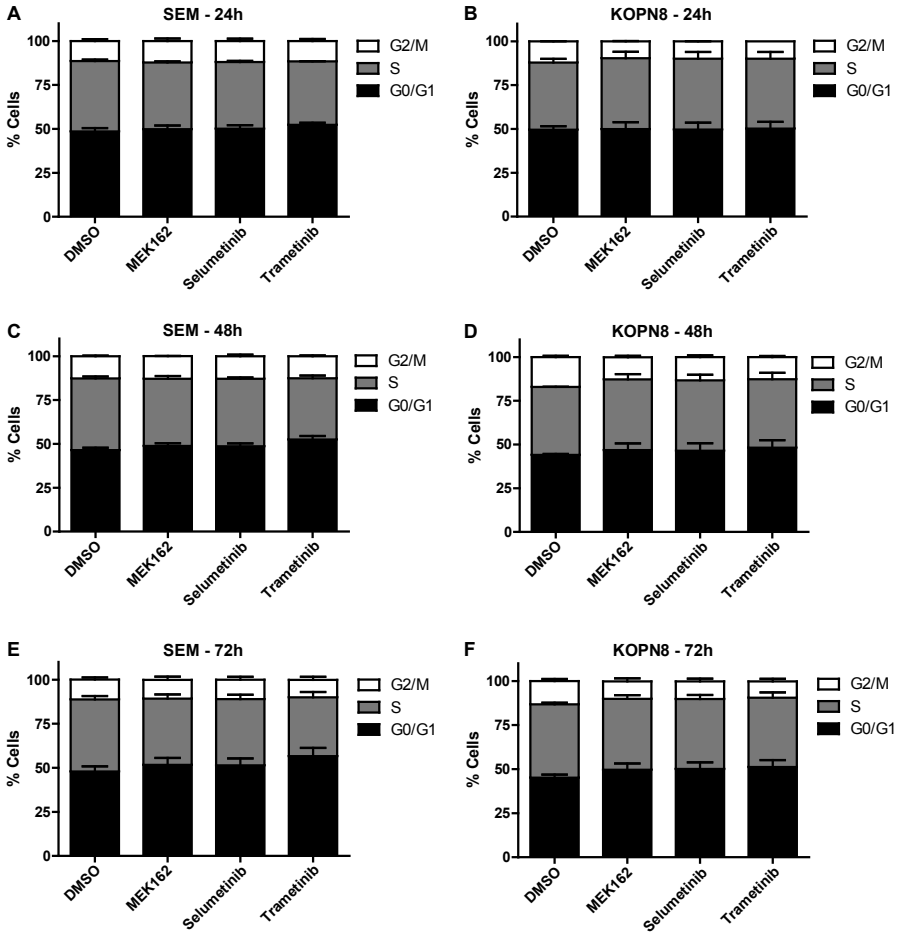

Supplemental Figure 6. Representative graphs of percentages SEM **(A,C,E)** or KOPN8 **(B,D,F)** cells in G2/M (white), S (grey) or G0/G1 (black) cell cycle stages, as analyzed by DNA staining. Cells were exposed to vehicle control (DMSO) or 500 nM MEK162, selumetinib or trametinib for 24, 48 or 72 hours (A and B, C and D, E and F, respectively).

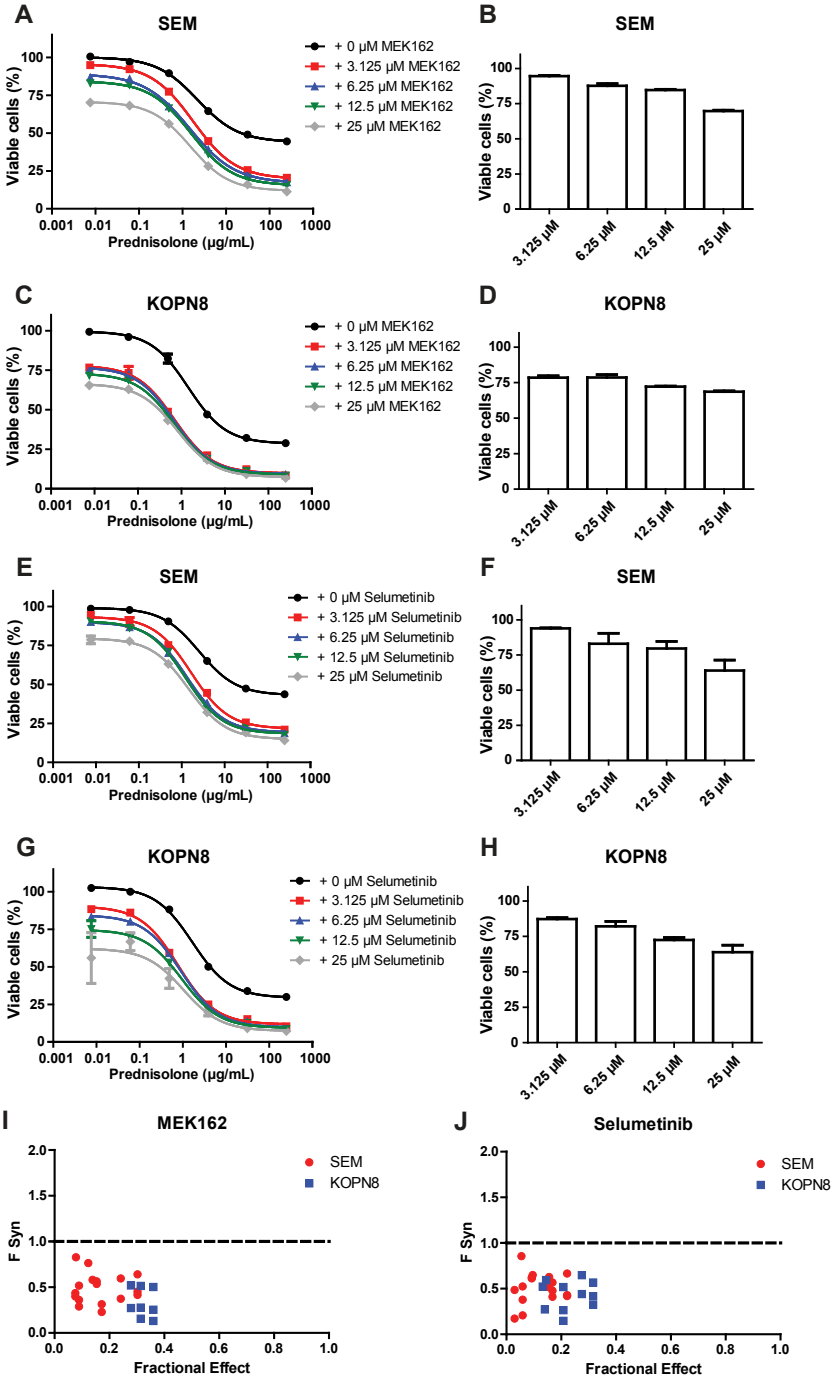
A
SEM
Viable cells (%)
Prednisolone (µg/mL)
+ 0 µM MEK162
+ 3.125 µM MEK162
+ 6.25 µM MEK162
+ 12.5 µM MEK162
+ 25 µM MEK162
B
SEM
Viable cells (%)
3.125 µM
6.25 µM
12.5 µM
25 µM
C
KOPN8
Viable cells (%)
Prednisolone (µg/mL)
+ 0 µM MEK162
+ 3.125 µM MEK162
+ 6.25 µM MEK162
+ 12.5 µM MEK162
+ 25 µM MEK162
D
KOPN8
Viable cells (%)
3.125 µM
6.25 µM
12.5 µM
25 µM
E
SEM
Viable cells (%)
Prednisolone (µg/mL)
+ 0 µM Selumetinib
+ 3.125 µM Selumetinib
+ 6.25 µM Selumetinib
+ 12.5 µM Selumetinib
+ 25 µM Selumetinib
F
SEM
Viable cells (%)
3.125 µM
6.25 µM
12.5 µM
25 µM
G
KOPN8
Viable cells (%)
Prednisolone (µg/mL)
+ 0 µM Selumetinib
+ 3.125 µM Selumetinib
+ 6.25 µM Selumetinib
+ 12.5 µM Selumetinib
+ 25 µM Selumetinib
H
KOPN8
Viable cells (%)
3.125 µM
6.25 µM
12.5 µM
25 µM
I
MEK162
F Syn
Fractional Effect
SEM
KOPN8
J
Selumetinib
F Syn
Fractional Effect
SEM
KOPN8

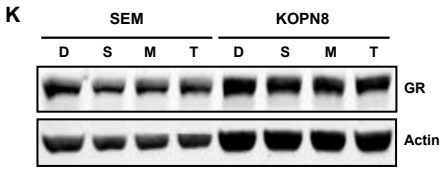

Supplemental Figure 7. (A) Dose-response curves of the SEM cell line exposed to prednisolone alone (black curve) or in combination with 3.125 μM, 6.25 μM, 12.5 μM or 25 μM MEK162 (red, blue, green and grey curves, respectively). Low concentrations of MEK162 sensitize cells towards prednisolone. **(B)** Response of SEM to the single MEK162 concentrations used in A. **(C)** Dose-response curves of KOPN8 treated with prednisolone (black curve), or in combination with the aforementioned MEK162 concentrations (shown in red, blue, green and grey, respectively). KOPN8 cells are also sensitized towards prednisolone by co-exposure with low concentrations of MEK162. **(D)** KOPN8 exposed to single MEK162 concentrations. **(E)** Dose-response curves of the SEM cell line exposed to either prednisolone alone (black), or in combination with selumetinib (at the same concentrations used for MEK162). Low concentrations of selumetinib can sensitize SEM cell towards prednisolone. **(F)** Effect of different single selumetinib concentrations in SEM. **(G)** Combined exposure to prednisolone and low selumetinib concentrations also sensitizes KOPN8 cells. **(H)** Response of KOPN8 towards single concentrations of selumetinib. **(I)** Combined exposure to prednisolone and MEK162 (n=3) was quantified using FSyn calculations (FSyn<1 indicates synergy) and plotted against fractional effect (i.e. inhibition of cell viability). In both SEM (red) and KOPN8 (blue), moderate to strong synergy was observed. **(J)** Combinatorial effect of prednisolone and selumetinib co-exposure (n=3) was quantified using FSyn calculations. Moderate to strong synergistic effects between prednisolone and selumetinib are observed for both SEM (red) and KOPN8 (blue). **(K)** Western blots of SEM and KOPN8 exposed for 48 hours to DMSO (D), selumetinib (S), MEK162 (M) or trametinib (T), detecting glucocorticoid receptor (GR) and loading control (Actin).

Chapter 4

Trametinib inhibits *RAS*-mutant *MLL*-rearranged acute lymphoblastic leukemia at specific niche sites and reduces ERK phosphorylation *in vivo*

Mark J.B. Kerstjens, Sandra Mimoso Pinhanços, Patricia Garrido Castro, Pauline Schneider, Priscilla Wander, Rob Pieters and Ronald W. Stam

Haematologica. 2018. Apr;103(4):e147-e150.

The majority (~80%) of infant ALL cases is characterized by chromosomal rearrangements involving the *Mixed Lineage Leukemia* (*MLL, or KMT2A*) gene, which confer a poor prognosis: event-free survival chances are at best 30-40%.[4] We and others showed (sub-clonal) *RAS* mutations occur in 14-36% of *MLL*-rearranged ALL cases, depending on *MLL*-translocation subtype.[20-22] *RAS* mutations diminish survival chances even further, with rapid occurrence of relapses and essentially no chance of survival.[21] Recently, we found that MEK inhibitors effectively killed *RAS*-mutant infant ALL cells *in vitro*, with trametinib being the most potent compound tested.[98] We therefore proposed that trametinib could be beneficial for *MLL*-rearranged infant ALL patients harboring additional *RAS* mutations. Here, we report preclinical evaluation of trametinib in a *RAS*-mutant *MLL*-rearranged infant ALL mouse xenograft model.

Since trametinib was previously investigated in mouse models for other malignancies and was accepted for treatment of *BRAF*-mutant melanoma,[99,100] we based our dosing regime on these studies, administering 5 mg/kg (low) or 30 mg/kg (high) trametinib 3 times per week through intraperitoneal injection in a toxicity assessment (n=3 mice per group). Within a week 2/3 mice in the 30 mg/kg trametinib group died, while the final mouse was humanely euthanized due to weight loss. The vehicle and 5 mg/kg trametinib doses were tolerable for up to 28 days, without signs of discomfort or weight loss (Sup.Fig.1A). One of the trametinib mice was smaller than its littermates, but there were no indications to exclude it from the study. Hematoxylin and eosin (H&E) staining of tissue slices revealed that high trametinib dosing induced kidney damage, which was absent in the vehicle and low trametinib groups (Sup.Fig.1B). Surprisingly, high dose trametinib also resulted in enhanced abundance of myeloid cells in the spleen (Sup.Fig.1C), which resembled splenic extramedullary hematopoiesis (EMH).[101] Moreover, we observed hematopoietic cell depletion in bone marrows of mice that received low trametinib doses, while this did not occur in the vehicle treated mice (Sup.Fig.1D). Although bone marrow tissue for high dose trametinib was unavailable, possibly high dose trametinib induces more severe bone marrow depletion, evoking splenic EMH.

To assess the efficacy of trametinib *in vivo*, we transplanted NSG mice with the *RAS*-mutant *MLL*-rearranged infant ALL cell line KOPN8 (10^6 cells; tail-vein injection), previously transduced with a luciferase-reporter (from here on referred to as KOPN8-SLIEW). After 1 week engraftment was assessed through intra-vital imaging. After randomization, vehicle or trametinib treatment (5 mg/kg, three times per week) commenced and leukemia progression was tracked by weekly intra-vital imaging. In both the vehicle and trametinib treated mice, systemic leukemia developed over a period of 2 weeks, although more severely in the vehicle mice, most evidently on day 14 (Fig.1A, left). Quantification of the intra-vital imaging revealed trametinib monotherapy delayed leukemia progression, but was insufficient to pre-

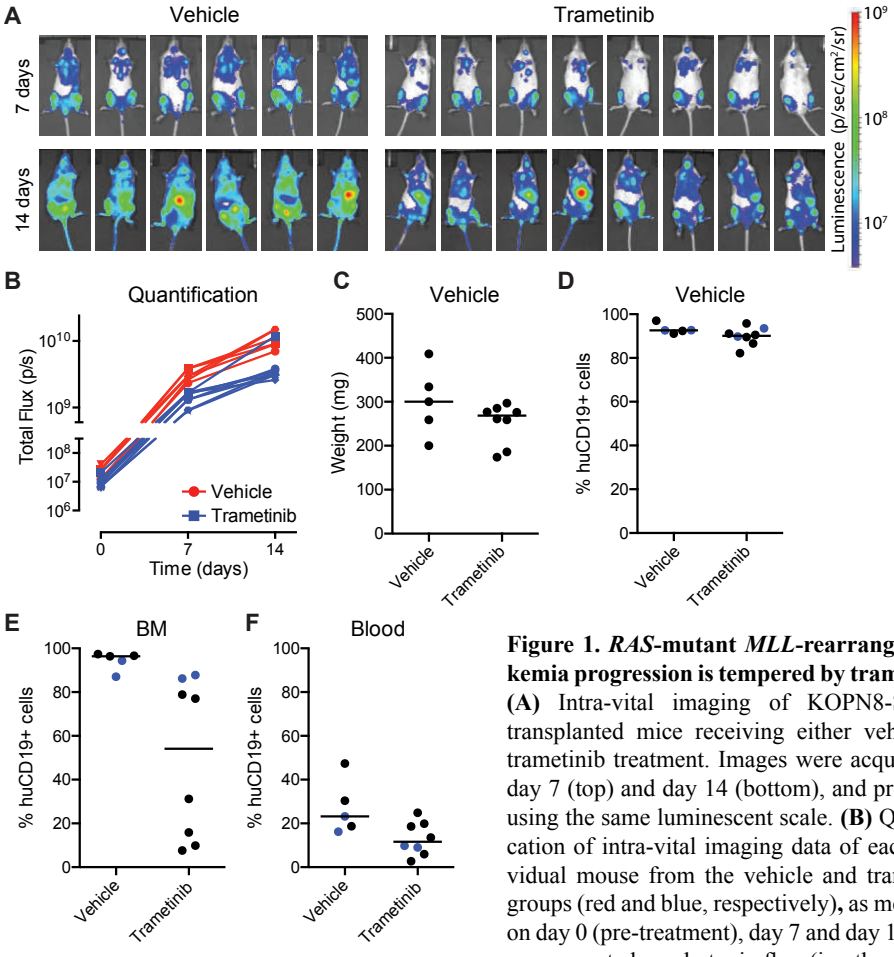

Figure 1. *RAS*-mutant *MLL*-rearranged leukemia progression is tempered by trametinib. **(A)** Intra-vital imaging of KOPN8-SLIEW transplanted mice receiving either vehicle or trametinib treatment. Images were acquired on day 7 (top) and day 14 (bottom), and presented using the same luminescent scale. **(B)** Quantification of intra-vital imaging data of each individual mouse from the vehicle and trametinib groups (red and blue, respectively), as measured on day 0 (pre-treatment), day 7 and day 14. Data are presented as photonic flux (i.e. the number of emitted photons per second). **(C)** Spleen weights of vehicle and trametinib mice. **(D,E,F)** Percentages of leukemic (huCD19+/msCd45-/Ter119-) cells detected in spleen, bone marrow and peripheral blood, respectively. The data from mice that received a trametinib bolus are indicated as blue dots.

vent leukemia outgrowth (Fig.1B). The modest effect of trametinib on leukemia progression led us to investigate whether its mechanism of action was achieved at all in our model. Therefore, 4 hours before sacrificing the mice (day 17), 2 mice from the vehicle group and 2 mice from the trametinib group were randomly selected to receive a bolus injection of trametinib (5 mg/kg) for analysis of ERK activation in tissue samples later on. Spleen, bone marrow and peripheral blood samples were extracted from all mice. As expected from the intra-vital imaging data, both treatment groups presented with splenomegaly, without a significant difference in spleen

weight (Fig.1C; Sup.Fig.2A). After processing the tissues, the presence of leukemic cells was analyzed using flow cytometry (example gating shown in Sup.Fig.2B).
The majority of cells derived from either vehicle or trametinib treated spleens represented human leukemia cells (Fig.1D). However, the leukemic load in bone marrow aspirates was reduced to 10-30% in 4 out of 8 trametinib treated mice, while the remaining mice presented with leukemic bone marrows similar to the vehicle treated group (80-95%) (Fig.1E). Additionally, we observed a reduction of leukemic cells in the peripheral blood of trametinib treated mice compared to vehicle (12% and 23%, respectively), although this difference was not statistically significant (Fig.1F). The mice that received a trametinib bolus-injection (blue dots) were comparable to the non-bolus mice. The bimodal effect observed in bone marrow aspirates did not correlate with gender, total or spleen weight, leukemic cells in the peripheral blood or age (Sup.Fig.2C).
To further investigate leukemic cell distribution in the bone marrows of trametinib and vehicle treated mice, we performed H&E staining on bone marrow tissue slices. Interestingly, in the vehicle bone marrows we observed severe leukemic cell infiltration, whereas the selected bone marrows of trametinib treated mice, with reduced leukemic load, actually showed hypocellularity (Fig.2A). Although these hypocellular bone marrows differ from healthy bone marrow, this is likely due to trametinib-induced leukemic cell death rather than toxicity, as the approval of trametinib for metastatic melanoma and recent clinical studies in other haematologic diseases suggest.[102]
Since *RAS* mutations in *MLL*-rearranged infant ALL have been implicated with enhanced central nervous system (CNS) infiltration,[103] we investigated fixated skull sections for presence of leukemic cells. Interestingly, trametinib substantially reduced leukemia infiltration into the leptomeningeal space in 2 out of 3 trametinib treated mice, whereas all vehicle mice presented with cell invasion (Fig.2B).
We electrophoretically resolved protein lysates of spleen and bone marrow samples and investigated ERK dephosphorylation as marker for trametinib efficacy. Interestingly, vehicle non-bolus spleen samples had evident ERK phosphorylation (pERK), while the vehicle mice that received a bolus presented with markedly lower pERK signal (Fig.2C). Moreover, trametinib inhibited ERK phosphorylation in all spleen isolates, both by successive trametinib injections (black bars), as well as a single bolus injection in vehicle group mice (white bars), as was confirmed by quantifying the relative pERK signal of these blots (Fig.2E). Additionally, the bone marrow samples of bolus and non-bolus mice (before purification by magnetic-activated cell sorting: MACS) contained comparable percentages of leukemic cells (Sup.Fig.3A). Interestingly, the vehicle bone marrow samples showed a similar ERK phosphorylation pattern as the spleen samples, with the trametinib bolus lowering the pERK level (Fig.2D), while in the trametinib group, the bolus injection was also accompanied

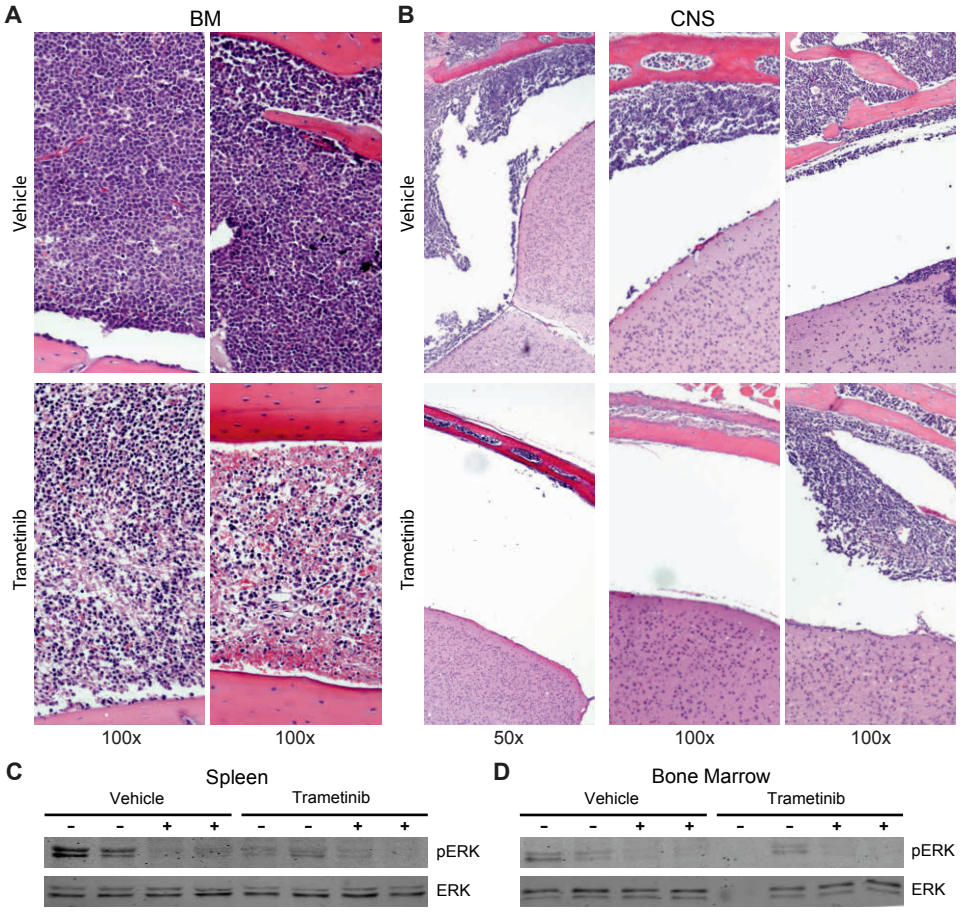

Figure 2. Trametinib impinges on niche distribution of *RAS*-mutant *MLL*-rearranged ALL cells and reduces ERK phosphorylation *in vivo*. (A) H&E stained bone marrow slides from 2 vehicle (top) and 2 trametinib (bottom) treated mice. **(B)** H&E stained slices from the skull of 3 vehicle (top) and 3 trametinib (bottom) treated mice. **(C)** pERK and total ERK levels were analyzed by western blot in MACS-enriched spleen isolates from vehicle or trametinib mice. Bolus trametinib injection samples are indicated by '+'. **(D)** pERK and total ERK levels determined by western blot of MACS-enriched bone marrow aspirates. Samples from mice that received a bolus trametinib injection are indicated by '+'. **(E,F)** The pERK/total ERK ratio as quantified from the western blots shown in C and D, respectively. Quantification data are presented as mean +/- sd.

by reduced ERK phosphorylation. Quantifying the blots revealed that in non-bolus bone marrows there was little difference between the vehicle and trametinib groups, though a bolus of trametinib effectively diminished ERK phosphorylation (Fig.2F). Hence, successive trametinib treatment did not result in maintained pERK reduction, as observed in the spleen, but bolus trametinib injections transiently decreased pERK levels in the bone marrow.

Although MEK inhibition previously proved effective in a *RAS*-mutant BCP-ALL xenograft model, trametinib could not substantially inhibit leukemia progression in our *MLL*-rearranged infant ALL model.[83] However, trametinib treatment did impinge on engraftment localization, specifically bone marrow and brain infiltration of *RAS*-mutant *MLL*-rearranged ALL cells. The difference in efficacy of MEK inhibition between *RAS*-mutant *MLL*-rearranged ALL and BCP-ALL might be explained by differences in cytogenetic subtype and associated outcome.

Interestingly, Prieto *et al.* showed that in mouse xenografts of human *MLL*-rearranged ALL cell line SEM, ectopic expression of $KRAS^{G12V}$ significantly promoted CNS infiltration, which together with our data suggests MEK inhibition might diminish CNS involvement.[103] Furthermore, MEK inhibitor selumetinib significantly reduced CNS infiltration in a pediatric *RAS*-mutant BCP-ALL xenograft model.[83]

Spleen-derived leukemic cells from the trametinib group showed sustained reduced pERK levels, whereas a bolus trametinib injection could also reduce pERK in the vehicle group. Furthermore, we observed bone marrow hypocellularity in 4 out of 8 mice after trametinib treatment, while ERK phosphorylation was reduced after a trametinib bolus in the mice with highly leukemic bone marrows. Possibly trametinib clearance reduces its effect or alternate signaling mechanisms restore pERK, and our dosing frequency is too low to induce sustained inhibition of ERK phosphorylation. Although more frequent dosing might improve efficacy, there is a risk for toxicity. However, other studies in patient-derived solid tumor xenografts have used daily oral dosing regimes (0.3 to 3 mg/kg), and while we chose intraperitoneal administration to better control trametinib levels, these protracted studies for some models resulted in better efficacy than we observed.

Survival chances for *MLL*-rearranged infant ALL patients carrying *RAS* mutations are close to zero.[21] Since trametinib reduces ERK phosphorylation, a key downstream effect of mutant RAS, this implies that trametinib treatment could revert the effect of *RAS* mutations in *MLL*-rearranged ALL, inducing a response to standard therapy that more resembles *RAS*-wildtype *MLL*-rearranged ALL. Moreover, glucocorticoid resistance remains a detrimental feature of *MLL*-rearranged infant ALL, and is associated with *RAS* mutations.[4,21,27,104] Previously, we and others have shown that MEK inhibitors trametinib, selumetinib and MEK162 could sensitize ALL to glucocorticoids.[95,98,105] This suggests that combination therapy of trametinib with glucocorticoids could be beneficial.

In conclusion, though trametinib monotherapy was unable to systemically inhibit *RAS*-mutant *MLL*-rearranged ALL *in vivo*, bone marrow leukemic burden was reduced in half of the mice, and trametinib effectively reduced ERK phosphorylation in leukemic cells from bone marrows and spleens. This illustrates the potential value of MEK inhibitors through reduction of CNS infiltration and possible potentiation of glucocorticoid sensitivity.

Acknowledgements
This work was supported through use of imaging equipment of the Applied Molecular Imaging Erasmus MC facility.

Supplemental Methods

In vivo xenografts

Animal experiments were performed in accordance with Dutch legislation and approved by the Erasmus MC Animal Ethical Committee, Rotterdam, The Netherlands (EMC3389). Immunodeficient NOD.Cg-*Prkdc*^{scid}*Il2rg*^{tm1Wjl}/SzJ (NSG) mice from in-house breeding received a tail-vein injection with the previously generated KOPN8-SLIEW luciferase reporter cell line (10^6 cells/mouse). After 1 week, mice underwent intra-vital bio-imaging (IVIS Spectrum Imaging System, Perkin Elmer) after injection of luciferin (RediJect D-Luciferin Bioluminescent Substrate, Perkin Elmer). Subsequently, mice were assigned to the respective treatment groups, and received vehicle (10% DMSO in PEG300; Sigma-Aldrich) or trametinib (5 mg/kg; MedChemExpress) intraperitoneally 3 times per week. Leukemia progression was monitored through weekly intra-vital imaging until the end of the study and acquired images were analyzed using Living Image software (Perkin Elmer), with equal exposure setting for all mice per time point.

At the end of the study, 2 vehicle and 2 trametinib mice received a bolus injection of trametininb (5 mg/kg) 4 hours prior to sacrifice. All mice were humanely euthanized through CO_2 asphyxiation and peripheral blood (PB) and tissues were harvested for further analyses. Leukemic burden in PB and infiltration into bone marrow (BM) and spleen were determined using a multicolor immunotyping flow cytometry approach. Hereto, blood was mixed with red blood cell (RBC) lysis buffer (155 mM NH_4Cl, 12 mM NH_4CO_3, 0.1 mM EDTA, pH 7.3-7.5). Bone marrows (tibia and femur) were flushed with PBS and resuspended to single cell suspension. Spleens were homogenized through a cell strainer (EASYstrainer, 70 µM, Greiner Bio-one), mixed with RBC lysis buffer and splenocytes were resuspended in PBS. Magnetic-activated cell sorting (MACS) was performed using anti-human CD19 magnetic particles (BD Biosystems). Example gating shown in Sup.Fig.3B-D.

Subsequent immunotyping flow cytometry was performed using 7-AAD, human CD19-APC, human CD45-PE, mouse Cd45-PE-Cy7 and mouse Ter119-PE-Cy7 (all BD Biosystems). Samples were measured on a MACSQuant flow cytometer (Miltenyi) and analyzed using FlowJo software.

Tissues were fixated in 4% formaldehyde and embedded in paraffin. Tissue slides were stained with hematoxylin and eosin (H&E). Images were acquired with a Leica digital microscope.

Western blot

Cell lysates were electrophoretically resolved on pre-cast SDS-polyacrylamide gels (AnyKD, TGX, Bio-Rad, Veenendaal, The Netherlands) and transferred to nitrocellulose membranes using the Transblot Turbo Transfer System (BioRad, Veenendaal,

The Netherlands). Membranes were blocked with 5% bovine serum albumin in TBS and probed with pERK or total ERK antibodies (Cell Signalling Technologies), followed by fluorophore-conjugated secondary antibodies. Blot mages were acquired and quantified using the Odyssey imaging system (LI-COR, Leusden, The Netherlands).

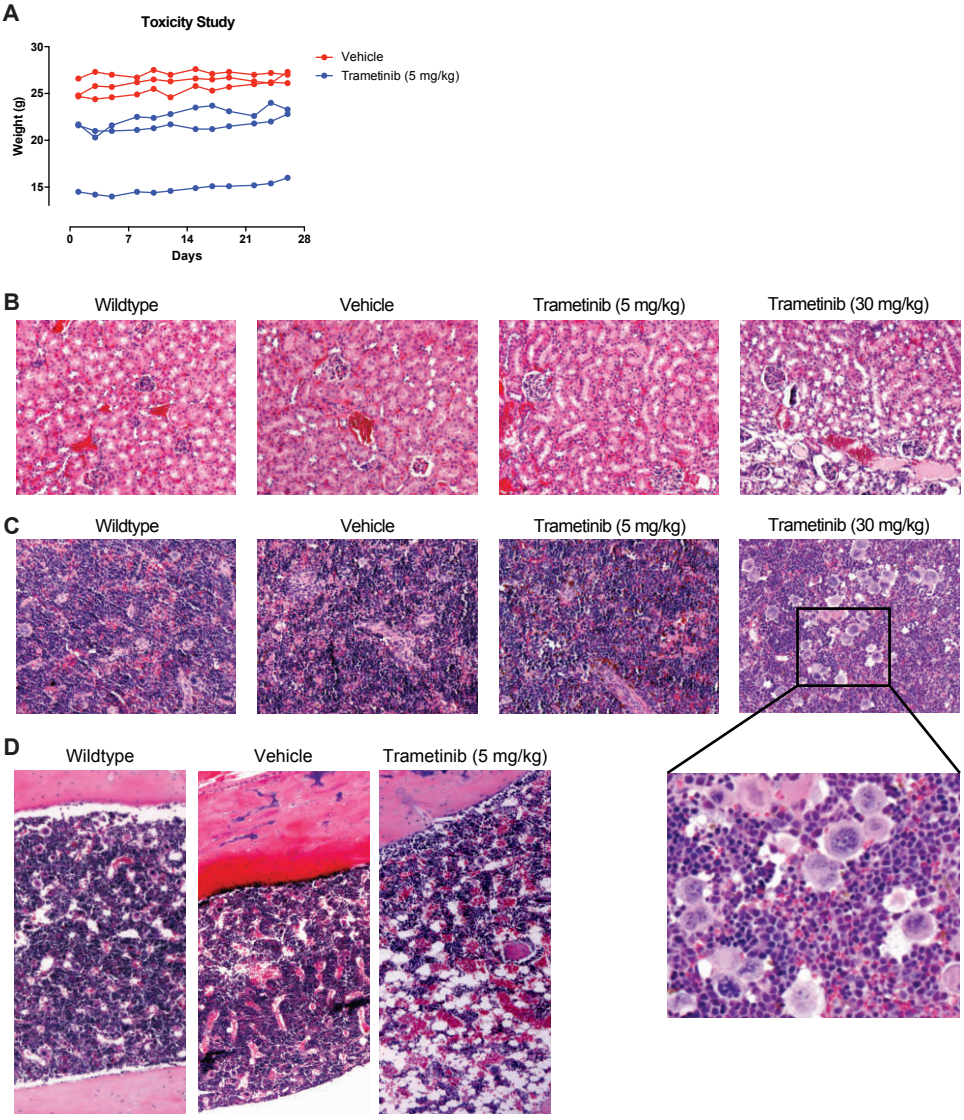

Supplemental Figure 1. (A) Progressive weight measurements of NSG mice injected with vehicle (n=3; red) or 5 mg/kg trametinib (n=3; blue). **(B)** Representative H&E stained kidney sections from wildtype mice and vehicle, 5 mg/kg trametinib or 30 mg/kg trametinib exposed mice (from left to right, respectively). **(C)** Representative H&E stained spleen sections from wildtype mice and vehicle, 5 mg/kg trametinib or 30 mg/kg trametinib exposed mice (from left to right, respectively). Part of the 30 mg/kg trametinib section has been enlarged for more detail. **(D)** Representative H&E stained bone marrow slides from wildtype (left), vehicle (center) and 5 mg/kg trametinib (right) treated mice.

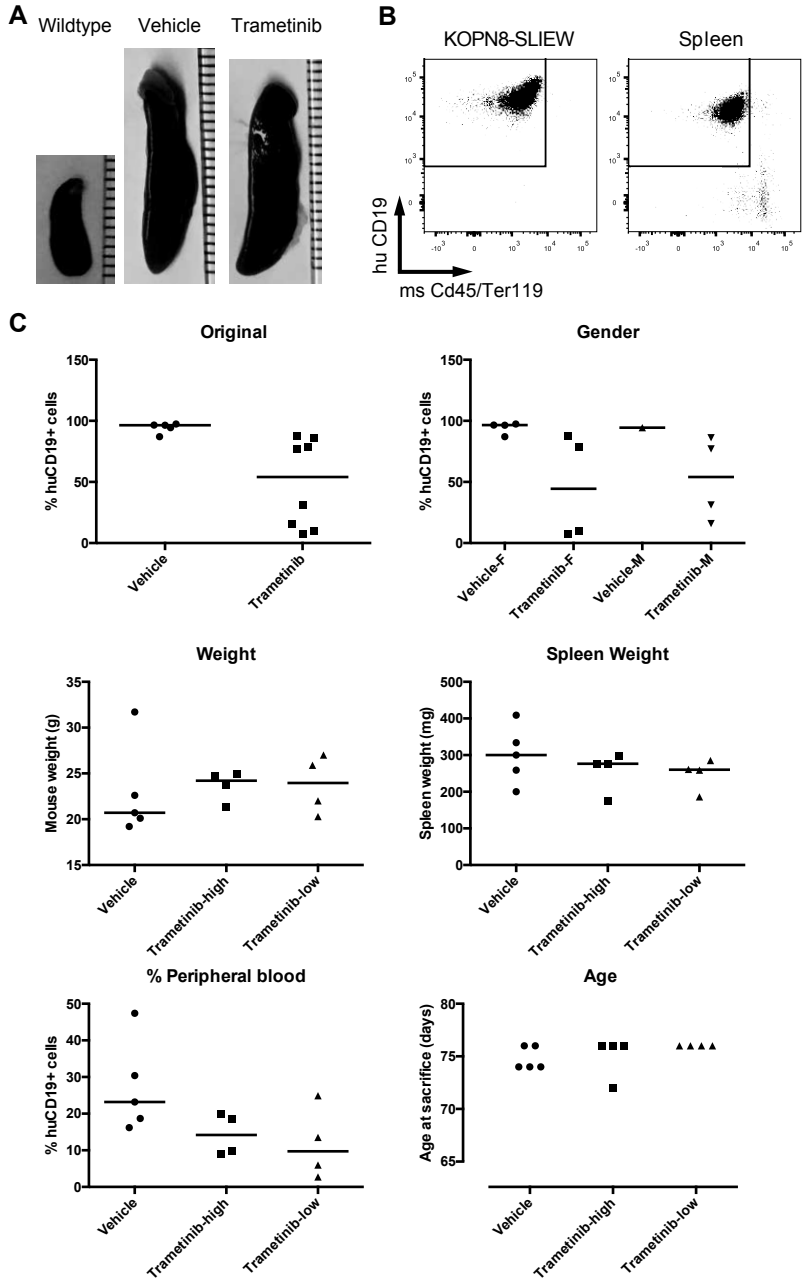

Supplemental Figure 2. (A) Pictures of spleens from wildtype (left), vehicle (center) and trametinib (right) group mice. **(B)** Exemplary gating strategy for determining the percentage human CD19-positive, mouse Cd45/Ter119-negative cells. Shown are FACS plots of pure KOPN8-SLIEW (left) and a

homogenized spleen sample from a mouse xenograft (right). **(C)** Graphs showing the percentage of leukemic cells in bone marrow aspirates from vehicle and trametinib treated mice as presented in Fig.1C (Original), as well as the same data subdivided for gender, or subdivisions of vehicle, and high and low leukemic bone marrows from the trametinib group for total weight, spleen weight, percentage leukemic cells in peripheral blood and age.

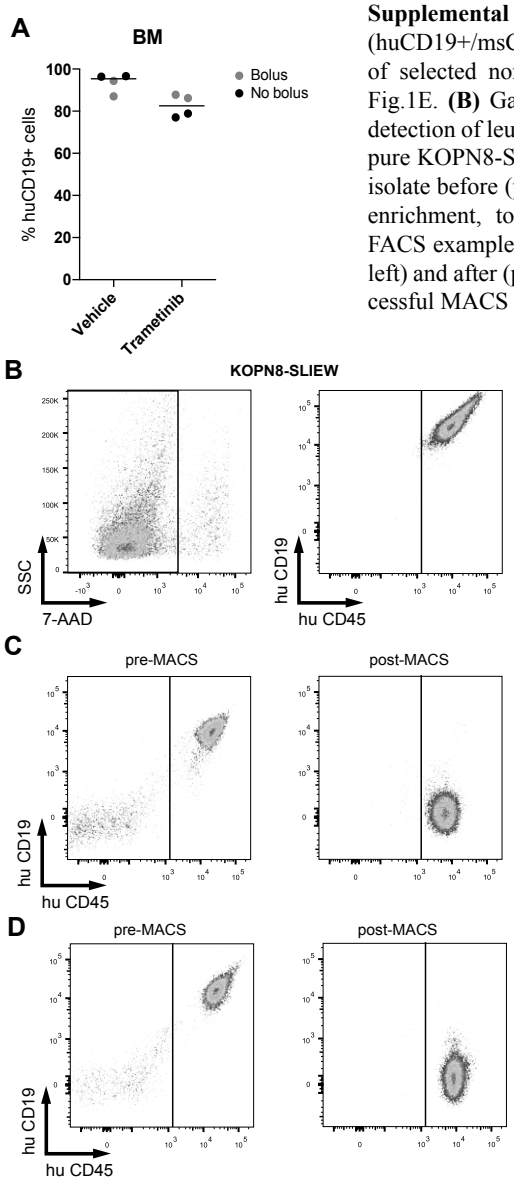

Supplemental Figure 3. (A) Percentages of leukemic (huCD19+/msCd45-/Ter119-) cells in bone marrow aspirates of selected non-bolus (black) and bolus (gray) mice from Fig.1E. **(B)** Gating strategy for post-MACS flow-cytometry detection of leukemic cells in isolated mouse tissues, based on pure KOPN8-SLIEW sample. **(C)** FACS example of a spleen isolate before (pre-MACS; left) and after (post-MACS; right) enrichment, to confirm successful MACS procedure. **(D)** FACS example of a bone marrow isolate before (pre-MACS; left) and after (post-MACS; right) enrichment, to confirm successful MACS procedure.

Chapter 5

S-Adenosylhomocysteine hydrolase inhibitor DZNep inhibits *MLL*-rearranged acute lymphoblastic leukemia *in vitro* and splenic engraftment *in vivo*

Mark J.B. Kerstjens, Sandra Mimoso Pinhanços, Patricia Garrido Castro, Pauline Schneider, Bertrand D. van Zelst, Priscilla Wander, Merel Willekes, Sandra G. Heil, Rob Pieters and Ronald W. Stam

Submitted.

Abstract

Acute Lymphoblastic Leukemia (ALL) in infants (< 1 year of age) is an aggressive hematologic malignancy. Chromosomal rearrangements involving the *Mixed Lineage Leukemia* (*MLL*, or *KMT2A*) gene characterize ~80% of the cases, and specifically this group has a poor prognosis. The aberrant epigenetic landscape associated with this disease has been the focus of drug discovery efforts, resulting in identification of different inhibitors awaiting further (pre)clinical evaluation. In this study, we employed an epigenetic drug screening approach to identify novel candidates to potentiate the treatment of *MLL*-rearranged infant ALL. We found S-Adenosylhomocysteine hydrolase (SAHH) inhibitors neplanocin and 3-deazaneplanocin (DZNep) inhibited leukemia cells *in vitro*, with *MLL*-rearranged ALL cell lines amongst the most sensitive. We confirmed DZNep strongly deregulates the balance between methyl donor S-Adenosylmethionine (SAM) and its demethylated product S-Adenosylhomocysteine (SAH), with particularly *MLL*-rearranged ALL cells showing SAM depletion, while slightly reducing histone methylation and EZH2 protein levels, but not *FHIT* promoter methylation. In an *MLL*-rearranged ALL xenograft model, DZNep reduced leukemia in the spleen, but was insufficient to prevent leukemia outgrowth. In summary, our data show DZNep monotherapy is insufficient to inhibit *MLL*-rearranged ALL *in vivo*, but the *in vitro* efficacy suggests further investigation in combination therapy could be valuable.

Introduction

Acute Lymphoblastic Leukemia (ALL) in infants (children < 1 year of age) is an aggressive hematologic malignancy. Approximately 80% of the cases carry chromosomal rearrangements involving the *Mixed Lineage Leukemia* (*MLL*, or *KMT2A*) gene, which are associated with a poor prognosis. The 5-year event-free survival (EFS) for *MLL*-rearranged infant ALL patients is only 30-40%, whereas for infant ALL patients carrying wildtype *MLL* genes the EFS is at least 75%.[4,6,8] The poor clinical outcome for *MLL*-rearranged infant ALL patients is associated with chemotherapy resistance, illustrating the necessity to develop novel therapeutic strategies.[27,104] The wildtype MLL protein functions as a methyl transferase of histone H3 at lysine 4 (K4), thereby initiating the formation of transcriptional elongation complexes.[9,10] *MLL* rearrangements give rise to chimeric MLL fusion proteins that have lost intrinsic H3K4 trimethylating capacity, but instead recruit the DOT1L methyltransferase, which is responsible for inducing active transcription through dimethylation of H3 on lysine 79.[13-15] This defective epigenetic regulation causes aberrant gene expression that is highly characteristic for *MLL*-rearranged infant ALL, and also discriminates it from *MLL* germline infant ALL and B-cell precursor (BCP) ALL in older children.[17] Interestingly, besides distorted histone methylation, *MLL*-rearranged infant ALL has been associated with increased DNA methylation of specific promoter regions, leading to suppression of genes, including tumor suppressor genes such as the *fragile histidine triad* (*FHIT*).[16,106] Evidently, targeting the epigenetic machinery represents a promising strategy against *MLL*-rearranged infant ALL. We and others have employed different drug discovery approaches, leading to the identification of DOT1L inhibitors (e.g. EPZ004777), demethylating agents (e.g. azacitidines), histone deacetylase (HDAC) inhibitors (e.g. panobinostat) and Bromodomain and extraterminal domain (BET) inhibitors (e.g. I-BET).[16,32-34,37,38] Clearly, there is potential for epigenetic drugs targeting *MLL*-rearranged ALL, which led us to explore the potential of additional epigenetic-based drugs for the treatment of this type of leukemia.

In the present study, we screened two epigenetic-based drug libraries for candidates effective against *MLL*-rearranged ALL cells. Through this drug screen we discovered S-adenosylhomocysteine hydrolase (SAHH) inhibitor neplanocin, and its derivative 3-deazaneplanocin (DZNep), as potential candidates, and proceeded our investigation focusing on DZNep, which has shown promising results in other malignancies. Although DZNep effectively inhibited *MLL*-rearranged ALL cell lines, as well as primary *MLL*-rearranged infant ALL patient samples *in vitro*, it was unable to block systemic leukemia in xenograft mouse models of human *MLL*-rearranged ALL, despite the impairment of leukemic infiltration in the spleen.

Materials & Methods

(Primary) cell culture

Cell lines were cultured in RPMI-1640 with GlutaMAX (Invitrogen Life Technologies, Waltham, MA, USA), 10% Fetal Calf Serum, 100 IU/mL penicillin, 100 IU/mL streptomycin and 0.125 μg/mL amphotericin B (Invitrogen Life Technologies) at 37°C under 5% CO_2 atmosphere. Cell line integrity was regularly checked by DNA fingerprinting.

Primary untreated samples from *MLL*-rearranged infant ALL patients were obtained at the Sophia Children's Hospital (Rotterdam, the Netherlands) as part of the INTERFANT protocol. The Erasmus MC Institutional Review Board approved these studies, and informed consent was obtained accordingly (Declaration of Helsinki). Processing of the samples occurred as described previously.[23] May-Grünwald-Giemsa counterstained cytospins confirmed leukemic blast percentage was >90%.

Flow cytometry

All samples were measured and analyzed using a MACSQuant flow cytometer (Miltenyi) and FlowJo software, respectively. The PE Annexin-V Apoptosis Detection Kit I (BD Pharmingen) was used according to manufacturer's protocol. Xenografted material was immunotyped using 7-AAD, human CD19-APC, human CD45-PE, mouse Cd45-PE-Cy7 and mouse Ter119-PE-Cy7 (all BD Biosystems).

Western blot

Protein samples were resolved on SDS-polyacrylamide gels (TGX, Bio-Rad, Veenendaal, The Netherlands) and transferred to nitrocellulose membranes using the Transblot Turbo Transfer System (BioRad, Veenendaal, The Netherlands). Membranes were probed with primary antibodies against PARP, Ubiquityl-H2B (K120), H2B, RNF20, RNF40 (Cell Signalling Technologies), H3K4, H3Ac, H3K9Ac (Acitve Motif), WAC (EMD Milipore) or H3 (Abcam) in 5% bovine serum albumin or skim milk in TBS. Blots were then probed with fluorophore-conjugated secondary antibodies and imaged using the Odyssey imaging system (LI-COR, Leusden, The Netherlands).

PCR

RNA was isolated using the QIAGEN RNeasy Mini Kit (QIAGEN), according to manufacturer's protocol. Reverse transcription was performed with MMLV RT (Promega) and the cDNA was used for quantitative reverse transcription PCR (qRT-PCR) using Sybr Green (Thermo Scientific) on an ABI Prism 7900 (Life Technologies, Bleiswijk, The Netherlands). Results were analysed using SDS 2.3 Software (Life Technologies, Bleiswijk, The Netherlands) and the dCT-method. Forward and

reverse primer sequences are: 5'-CACGCTTGACACTCACACT-3' and 5'-CAGGGTCTGGTGTTTTGTA-3' (HOXA9), 5'-GTCGGAGTCAACGGATT-3' and 5'-AAGCTTCCCGTTCTCAG-3' (GAPDH).
DNA isolation was performed with the DNeasy Blood & Tissue kit (QIAGEN), followed by bisulfite conversion with the EZ DNA methylation-Lightning kit (Zymo Research). Methylation-specific PCR for the FHIT promoter was performed as previously described[106], and product formation was analyzed on agarose gels.

Liquid chromatography-tandem mass spectrometry

Cell pellets were snap-frozen in liquid nitrogen and stored at -80°C until use. After thawing on ice and subsequent solid phase extraction (SPE), SAM and SAH levels were determined using liquid chromatography-tandem mass spectrometry (LC-MS/MS) according to Gellekink *et al*.[17] Hereto, 10 µl sample was injected onto an Atlantis C-18 column (Waters) and eluted in a gradient of methanol in aqueous acetic acid (0.1%). A SAM and SAH calibration curve was used for quantifying the samples.

Animal experiments

Animal experiments were performed according to Dutch legislation and approved by the Erasmus MC Animal Ethical Committee, Rotterdam, The Netherlands (EMC3389). Immunodeficient NOD.Cg-*Prkdc*^{scid}*Il2rg*^{tm1Wjl}/SzJ (NSG) mice were xenografted with the SEM-SLIEW luciferase reporter cell line (10^6 cells) through tail-vein injection. The SLIEW luciferase construct was a kind gift from Prof. Dr. Olaf Heidenreich from the Northern Institute for Cancer Research, Newcastle, UK. Intra-vital bio-imaging (IVIS Spectrum Imaging System, Perkin Elmer) after injection of luciferin (RediJect D-Luciferin Bioluminescent Substrate, Perkin Elmer) was used to track leukemia progression. Acquired images were analyzed using Living Image software (Perkin Elmer), with equal exposure setting for all mice per time point. The respective treatment groups received vehicle (10% DMSO in PEG300; Sigma-Aldrich) or DZNep (5 mg/kg; MedChemExpress) intraperitoneally 3 times per week. At the end of the study, all mice were humanely euthanized through CO_2 asphyxiation and relevant tissues (i.e. peripheral blood, bone marrow, spleen) were harvested for further analyses. Tissue slides were acquired through fixation (4% formaldehyde), paraffin embedding and subsequent staining with hematoxylin and eosin (H&E). Images were acquired with a Leica digital microscope.

Results

HC toxin, neplanocin and 3-deazaneplanocin inhibit *MLL*-rearranged ALL cell lines *in vitro*

We performed drug library screens using the Screenwell Epigenetics Library (43 compounds, ENZO Life Sciences) and Epigenetics Screening Library (59 compounds, Cayman Chemical), which when combined consist of 84 unique epigenetic compounds, for anti-leukemic activity against *MLL*-rearranged ALL cell lines SEM and RS4;11. For this, we adopted 4-day MTS-assays using drug concentrations of 1 μM and 100 nM. Interestingly, at the 1 μM concentration, several drugs affected cell viability in both SEM and RS4;11 by >75% (Fig.1A). The lower concentration of 100 nM, only identified 3 drugs that effectively inhibited the *MLL*-rearranged cell lines to this magnitude, including HC toxin, neplanocin and 3-deazaneplanocin (DZNep) (Fig.1B).

HC toxin is an HDAC inhibitor, whereas neplanocin and its derivative DZNep have been developed as S-adenosylhomocysteine hydrolase (SAHH) inhibitors. Since HDAC inhibitors were previously identified as effective drugs against *MLL*-rearranged ALL cells, and the HDAC inhibitor HC toxin was identified as a potential hit, we investigated the response of SEM and RS4;11 to all HDAC inhibitors present in the drug libraries. While we found all HDAC inhibitors, including the previously tested trichostatin A (TSA) and vorinostat (SAHA)[34], effectively inhibited the cell lines at 1 μM concentration (Fig.1C), HC toxin was the most potent HDAC inhibitor, inducing cell death in nearly 100% of the leukemic cells at 100 nM concentration (Fig.1D).

We previously found another HDAC inhibitor, i.e. Panobinostat (or LBH589) to be highly effective against *MLL*-rearranged ALL.[34,35] Since panobinostat was not present in the here used drug libraries, we compared the effects of HC toxin and panobinostat in full dose-response curves and found both compounds inhibited the *MLL*-rearranged ALL cell lines with comparable IC_{50} values (Sup.Fig.1A and B). As HC toxin, although highly effective, did not demonstrate superior effects over panobinostat, we decided to further focus on the identified SAHH inhibitors, especially since little is known about SAHH inhibition in the context of *MLL*-rearranged ALL. Like HC toxin, the SAHH inhibitors neplanocin and DZNep effectively reduced *MLL*-rearranged ALL cell viability at 100 nM concentrations (Fig.1E).

DZNep inhibits *MLL*-rearranged infant ALL cells by inducing apoptosis

To validate the results from our drug library screens, we exposed the *MLL*-rearranged ALL cell lines SEM, RS4;11, KOPN8 and BEL-1, the AML cell lines MV4;11 (also *MLL*-rearranged) and Kasumi-1, and the BCP-ALL cell lines REH, 697 and Sup-B15 to varying concentrations of neplanocin and DZNep, and assessed cell viability after

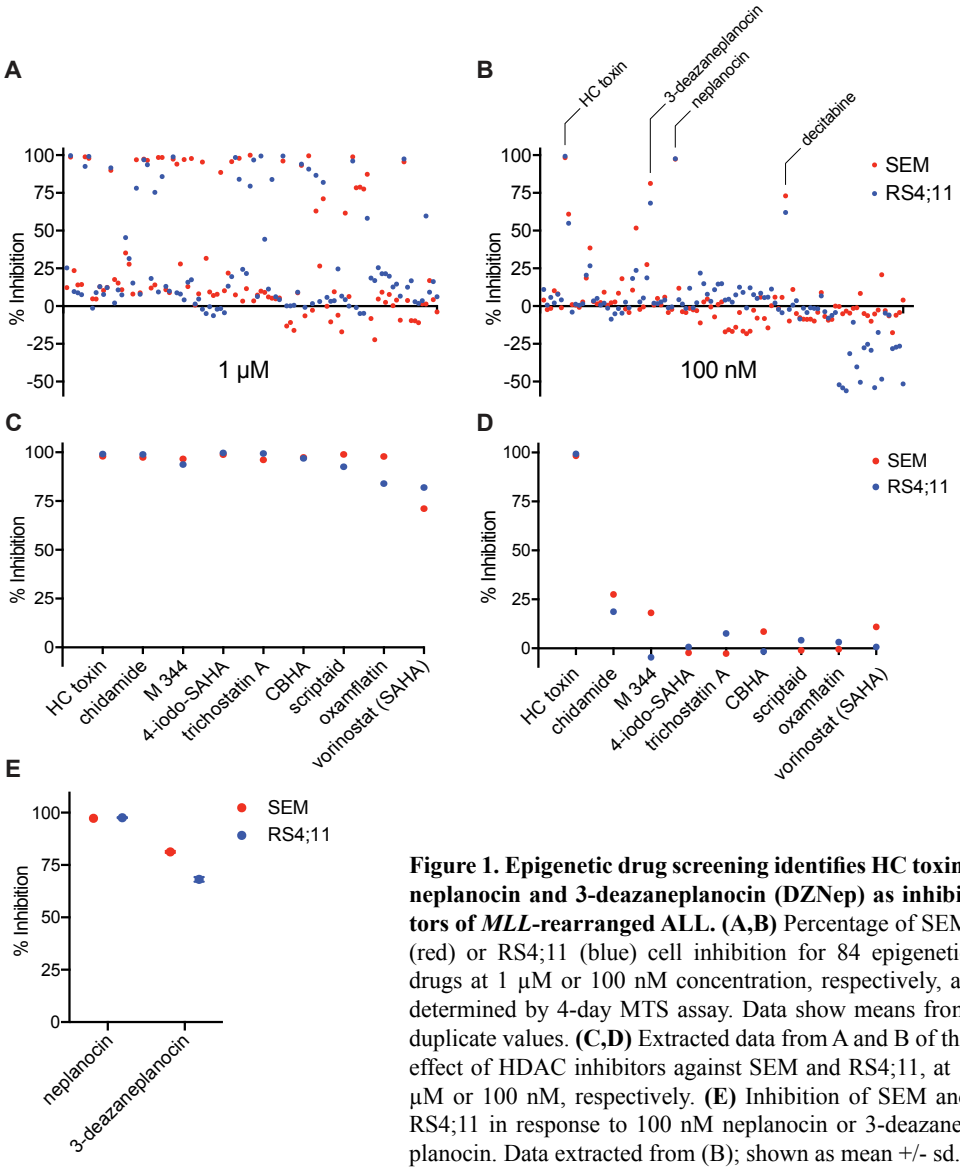

Figure 1. Epigenetic drug screening identifies HC toxin, neplanocin and 3-deazaneplanocin (DZNep) as inhibitors of *MLL*-rearranged ALL. (A,B) Percentage of SEM (red) or RS4;11 (blue) cell inhibition for 84 epigenetic drugs at 1 µM or 100 nM concentration, respectively, as determined by 4-day MTS assay. Data show means from duplicate values. **(C,D)** Extracted data from A and B of the effect of HDAC inhibitors against SEM and RS4;11, at 1 µM or 100 nM, respectively. **(E)** Inhibition of SEM and RS4;11 in response to 100 nM neplanocin or 3-deazaneplanocin. Data extracted from (B); shown as mean +/- sd.

4 days of exposure. Interestingly, neplanocin most potently inhibited the *MLL*-rearranged ALL cell lines SEM and RS4;11 at low nanomolar concentrations, while also effectively inhibiting most of the other leukemic cell lines at slightly higher concentrations (Fig.2A). DZNep also effectively inhibited the leukemic cell lines tested, with the SEM cell line being the most sensitive (Fig.2B).

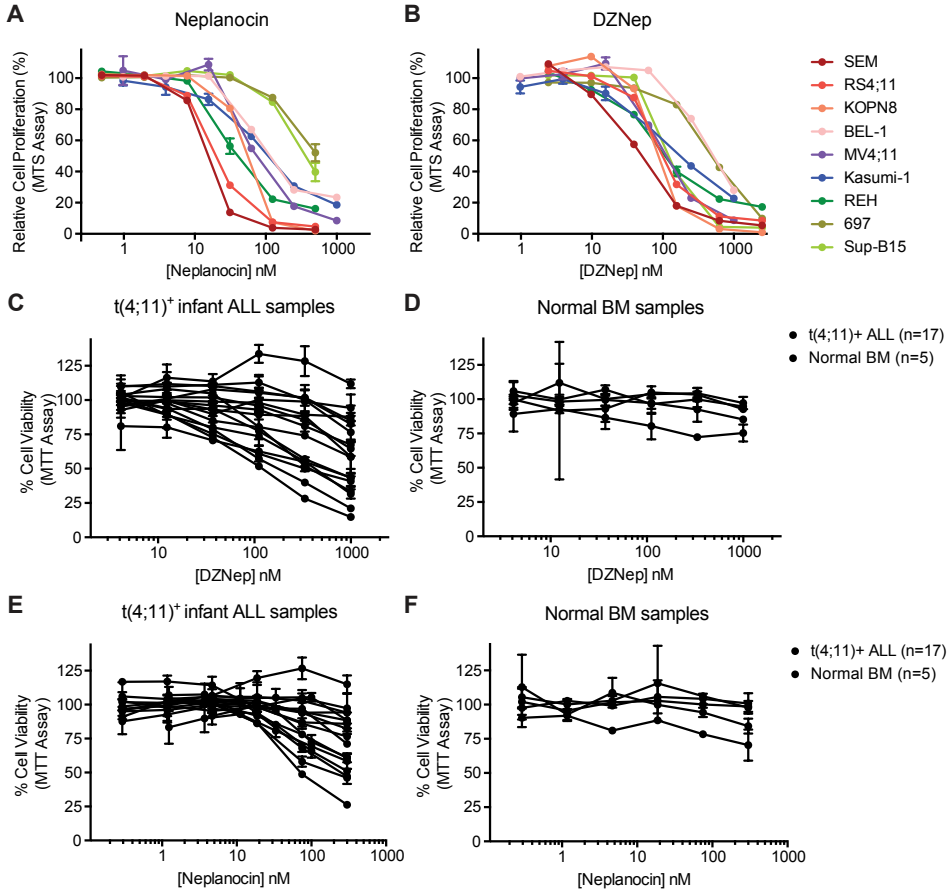

Next, we exposed primary *MLL*-rearranged infant ALL samples (n=17), as well as normal (non-leukemic) bone marrow aspirates (n=5), to DZNep and neplanocin and assessed cell viability after 4 days of exposure. Interestingly, although the efficacy of DZNep on some of the patient-derived *MLL*-rearranged infant ALL samples was comparable to that of the cell lines, the IC_{50} values were higher in most of the patient samples (Fig.2C). Still, the healthy bone marrow derived cells remained unaffected by DZNep up to 1 μM concentration (Fig.2D). Additionally, exposing the primary samples to neplanocin yielded a similar response among *MLL*-rearranged infant ALL samples and no response in the healthy bone marrow samples (Fig.2E and F, respectively). Although the IC_{50} values for neplanocin were slightly lower than for DZNep, the recent promising results for DZNep in *in vivo* models of other malignancies led us to investigate DZNep further as lead candidate.[107-109]

To better understand DZNep's anti-leukemic effects, we further investigated the

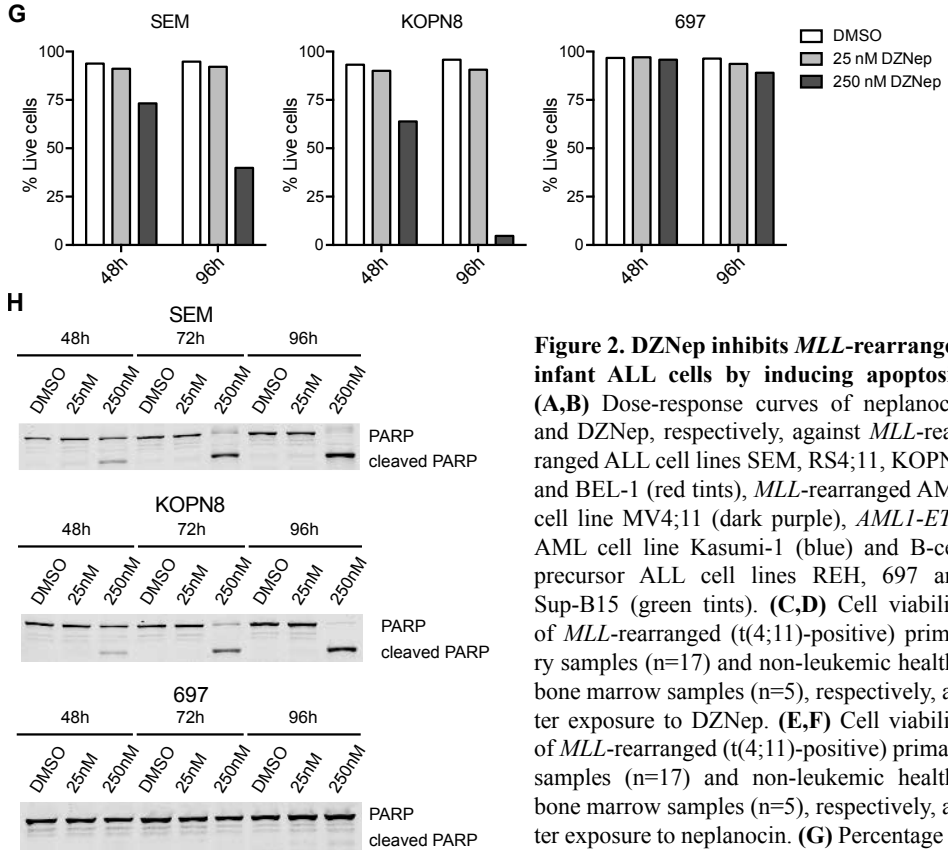

Figure 2. DZNep inhibits *MLL*-rearranged infant ALL cells by inducing apoptosis. (A,B) Dose-response curves of neplanocin and DZNep, respectively, against *MLL*-rearranged ALL cell lines SEM, RS4;11, KOPN8 and BEL-1 (red tints), *MLL*-rearranged AML cell line MV4;11 (dark purple), *AML1-ETO* AML cell line Kasumi-1 (blue) and B-cell precursor ALL cell lines REH, 697 and Sup-B15 (green tints). **(C,D)** Cell viability of *MLL*-rearranged (t(4;11)-positive) primary samples (n=17) and non-leukemic healthy bone marrow samples (n=5), respectively, after exposure to DZNep. **(E,F)** Cell viability of *MLL*-rearranged (t(4;11)-positive) primary samples (n=17) and non-leukemic healthy bone marrow samples (n=5), respectively, after exposure to neplanocin. **(G)** Percentage of live SEM, KOPN8 or 697 cells (left, center and right, respectively), as determined by Annexin-V/7-AAD staining, after 48 or 96 hours exposure to vehicle (white), 25 nM DZNep (light grey) or 250 nM DZNep (dark grey). **(H)** Immunoblots showing full length PARP and PARP cleavage after exposure to DZNep in SEM, KOPN8 and 697 cell lines (top, center and bottom, respectively).

mechanism of leukemic cell inhibition. Hereto, we exposed SEM, KOPN8 and 697 cells to vehicle (DMSO), 25 nM or 250 nM DZNep and used flow cytometry to assess the fraction of live (non-apoptotic cells) by AnnexinV staining and 7-AAD exclusion after 48 and 96 hours. Interestingly, in both SEM and KOPN8 the percentage of live cells progressively declined over time, whereas 697 cells were hardly affected at both DZNep concentrations (Fig.2G). Furthermore, we could confirm apoptosis by detection of PARP cleavage in DZNep exposed SEM, KOPN8 and 697 cell lysates on western blots (Fig.2H). Additionally, we investigated cell cycle progression in SEM and 697 cells, and found a moderate G_0/G_1 arrest after 48 hours, possibly associated with the observed enhanced apoptosis (Sup.Fig.1C).

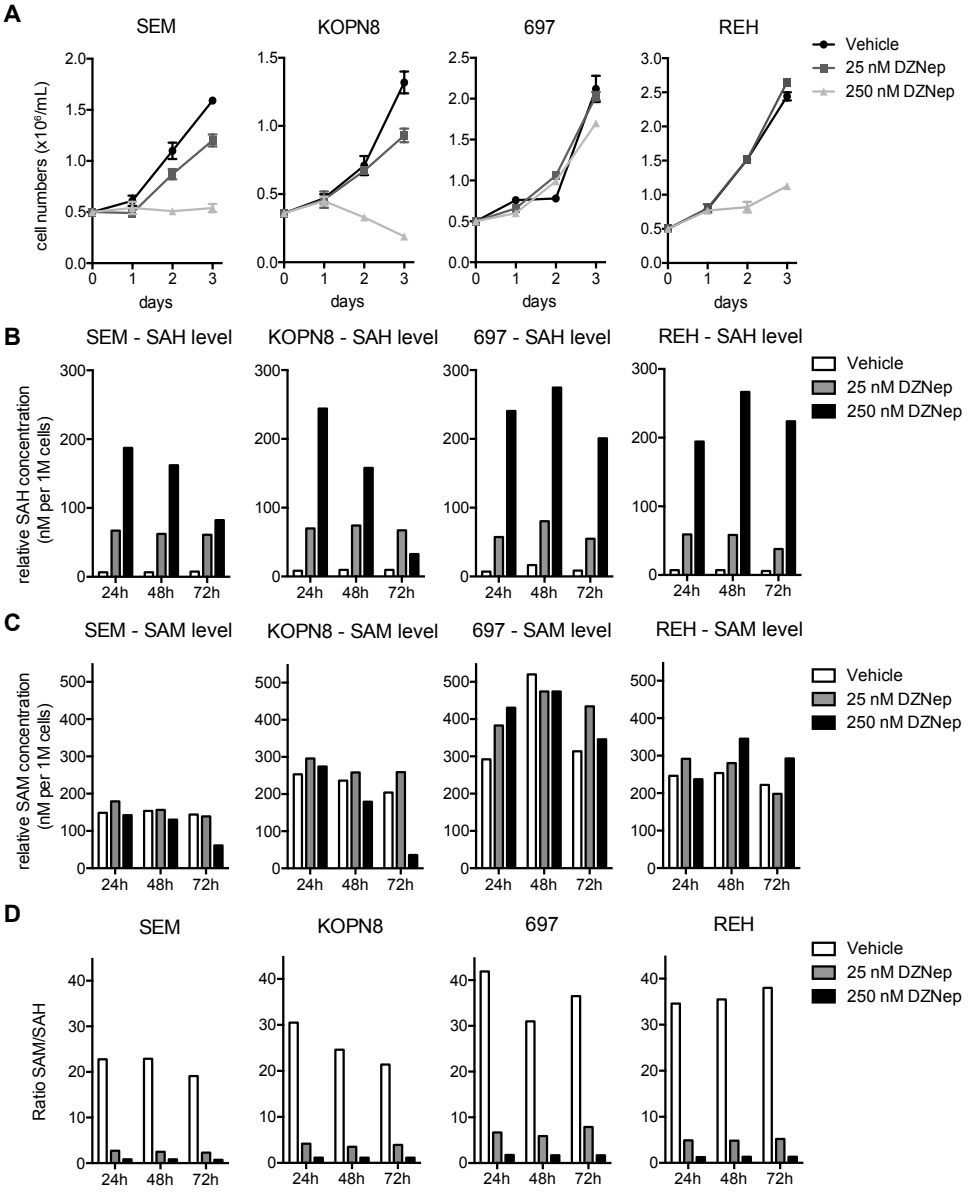

Figure 3. DZNep effectively alters SAH and SAM levels in ALL cells. (A) SEM, KOPN8, 697 or REH cell numbers after exposure to DMSO (control), or DZNep (25 or 250 nM) for 1 to 3 days. **(B,C)** Relative S-adenosylhomocystein (SAH) and S-adenosylmethionine (SAM) concentrations, respectively, (per 10^6 cells) in SEM, KOPN8, 697 or REH as determined by LC-MS/MS. Samples were assayed after exposure to vehicle (white), 25 nM DZNep (grey) or 250 nM DZNep (black) for 24, 48, or 72 hours. **(D)** The ratio between levels of SAM (C) and SAH (B) for each time point, as measure for methylation potential.

DZNep effectively alters SAH and SAM levels in ALL cells

SAHH plays a key role in the methionine cycle, replenishing the biochemical methyl donor S-adenosylmethionine (SAM). In order to supply methyl groups for various methylation processes in the cell, SAM needs to be converted into S-adenosylhomocysteine (SAH) by methyl transferases. In turn, SAH is converted into homocysteine and subsequently into methionine to finally be transformed into SAM. In this cycle, SAHH is responsible for converting SAH into homocysteine, and therefore the inhibition of SAHH leads to a disrupted balance in SAM and SAH molecules, and a reduction in the amount of methyl donor for methylation processes.[110,111] To investigate whether DZNep inhibited its target SAHH, we adopted a liquid chromatography–tandem mass spectrometry (LC-MS/MS) approach to detect SAH and SAM levels in the cell lines SEM, KOPN8, 697 and REH either in the absence or presence of DZNep, at different time points, and normalized these to cell concentration at the respective condition (as shown in Fig.3A). Interestingly, SAH accumulated rapidly and in a dose-dependent manner in all samples exposed to DZNep, including the less sensitive ALL cell line 697 (Fig.3B). Additionally, we observed a strong decrease of SAM levels in SEM and KOPN8 cells after 48 to 72 hours of exposure to 250 nM DZNep, while SAM levels in 697 and REH were unaffected by DZNep exposure up to 72 hours (Fig.3C). Hence, although SAHH was clearly inhibited in all cell lines, this led to a substantial reduction in available SAM only in the *MLL*-rearranged ALL cell lines. The cellular methylation potential has indeed been associated with SAM and SAH levels, but also with the ratio between the two.[112-114] Therefore, we also compared the SAM/SAH ratio between the different samples. Interestingly, we found sharply reduced SAM/SAH ratios in each of the cell lines already after 24 hours of DZNep exposure (Fig.3D). Although the SAM/SAH ratio was also affected in the 697 cell line, the SAM levels in the presence of DZNep and of the DMSO control are comparable, suggesting that this cell line is not challenged by a lack of available methyl groups. In contrast, the *MLL*-rearranged ALL cell lines SEM and KOPN8 clearly show reduced levels of the methyl donor SAM, and therefore should experience an impaired availability of methyl groups for various methylation processes.

Although SAHH was originally postulated as the target for DZNep, multiple studies have suggested DZNep exerts its function through depletion of EZH2.[115-118] We analyzed DZNep-treated cell lysates for EZH2 protein expression and observed a reduction of EZH2 in SEM, as well as a swift reduction in KOPN8 after 48 hours, though less apparent after 96 hours, while EZH2 levels in 697 samples drop after 96 hours exposure to 250 nM DZNep (Sup.Fig.2).

To summarize, in leukemic cells, DZNep is effectively targeting SAHH, which results in the accumulation of SAH, whereas SAM depletion only seems to occur in *MLL*-rearranged ALL cell lines and not in BCP-ALL cells. Similarly, DZNep may to

some extent reduce the protein expression levels of EZH2.

DZNep affects histone modifications

Since DZNep altered SAM and SAH levels in a way associated with loss of methylation capacity, we investigated whether the sensitivity of *MLL*-rearranged ALL cells to DZNep is caused by reduced histone and DNA methylation. Hereto, we exposed SEM and KOPN8 cells to DZNep (25 and 250 nM), isolated protein lysates after 48, 72 and 96 hours and analyzed several posttranslational histone modifications

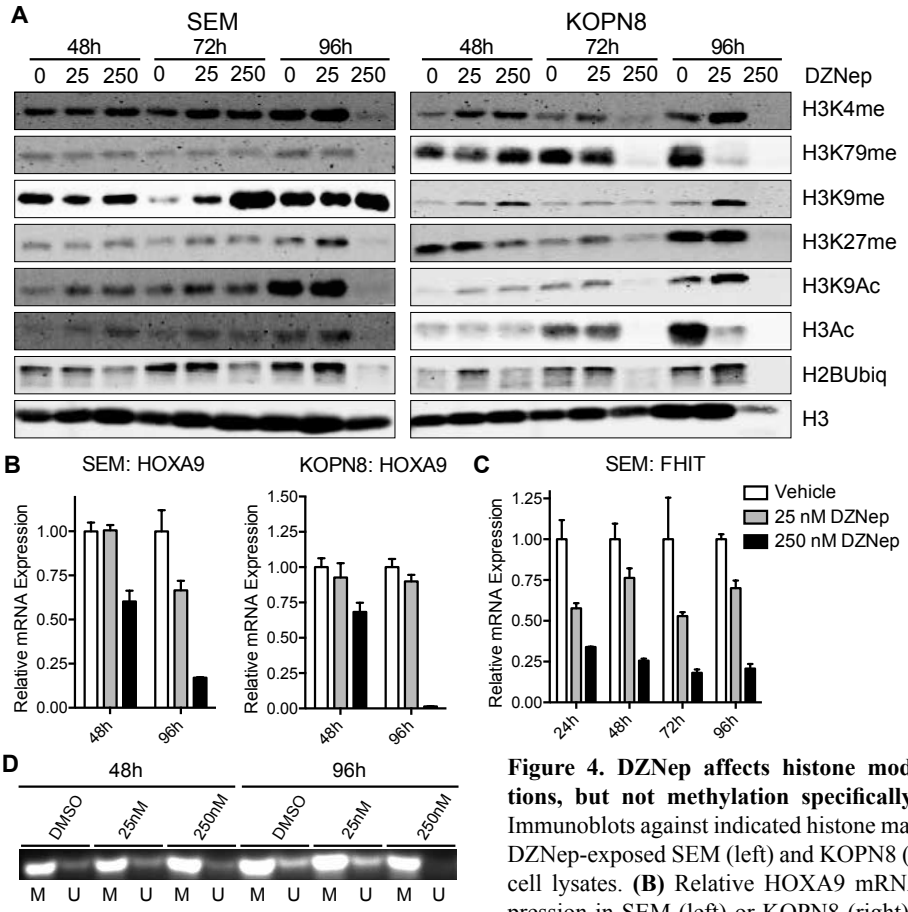

Figure 4. DZNep affects histone modifications, but not methylation specifically. (A) Immunoblots against indicated histone marks in DZNep-exposed SEM (left) and KOPN8 (right) cell lysates. **(B)** Relative HOXA9 mRNA expression in SEM (left) or KOPN8 (right) samples after exposure to vehicle (white), 25 nM DZNep (grey) or 250 nM DZNep (black) for 48 or 96 hours. **(C)** Relative mRNA expression of tumor suppressor FHIT in SEM after exposure to vehicle (white), 25 nM DZNep (grey) or 250 nM DZNep (black). **(D)** Image of resolved products of methylation-specific PCR for the *FHIT* promoter region. Methylated (M) and unmethylated (U) specific primer sets are as indicated.

by western blotting (Fig.4A). Surprisingly, the *MLL*-rearranged ALL characteristic trimethylation of histone 3 at lysine 4 (H3K4me3) and dimethylation of lysine 79 (H3K79me2) were only affected after 72 hours in KOPN8 cells, and after 96 hours in SEM cells, which was similar for H3K9 (in KOPN8 cells only) and H3K27 methylation. We also observed a comparable reduction in overall acetylation of histone 3 (H3Ac), and on lysine 9 (H3K9Ac) more specifically. Additionally, loss of ubiquitination of histone 2B (H2BUbiq) was detected from 48 hours onwards. Though the overall signal seemed higher, similar results (relative to DMSO control) were obtained for neplanocin-treated SEM and KOPN8 samples (Sup.Fig.3A). Thus, DZNep-induced depletion of SAM supposedly leads to impaired methylation on various lysine residues at histone 3, as well as to reduced acetylation and ubiquitination at other histone sites. While it is unlikely that an impaired methyl pool is directly responsible for the reduced acetylation and ubiquitination, it seems more likely that the effects on acetylation and ubiquitination are indirect consequences of the impaired methylation at histone 3. Interestingly, DZNep exposure diminished mRNA expression of MLL fusion target HOXA9 in SEM and KOPN8 (Fig.4B), while neplanocin reduced HOXA9 expression in SEM and KOPN8 as well (Sup.Fig.3B).

Next we asked whether DZNep exposure also leads to impaired methylation at the DNA. Previously, we found that promoter hypermethylation of the *FHIT* tumor suppressor gene was characteristic for *MLL*-rearranged infant ALL, which was accompanied by low *FHIT* expression. Hypothetically, drug-mediated demethylation should increase *FHIT* expression. Hence, we investigated *FHIT* mRNA expression levels and *FHIT* promoter methylation in SEM after exposure to DZNep. Surprisingly, already after 24 hours of exposure to DZNep, the already low *FHIT* expression in SEM cells further dropped dose-dependently (Fig.4C). Furthermore, using bisulphite conversion and methylation-specific PCR, we found an increase in *FHIT* promoter methylation levels, especially after 96 hours exposure to DZNep (Fig.4D), which appeared to be in line with the observed lowering of *FHIT* expression in response to DZNep exposure. This suggests that DZNep does not inhibit DNA methylation, at least not at the *FHIT* promoter.

DZNep monotherapy reduces leukemia in the spleen

To further evaluate DZNep as a therapeutic option, we investigated its efficacy in an *MLL*-rearranged ALL xenograft mouse model. In a toxicity study, both vehicle and dosages of 5 mg/kg on a 3 times per week intra-peritoneal injection schedule were well tolerated by immunodefcient NOD.Cg-*Prkdc*^{scid}*Il2rg*^{tm1Wjl}/SzJ (NSG) mice (Sup. Fig.4A). Surprisingly, necropsy of the mice revealed DZNep induced splenomegaly, when compared to vehicle treated or wildtype mice, and hematoxylin and eosin (H&E) staining of spleen tissue sections indicated DZNep induces hypercellularity (Sup.Fig.4B and C). Since the mice showed no signs of acute toxicity, we transplant-

ed NSG mice (n=15) with luciferase-expressing SEM cells (10^6 cells, intravenously) and divided them over the vehicle (n=8) and DZNep (n=7) treatment groups. Leukemia progression was tracked with weekly intra-vital bioluminescent imaging, and after 20 days both groups presented with systemic leukemia (Fig.5A). Quantifying the total flux (emitted photons/second) of the intra-vital imaging showed leukemia progression occurred in similar fashion for vehicle and DZNep treated mice (Fig.5B). After sacrificing the mice (day 28), the necropsy revealed that mice from both groups presented with splenomegaly (Fig.5C), with DZNep treated mice having slightly larger spleens than vehicle treated mice (Fig.5D). Following processing of the spleen, bone marrow, and peripheral blood samples from both treatment groups, we investigated the presence of leukemic cells in these samples through a multicolor flow cytometry approach. Interestingly, the spleen isolates from the vehicle mice on average showed 56% leukemic cells, while the DZNep mice on average only showed 9% leukemic cells in the spleen (Fig.5E). No differences in leukemic infiltration of

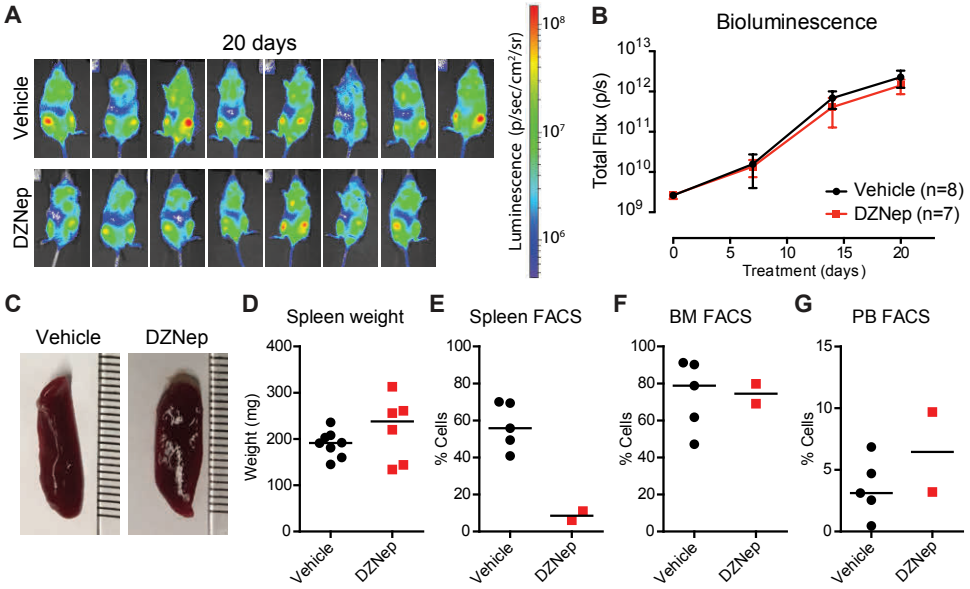

Figure 5. DZNep lacks inhibitory capacity for systemic ALL *in vivo*, but reduces leukemia in the spleen. (A) Intravital imaging of SEM-SLIEW transplanted mice after 20 days of treatment with vehicle (top) or 5 mg/kg DZNep (bottom). All images use the same luminescent scale, as shown on the right. **(B)** Quantification of the bioluminescence measured in (A) for vehicle (black) and DZNep (red) groups of mice. **(C)** Representative images of spleens from a vehicle (left) and DZNep (right) mouse. **(D)** Spleen weights from individual mice of the vehicle (black) and DZNep (red) groups. Group medians are indicated by horizontal bars. **(E,F,G)** Flow cytometry analysis of leukemic infiltration of spleen, bone marrow and peripheral blood, respectively. Vehicle and DZNep samples are indicated by black and red, respectively.

bone marrow or peripheral blood were observed between the two groups (Fig.5F and G). Further analysis of two bone marrow sections suggested that DZNep slightly reduced leukemic load in the bone marrow (Sup.Fig.5A). Interestingly, spleen tissue sections of DZNep treated mice did not reflect the reduction in leukemic cells, possibly due to DZNep-induced non-leukemic hypercellularity which we also observed in the toxicity study (Sup.Fig.5B).

Discussion

Acute lymphoblastic leukemia (ALL) in infants has a very poor clinical outcome. Rearrangements in the *MLL* gene occur in the majority (80%) of cases, and lead to epigenetic perturbations that differentiate this leukemia subtype from ALL in older children, both in gene expression and in clinical prognosis. Previously, we and others reported different therapeutic strategies impinging on epigenetic readers and modifiers. In this study, we employed an *in vitro* screening approach of epigenetic drugs to identify the next generation of epigenetic therapeutics and investigate their potential against *MLL*-rearranged ALL.

The screen yielded HDAC inhibitor HC toxin, and S-Adenosylhomocysteine hydrolase (SAHH) inhibitors neplanocin and its derivative 3-deazaneplanocin (DZNep) as promising compounds. HC toxin showed similar potency and efficacy as the previously identified panobinostat (LBH-589).[34] Furthermore, the mechanism behind inhibition of SAHH suggested the promising strategy to deplete methylation potential, thereby hypothetically incapacitating both histone and DNA methylation in *MLL*-rearranged ALL cells. Therefore, we selected neplanocin and DZNep for further studies. Validation in different leukemia cell lines indicated that although *MLL*-rearranged cell lines were amongst the most sensitive, both neplanocin and DZNep effectively inhibited ALL and AML cell lines, irrespective of *MLL* status. Interestingly, we observed IC_{50} values in nanomolar range for our leukemia cell lines, whereas in other malignancies (i.e. breast cancer, colorectal cancer and prostate cancer) IC_{50} values are generally in the order of micromolars, with a 10- to 200-fold difference to our data.[116,119] Additionally, patient-derived ALL samples have higher IC_{50} values than the cell lines, possibly explained by the limited dividing potential of primary samples *in vitro*. Still, although the response of primary *MLL*-rearranged infant ALL samples to DZNep and neplanocin is ambiguous, healthy, non-leukemic samples show no response to SAHH inhibition.

Hypothetically, inhibition of SAHH would lead to reduction of methylation potential, thereby affecting histone and DNA methylation in *MLL*-rearranged infant ALL. We found a strong alteration of SAM and SAH levels in response to DZNep treatment within 24 hours, which suggests the anti-leukemic effect of DZNep

is dependent on SAHH inhibition. Furthermore, DZNep modestly affected histone methylation, which correlated with reduced expression of MLL target gene HOXA9. Possibly, DZNep exposure also impacts expression of other MLL target genes.[30,31] Also, histone acetylation was reduced and the loss of H2B ubiquitination was prominent already after 24 to 48 hours of exposure. The latter was an interesting finding, since previous work in our group found depletion of H2B ubiquitination through suppression of the RNF20/RNF40/WAC ubiquitin ligase complex to be associated with the anti-leukemic effect of the HDAC inhibitor panobinostat (LBH-589).[35] We could confirm DZNep reduced protein levels of RNF20, RNF40 and WAC in SEM cell lysates (Sup.Fig.6), and this observation correlates with the observed decrease in H2B ubiquitination in Figure 4A.

Possibly, the reduced histone ubiquitination and acetylation are an indirect consequence of the disturbed methylation potential by DZNep. Additionally, promoter methylation of *FHIT* was not reduced and *FHIT* expression was actually decreased in SEM cells. Various studies have linked DZNep activity to different mechanisms. Miranda *et al*. found DZNep affected global histone methylation in breast cancer and bladder cancer cells, whereas Zhang *et al*. ascribed the effect of DZNep on breast cancer cells to inhibition of H3K79 methylation.[119,120] Alternatively, Tan *et al*. found depletion of components of the PRC2 complex and subsequent loss of H3K27 methylation, followed by reactivation of expression of distinct genes as mechanism of action for DZNep.[116] Intriguingly, our study confirms the original SAHH inhibitory properties of DZNep, but with different subsequent effects on histone modifications and this might not be methylation-dependent.[115,121] These differences could indicate DZNep exerts its anti-cancer function in a context-dependent manner. However, another possible explanation could lie in the balance between SAM and SAH and the methylation of mRNA, which is required for translation. Fernandez-Sanchez *et al*. found that inhibition of *SAHH* expression or SAHH activity repressed Myc-mediated mRNA cap methylation, reducing Myc-induced protein synthesis.[122] Hence, DZNep might deregulate protein synthesis through indirect inhibition of mRNA methylation, which might explain the sensitivity of *MLL* germline leukemia cells.

Surprisingly, investigation of DZNep in an *MLL*-rearranged xenograft mouse model showed no significant reduction in systemic leukemia, although splenic localization of leukemic cells was decreased. In contrast, Gannon *et al*. previously showed in a squamous cell carcinoma xenograft model that similar or lower DZNep doses could inhibit tumor growth.[123] Moreover, the cell lines used in this model were less sensitive to DZNep exposure *in vitro* than our leukemic cell lines. Additionally, similar results were reported for the *in vivo* efficacy of DZNep in mantle cell lymphoma.[124] However, these studies used sub-cutaneous transplantation, which regarding our data could suggest DZNep distribution and tumor localization *in vivo* is pivotal to treatment efficacy. This is supported by Zhou *et al*., who show in sub-cutaneous

xenografts with the *MLL*-rearranged AML cell line MOLM14, tumor volume hardly increases when treated with DZNep, whereas DZNep treatment after intra-venous transplantation induces some prolonged survival, but is insufficient to prevent leukemia outgrowth.[125] Interestingly, in a mouse transplantation model with *MLL*-rearranged mouse leukemia stem cells, DZNep treatment could not prevent leukemia outgrowth, but lengthened survival slightly.[118] A pharmacokinetics study in mice reported accumulation of radiolabeled DZNep in liver and kidneys shortly (2-24 hours) after a single intravenous dose, and showed plasma protein binding, which might explain the limited efficacy we observed *in vivo*.[126] Additionally, in this study, DZNep levels in the spleen remained, after liver and kidneys, higher than in other internal organs after 24 hours, though the specific cause for DZNep-mediated splenomegaly remains elusive. Possibly prolonged dosing further increases DZNep accumulation in the spleen, leading to inhibition of leukemic cells at this specific niche.
Despite the conclusion that DZNep monotherapy is insufficient to inhibit *MLL*-rearranged infant ALL *in vivo*, there is ongoing interest for its potential in anti-cancer combination therapy. For example, *in vitro* and *in vivo* combination treatment of DZNep with HDAC inhibitor panobinostat synergistically inhibited mantle cell lymphoma and AML.[107,124] Since we observed DZNep reduced expression of MLL target HOXA9, DZNep might support *MLL*-rearranged infant ALL treatment as part of combination therapy, possibly together with the very promising HDACi panobinostat.[34]
SAHH inhibition remains an interesting approach for anti-cancer therapy. Recently, Jiang *et al*. reported D9, a novel DZNep derivative, that inhibited different AML cell lines *in vitro*, and reduced tumor volume and prolonged survival in an *MLL*-rearranged AML xenograft model.[127] Hence, perhaps improved SAHH inhibitors could play a role in future combination therapy protocols for different malignancies, including *MLL*-rearranged infant ALL.
In summary, through screening of epigenetic drugs we found SAHH inhibitor DZNep as promising option against *MLL*-rearranged infant ALL cells *in vitro*. Although DZNep monotherapy was insufficient to block leukemia progression *in vivo*, we did observe reduced splenic infiltration. Since DZNep and panobinostat showed enhanced anti-cancer effects, further research into (epigenetic) combination therapies involving DZNep is warranted.

Supplemental Figures

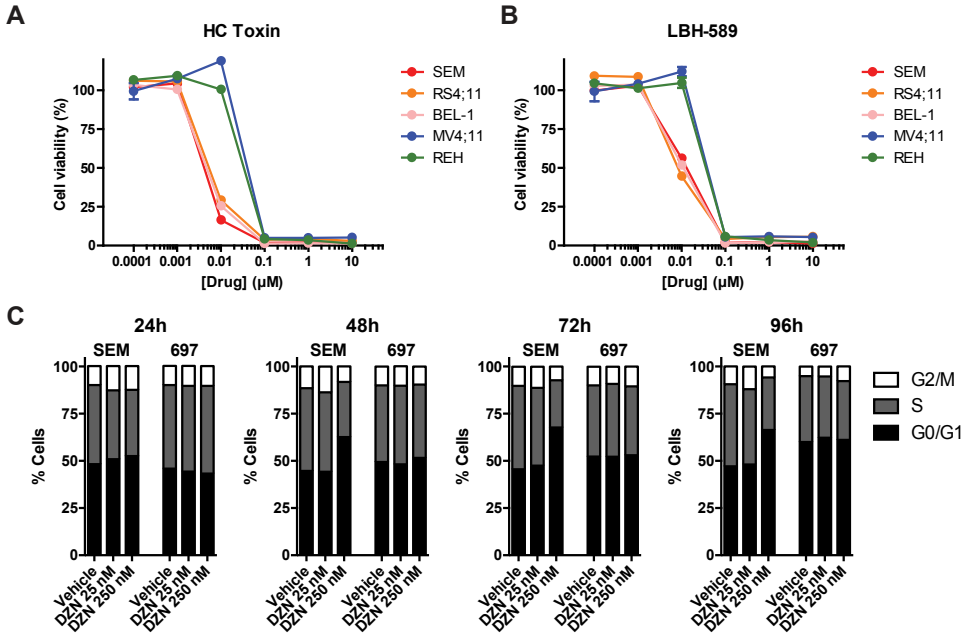

Supplemental Figure 1. (A,B) Dose-response curves of HC Toxin and LBH 589 (panobinostat), respectively, against *MLL*-rearranged ALL cell lines SEM, RS4;11 and BEL-1 (red tints), *MLL*-rearranged AML cell line MV4;11 (blue) and B-cell precursor ALL cell line REH (green). **(C)** Percentage of SEM or 697 cells in G0/G1 (black), S (grey) or G2/M (white) cell cycle stage, as determined by propidium iodide staining, after 24, 48, 72 or 96 hours exposure to vehicle, 25 nM DZNep or 250 nM DZNep.

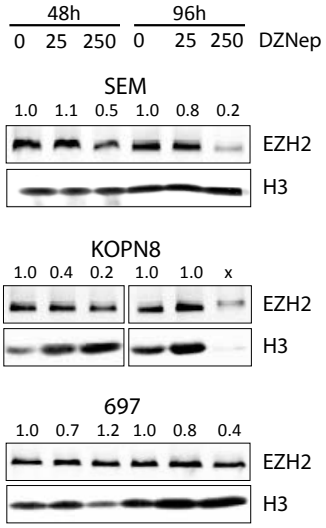

Supplemental Figure 2. Immunoblots showing EZH2 levels after 48 or 96 hours exposure to 25 or 250 nM DZNep in SEM, KOPN8 and 697 cell lines (top, center and bottom, respectively). Quantification of bands relative to the DMSO (0) control of the respective timepoint is shown above each lane.

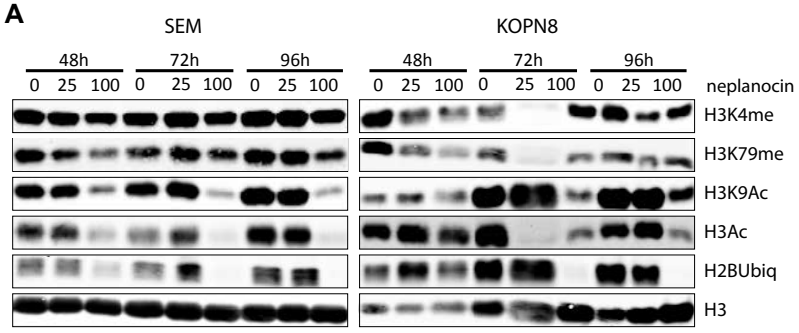

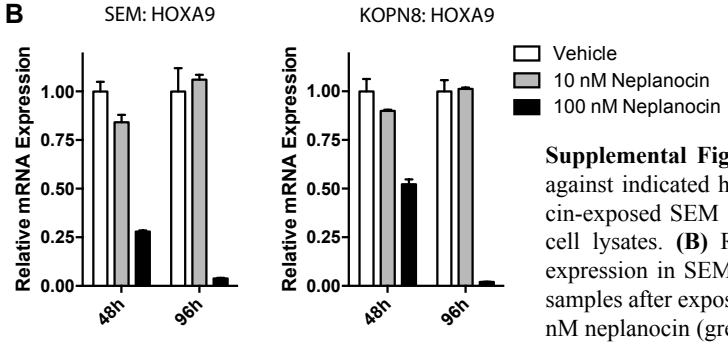

Supplemental Figure 3. (A) Immunoblots against indicated histone marks in neplanocin-exposed SEM (left) and KOPN8 (right) cell lysates. **(B)** Relative HOXA9 mRNA expression in SEM (left) or KOPN8 (right) samples after exposure to vehicle (white), 10 nM neplanocin (grey) or 100 nM neplanocin (black) for 48 or 96 hours.

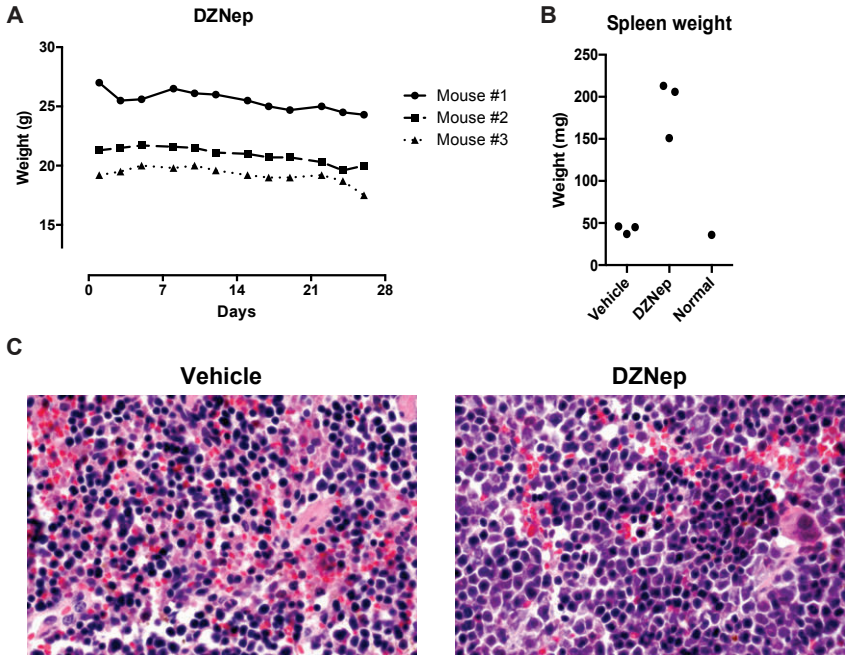

Supplemental Figure 4. (A) Progressive weight measurements of non-leukemic NSG mice injected with 5 mg/kg DZNep (n=3). **(B)** Spleen weight of vehicle, DZNep and wildtype (normal) mice. **(C)** Representative hematoxylin and eosin (H&E) stained spleen tissue-sections of vehicle and DZNep mice.

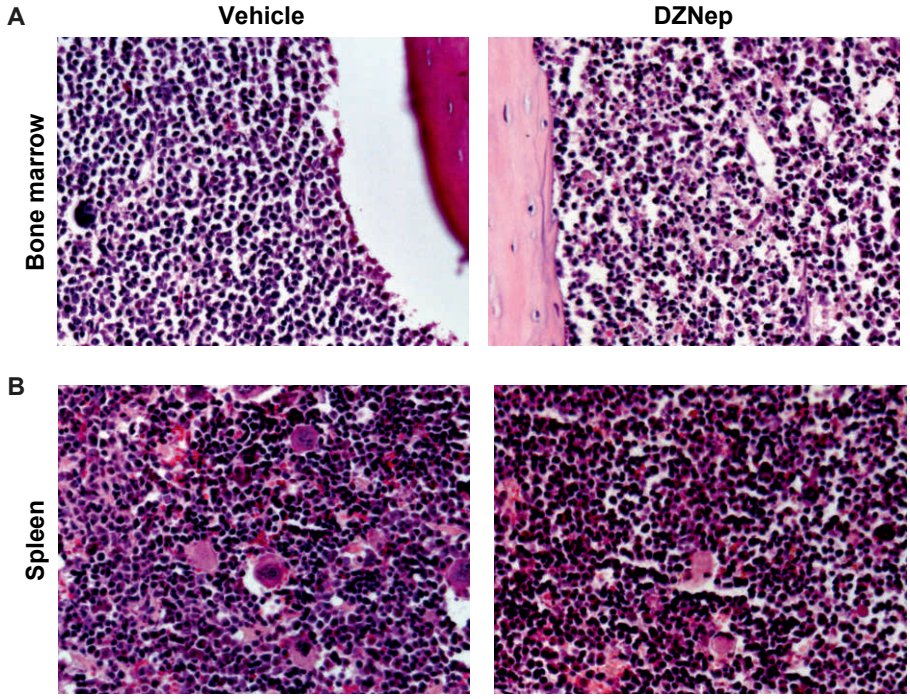

Supplemental Figure 5. (A,B) Representative hematoxylin and eosin (H&E) stained bone marrow and spleen tissue-sections of vehicle (left) or DZNep (right) treated leukemic mice, respectively.

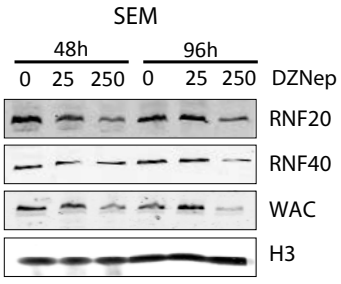

Supplemental Figure 6. Immunoblots showing (from the top down) RNF20, RNF40 and WAC levels after 48 or 96 hours exposure to 25 or 250 nM DZNep in SEM cells.

Chapter 6

General Discussion and Future Perspectives

Drug discovery and *MLL*-rearranged infant ALL

One of the most pressing drug development challenges in general is the high rate of attrition.[128] This is especially true for oncology drugs in clinical trials, which over the time period 2003-2011 reached a mere 6,7% likelihood of approval (i.e. the percentage of drugs that progress from phase 1 to FDA-approval).[129] Clearly, improvements in drug discovery and development are needed, with an emphasis on prediction of clinical safety profiles and efficacy. Input from studies on approved drugs, as well as drug failures, has played an important role in the development of predictive tools for classification of drug-like properties in medicinal chemistry.[130,131] However, progression of novel molecular entities from discovery towards clinical application is slow. Moreover, for drugs to make the transition to pediatric clinical investigation, extensive clinical data in adults is required, further protracting the application of *de novo* therapeutics in children. Additionally, *MLL*-rearranged infant acute lymphoblastic leukemia (ALL) is a rare disease that differs significantly from ALL in older children and adults, which further complicates clinical investigation.[5] While significant advances have been made over the past decades, including the initiation of infant-specific treatment protocols and improved risk stratification, lifting *MLL*-rearranged infant ALL survival chances to approximately 40-50% nowadays, the balance between therapeutic efficacy and toxicity of the current chemotherapeutics is delicate.[4,48] Hence, novel therapeutic strategies for *MLL*-rearranged infant ALL patients are clearly needed. Although the discovery of druggable targets and associated therapeutic small molecules is generally a valid approach, so far this has not led to improved outcome for these patients. This has led us to investigate drug repurposing as a tool to identify already approved therapeutics for which implementation into clinical trials can occur much quicker.

Drug repurposing

Drug repurposing has received extensive interest and has formed the basis for one of the research approaches in this thesis.[40] As reported in chapter 2, screening of over 3500 FDA-approved or off-patent drugs yielded a number of promising hits and resulted in the identification of topoisomerase I inhibitor SN-38 *in vitro*, and the successful pre-clinical efficacy assessment of the SN-38 prodrug irinotecan in *MLL*-rearranged *in vivo* xenograft mouse models. The amount of data on clinical use of irinotecan against other types of cancer, in both adult and pediatric cancer patients, is extensive and should provide medical practitioners with important information on pharmacodynamics and pharmacokinetic properties, to expedite the transition towards implementation in infant ALL treatment protocols. The drug repurposing approach may potentially increase accessibility and reduce costs of therapeutics, and its usefulness has been shown in different diseases, including vaccinia virus infection, multi-drug resistant tuberculosis, Parkinson's Disease and cancer.[132-135] Moreover,

it is particularly well suited for rare (orphan) and neglected diseases, which suffer from reserved interest of big pharmaceutical companies.[136,137] Our data exemplify the value of investigating drug repurposing as an alternative to target discovery and *de novo* drug design efforts for rare and aggressive diseases. Interestingly, adaptations of the drug repurposing approach are also being employed as tools in drug discovery. For example, chemical informatics databases with information on drug structures and associated targets predict targets for new drugs or vice versa, as well as potential off-target effects, whereas profiling of drug-induced alterations in gene expression have aided drug discovery and repositioning.[34,138-140] More recently, Legehar *et al.* have developed an approved drug database describing a plethora of parameters (i.e. ADMET information, molecular descriptors, targets and bioactivity) for thousands of small molecules and biologics.[141] These and new developments are expected to make a significant contribution to future drug discovery in general.

Targeted therapies for *MLL*-rearranged infant ALL

Our drug library screening reported in chapter 2, besides identifying SN-38/irinotecan as promising, though not *MLL*-rearranged ALL specific, therapeutic strategy, also indicated that in a large panel of FDA-approved drugs no *MLL*-rearranged infant ALL specific inhibitors could be identified. Considering the clinical and biological distinction from *MLL* germline infant ALL and BCP-ALL in older children, this implies that novel therapies against disease-specific mechanisms of *MLL*-rearranged ALL are needed.[16,17,28]

In chapter 3 we investigated targeted therapeutic options for *MLL*-rearranged infant ALL patients harboring additional *RAS* mutations, an infant ALL subgroup (24%) with an extremely poor prognosis, by testing inhibitors against RAS-pathway components.[21] While we found that MEK inhibitors inhibited *RAS*-mutant *MLL*-rearranged infant ALL patient cells and induced sensitization to prednisolone *in vitro*, the *in vivo* validation of MEK inhibitor trametinib showed limited systemic efficacy as monotherapy, but still managed to affect leukemic cell localization and reduce ERK phosphorylation (chapter 4). Although trametinib affected ERK phosphorylation in our xenograft mouse models, the dosing regime might not have been frequent enough to induce a sustained effect. However, more frequent dosing of trametinib is hampered by the toxicity we observed at higher dosages.

Previously, inhibition of downstream RAS signaling, especially at the level of MEK/ERK, has been shown to contribute to enhanced sensitization towards glucocorticoids in non-infant childhood ALL.[95] Since *MLL*-rearranged infant ALL is notorious for its resistance to glucocorticoids, most evidently in *RAS*-mutant leukemia, MEK inhibition could be a valuable option for combination therapy, and further pre-clinical *in vivo* validation is warranted. With trametinib approved for metastatic melanoma, and several clinical trials in progress, addition of trametinib to infant ALL

treatment protocols might be an option for overcoming glucocorticoid resistance.
Since *MLL*-rearranged ALL is characterized by aberrant epigenetic regulation, illustrated by perturbed histone modifications and DNA methylation patterns resulting in a distinct gene expression profile, it is no surprise that therapeutic strategies impinging on epigenetic modifiers (both "writers" and "readers") have been the core subject of targeted drug discovery research. In chapter 5 we screened two small epigenetic drug libraries for inhibitors of *MLL*-rearranged ALL cells. Amongst the most effective compounds we found histone deacetylase (HDAC) inhibitors, as well as S-adenosylhomocysteine hydrolase (SAHH) inhibitors. The mechanism of action for the latter was particularly intriguing, since SAHH plays a key role in replenishing the methyl donor S-adenosylmethionine (SAM).[115] Although we showed SAHH inhibitor DZNep killed leukemic cells (but not healthy bone marrow) *in vitro*, this was not *MLL*-rearanged ALL specific, as BCP-ALL cells with other translocations were affected to a comparable extent. Furthermore, while we observed increased SAH and reduced SAM levels, this did not drastically influence methylation, and although DZNep reduced splenic infiltration *in vivo* in xenograft mouse models of *MLL*-rearranged ALL, no difference in systemic leukemia was detected. Since DZNep, added to combination chemotherapy, showed enhanced anticancer effects in other malignacies, further investigation into synergistic (epigenetic) drug combinations might be promising.[107,124] In fact, several other epigenetic drug candidates, like azacytidine, are currently under investigation in *MLL*-rearranged infant ALL.

Epigenetic therapies in development

Although there is ambiguity about which specific HDAC isoforms are essential in ALL, different preclinical studies have reported promising results for HDAC inhibitors, and *MLL*-rearranged infant ALL cell lines and patient samples are particularly sensitive towards HDAC inhibition.[34,142] Moreover, as we recently showed, HDAC inhibitor panobinostat effectively impedes *MLL*-rearranged infant ALL progression in xenograft mouse models of both cell line and patient-derived *MLL*-rearranged infant ALL cells.[35] Furthermore, our study also suggests inhibition of an H2B ubiquitin ligase complex as key in the mechanism of action of panobinostat in *MLL*-rearranged infant ALL. The recent approval of panobinostat for multiple myeloma in adults will hopefully expedite transition towards clinical investigation for pediatric malignancies as well.[143]
Additionally, due to promoter hypermethylation in *MLL*-rearranged ALL, demethylating agents have been investigated extensively, with nucleoside analogues decitabine, 5-azacytidine and clofarabine as most promising compounds.[16] Interestingly, the first two drugs have been FDA-approved for myeloid malignancies in adults, which might expedite transition towards clinical application in pediatric cancer.[144] Moreover, clinical trials for 5-azacytidine as addition to current *MLL*-rearranged

infant ALL treatment protocols are underway, while clofarabine will be investigated for infant patients.

The histone methyltransferase DOT1L is pivotal to *MLL*-rearranged ALL maintenance and can be targeted by a small molecule inhibitor (EPZ-5676).[32] Furthermore, EPZ-5676 is under phase 1 clinical investigation for *MLL*-rearranged leukemia in adults, as well as pediatric patients. Recently, a study on two *MLL*-rearranged AML cell lines showed synergistic enhancement of anti-leukemic effects for EPZ-5676 in combination with standard AML therapies, as well as a number of epigenetic therapeutics.[145] With limited *in vivo* data on DOT1L inhibitors in *MLL*-rearranged ALL models, and *MLL*-rearranged ALL cell lines being less sensitive to EPZ-5676 than AML cells, it is currently unclear whether DOT1L inhibitors could be beneficial for *MLL*-rearranged infant ALL.

Another interesting class of epigenetic inhibitors targets the BET protein family (i.e. BRD2-4 and BRDT), which mediates formation of MLL fusion protein complexes that drive transcription.[37] Recently, we found I-BET151 deregulates BRD4 chromatin recruitment and effectively impedes primary *MLL*-rearranged ALL progression *in vivo*.[146] Other BET inhibitors are under clinical investigation for different solid and hematologic cancers in adults.

Conclusion

Through drug repurposing we identified SN-38 and irinotecan as possible effective drugs for *MLL*-rearranged infant ALL. The future of targeted therapies for *MLL*-rearranged infant ALL lies with the further development of novel epigenetic drugs and disruption of interactions within MLL-associated protein complexes, such as recently reported MLL-Menin inhibitors.[56,147] The progression of these promising therapeutics in (pre)clinical trials, especially the investigation of epigenetic combination treatment protocols, is of great interest and hopefully will have a positive impact on the treatment of *MLL*-rearranged infant ALL in the near future.

Chapter 7

Nederlandse samenvatting voor niet-ingewijden

Bloed

Ons lichaam bestaat uit meer dan 30 triljoen (30.000.000.000.000) cellen, die samenwerken om ons gezond te houden. Om de verschillende celtypes in ons lichaam te laten functioneren, hebben wij ongeveer 5 liter bloed, met ook weer verschillende soorten cellen met elk hun eigen belangrijke taak. Zo bestaat ons bloed uit cellen die zuurstof en koolstofdioxide transporteren (rode bloedcellen), cellen die zorgen dat bloed stolt bij een wondje (bloedplaatjes), en cellen die bescherming bieden tegen ziekteverwekkers (witte bloedcellen). Al deze verschillende bloedcellen stammen af van één voorloper cel, ook wel bloedstamcel genoemd. Dit type stamcel heeft her vermogen om zichzelf zeer vaak te vermenigvuldigen, en kan zich ook via verscheidene stappen verder ontwikkelen (rijpen) en zo veranderen in de verschillende bloedcellen. Dit wordt ook wel differentiëren genoemd. Tijdens de embryonale ontwikkeling vindt de productie van bloedcellen voornamelijk plaats in de lever, tot ongeveer 2 maanden voor de geboorte, wanneer het beenmerg de belangrijkste plek van de bloedaanmaak wordt.

Leukemie

Wanneer onrijpe witte bloedcellen (die nog niet functioneel zijn) ongeremd gaan delen, ontstaat er leukemie, ook wel bloedkanker genoemd. De voortgang van leukemie kan snel en agressief zijn, wat ook wel acute leukemie genoemd wordt. Aan de andere kant kan de deling en verspreiding van de cellen langgerekt zijn, wanneer er sprake is van chronische leukemie. Naarmate de leukemie zich verder ontwikkelt, verdringen de onrijpe witte bloedcellen de gezonde bloedcellen, wat ervoor zorgt dat de aanmaak van rode bloedcellen, bloedplaatjes en gezonde witte bloedcellen geblokkeerd wordt. Dit belemmert zuurstof/koolstof dioxide transport, bloedstolling en het afweersysteem. Binnen acute leukemie, wordt er onderscheid gemaakt aan de hand van de voorloper cel waar de leukemie uit ontstaan is. Zo kan er sprake zijn van acute myeloïde leukemie (AML) of acute lymfatische leukemie (ALL). Kinderen met leukemie hebben in de meeste gevallen acute lymfatische leukemie, waarvan in Nederland ongeveer 125 nieuwe gevallen per jaar worden vastgesteld. De afgelopen decennia is de behandeling van ALL bij kinderen sterk verbeterd. Dit komt onder andere door het gebruik van chemotherapie, meer kennis over deze ziekte en het beter kunnen identificeren van risicofactoren voor een slechte prognose. Hierdoor is de overlevingskans van kinderen met ALL van minder dan 10% in de jaren ’60 inmiddels gestegen tot ongeveer 90% overleving. Helaas hebben deze ontwikkelingen niet voor alle kinderen met ALL tot zo’n geweldige verbetering geleid, in het bijzonder niet voor de allerjongste patiëntjes, namelijk de zuigelingen (kinderen jonger dan 1 jaar).

MLL-herschikte acute lymfatische leukemie bij zuigelingen

In Nederland wordt jaarlijks bij 5 zuigelingen acute lymfatische leukemie gediagnostiseerd. De meerderheid van deze baby's (~80%) heeft een specifiek defect in het DNA. Van de 46 chromosomen in een cel, zijn er in dit geval 2 gebroken en verkeerd weer aan elkaar gelijmd, precies op een stuk dat codeert voor het *MLL* gen. Hierdoor is een stuk van het *MLL* gen aan een ander gen geplakt, wat ook wel een *MLL*-herschikking wordt genoemd. Bij de zuigelingen die géén *MLL*-herschikking hebben (~20% van de zuigelingen met ALL) is de overleving op de lange termijn ~75%, dus redelijk in de buurt van de overleving bij oudere kinderen met ALL. Maar zuigelingen met een *MLL*-herschikking hebben een veel slechtere prognose, met ongeveer 50% kans op overleving.

Het "gezonde" *MLL* gen wordt in de cel omgezet naar het MLL eiwit, dat betrokken is bij het reguleren van de bloedaanmaak. Normaalgesproken zijn er in (bloed voorloper) cellen verschillende signalen nodig om de cel bijvoorbeeld te laten delen of te differentiëren. Dat betekent dat de werking van het MLL eiwit onder controle staat van weer andere signalen en eiwitten. Maar in cellen met een *MLL*-herschikking worden er eiwitten aangemaakt die voor de helft uit MLL bestaan, en voor de andere helft uit een ander eiwit. Deze fusie-eiwitten kunnen nog wel allerlei processen in de cel aan- of uitzetten, maar zijn niet meer gevoelig voor de strenge controle die er in de cel is. Zo treden er in de leukemie cellen veranderingen op die *MLL*-herschikte ALL onderscheiden van ALL bij zuigelingen zonder *MLL*-herschikking en ALL bij oudere kinderen.

Hoewel de *MLL*-herschikking vaak de drijvende factor is bij ALL in zuigelingen, is er ook onderzoek gedaan andere fouten in het DNA die bijdragen aan de slechte prognose. Zo is er recent vastgesteld dat bij sommige patiënten een deel van de leukemiecellen een mutatie heeft in het *RAS* gen. Deze mutatie wordt geassocieerd met resistentie tegen chemotherapie en dus een nog slechtere prognose.

Ziektebeeld en huidige therapieën

Bij *MLL*-herschikte ALL zijn de leukemie cellen te herkennen als zeer onrijp, wat betekent dat ze nog dicht tegen het voorloper cel stadium aan zitten en dus nauwelijks gedifferentieerd zijn. Naast onrijpe witte bloedcellen, zijn er een aantal klinische kenmerken die *MLL*-herschikte leukemie karakteriseren en een indicator zijn voor een slechte prognose, waaronder leeftijd bij diagnose (<6 maanden), hoog aantal witte bloedcellen, beperkte effectiviteit van chemotherapie (prednison) gedurende de eerste week behandeling en infiltratie van leukemiecellen in het centraal zenuwstelsel. Hoewel het merendeel (~85%) van zuigelingen met *MLL*-herschikte ALL in eerste instantie goed reageert op de behandeling, komt de leukemie bij twee derde van de patiënten terug (ook wel relapse genoemd), resulterend in slechts 50% kans op overleving. Het huidige behandelingsprotocol wordt internationaal toegepast, en

bestaat uit een 2-jarige behandeling met verschillende chemotherapeutica, met onder andere glucocorticoïden (prednison, dexamethason), antimetabolieten (cytarabine, methotrexaat), asparaginase, daunorubicine en vincristine. Daarnaast komen patiënten die wel goed reageren op therapie in aanmerking voor stamcel transplantatie. Helaas is intensiever behandelen van patiënten niet mogelijk, omdat dit zou resulteren in verhoogde toxiciteit en behandeling-gerelateerde sterfte. Gezien het hoge aantal relapsen bij *MLL*-herschikte leukemie bij zuigelingen, moeten we concluderen dat de huidige behandeling niet genoeg is voor genezing. Daarom focust het recente onderzoek naar behandelmethodes voor deze ziekte zich op de ontwikkeling van nieuwe en meer doelgerichte medicijnen.

Medicijnontwikkeling in een notendop

Bij de ontwikkeling van nieuwe medicijnen, richt het onderzoek zich in eerste instantie op het begrijpen van het ziektebeeld en waardoor dit veroorzaakt wordt. Vaak is er een fout in het DNA, wat resulteert in de aanmaak van een eiwit wat niet meer werkt, of juist te actief is. De volgende stap is het vinden van een chemische structuur die in staat is om de werking van het eiwit te repareren. De chemische stof zal met het eiwit een specifieke interactie moeten aangaan, oftewel: aan het eiwit moeten binden. Dit wordt ook wel vergeleken met een slot (het eiwit) en een sleutel (de chemische stof), waarbij het kan zijn dat de sleutel het slot moet openmaken (herstellen van de functie van het eiwit) of het slot juist moet blokkeren (een overactief eiwit moet remmen). Als er een aantal stoffen gevonden of gemaakt zijn, worden die in verschillende lab experimenten getest, voordat een selectie van de meest veelbelovende middelen in diermodellen worden getest. Dit wordt gedaan om vast te stellen of de stof in een complex model goed werkt en veilig is om uiteindelijk in mensen getest te kunnen worden. Als in deze proeven goede resultaten behaald zijn, doorloopt het beste middel een aantal opeenvolgende klinische studies, waarbij gebruik van het middel bij o.a. gezonde volwassenen en specifieke groepen (volwassen) patiënten onderzocht wordt, voordat het medicijn goedgekeurd kan worden voor gebruik. De periode van begin van het onderzoek tot het goedkeuren van een medicijn bestrijkt gemiddeld 12-15 jaar. Maar omdat kinderen niet zomaar kleine volwassenen zijn, is er nog extra onderzoek nodig voordat een goedgekeurd medicijn bij kinderen, laat staan zuigelingen, toegepast kan worden.

Ontwikkeling van nieuwe doelgerichte medicijnen tegen *MLL*-herschikte acute lymfatische leukemie bij zuigelingen

Omdat er dringend iets gedaan moet worden aan de prognose van zuigelingen met *MLL*-herschikte ALL, hebben we een andere benadering gekozen. In hoofdstuk 2 van dit proefschrift hebben we meer dan 3500 medicijnen, die eerder zijn goedgekeurd en gebruikt worden voor de behandeling van verscheidene ziektes, getest op

geïsoleerde leukemiecellen van zuigelingen en oudere kinderen. Hiermee hoopten we een aantal middelen te vinden die de leukemiecellen kunnen doden en mogelijk geschikt zouden zijn als medicijn tegen *MLL*-herschikte ALL bij zuigelingen. Omdat deze middelen al eerder uitgebreid getest zijn in volwassenen, verwachtten we dat de overgang van een nieuw middel uit onze studies, naar daadwerkelijke toepassing in de kliniek, drastisch verkort zou kunnen worden. Onze lab experimenten wezen uit dat de stof 7-ethyl-10-hydroxycamthotecin (SN-38) bij lage concentraties zeer effectief leukemie cellen kon doden. Verder onderzoek in muismodellen wees uit dat een voorlopermedicijn (irinotecan) dat in het lichaam omgezet wordt naar SN-38, zeer effectief leukemiecellen in de muis kon blokkeren. Irinotecan was zelfs in staat om vergevorderde leukemie in muizen terug te dringen tot een niveau dat de leukemiecellen niet meer te detecteren waren. Hoewel de resultaten van SN-38 en irinotecan zeer veelbelovend zijn, is de werking van deze middelen niet specifiek: van snel delende cellen in het lichaam kan verwacht worden dat zij ook een bepaalde gevoeligheid hebben voor deze chemotherapeutica. Daarom gaat het onderzoek door naar middelen die specifieker op de genetische fouten in *MLL*-herschikte leukemie aangrijpen.

In hoofdstuk 3 hebben we onderzoek gedaan naar *MLL*-herschikte ALL cellen met extra *RAS* mutaties, wat geassocieerd wordt met een zeer slechte prognose, mede door verhoogde resistentie tegen de behandeling met prednison. Hiertoe hebben we een aantal medicijnen getest die aangrijpen op eiwitten en processen die betrokken zijn bij de werking van het (gemuteerde) RAS eiwit. Het was interessant om te zien dat chemische stoffen die de werking van het eiwit MEK blokkeren, effectief leukemiecellen konden doden in lab experimenten. Daarnaast ontdekten we dat deze MEK inhibitors de leukemiecellen gevoeliger konden maken voor prednisolon, de werkzame vorm van prednison. Vanwege deze veelbelovende resultaten, besloten we de meest effectieve MEK inhibitor (trametinib) verder te onderzoeken in een muismodel. In hoofdstuk 4 beschrijven we de experimenten. Hoewel we geen overduidelijke remming van de leukemiecellen zagen in de muizen die behandeld werden met trametinib, vonden we toch interessante aanknopingspunten. Zo bevatte het beenmerg van een aantal behandelde muizen nauwelijks nog leukemiecellen. Ook was de infiltratie van het centrale zenuwstelsel door de leukemiecellen teruggedrongen als gevolg van de behandeling met trametinib. Verder onderzoek naar een combinatie behandeling met trametinib en prednisolon zou van toegevoegde waarde kunnen zijn.

Hoofdstuk 5 beschrijft het onderzoek naar middelen die directer aangrijpen op processen waarbij het MLL eiwit betrokken is. Hiervoor zijn 84 verschillende medicijnen (deels nog in ontwikkeling) getest voor hun remmende werking op leukemiecellen. Neplanocin en 3-deazaneplanocin (DZNep), twee middelen die erg op elkaar lijken, kwamen hieruit naar voren als interessant optie, mede door hun mogelijke

werkingsmechanisme. Hoewel beide middelen effectief leukemiecellen remden, en geen gezonde beenmergcellen, was dit niet specifiek voor *MLL*-herschikte leukemie. Daarnaast wees verder onderzoek in een muismodel uit dat DZNep op zichzelf niet in staat was om leukemie te remmen. Recente onderzoeken naar DZNep als onderdeel van combinatiebehandeling tegen andere vormen van kanker, leverden veelbelovende resultaten op. Dit biedt aanknopingspunten om de mogelijkheden voor DZNep in combinatie met andere medicijnen tegen *MLL*-herschikte leukemie te onderzoeken.

Conclusie

In dit proefschrift hebben we verschillende mogelijke therapieën tegen *MLL*-herschikte ALL bij zuigelingen onderzocht, en SN-38 gevonden als veelbelovend middel. Naar verwachting zal onderzoek naar specifieke(re) medicijnen tegen dit type leukemie zich focussen op het blokkeren van de processen rondom het MLL-fusie eiwit. Daarbij zal de effectiviteit van deze middelen als onderdeel van combinatiebehandelingen een grote rol spelen, en hopelijk op relatief korte termijn een belangrijke bijdrage leveren aan de prognose voor zuigelingen met *MLL*-herschikte acute lymfatische leukemie.

Appendix

- References
- About the author
- List of publications
- PhD portfolio
- Dankwoord

References

1. Sender, R., Fuchs, S. & Milo, R. Revised Estimates for the Number of Human and Bacteria Cells in the Body. *PLoS Biol* **14**, e1002533 (2016).
2. Thomas, D.B. & Yoffey, J.M. Human Foetal Haematopoiesis. Ii. Hepatic Haematopoiesis in the Human Foetus. *Br J Haematol* **10**, 193-197 (1964).
3. Hunger, S.P. & Mullighan, C.G. Acute Lymphoblastic Leukemia in Children. *N Engl J Med* **373**, 1541-1552 (2015).
4. Pieters, R.*, et al.* A treatment protocol for infants younger than 1 year with acute lymphoblastic leukaemia (Interfant-99): an observational study and a multicentre randomised trial. *Lancet* **370**, 240-250 (2007).
5. Meyer, C.*, et al.* The MLL recombinome of acute leukemias in 2013. *Leukemia* **27**, 2165-2176 (2013).
6. Hilden, J.M.*, et al.* Analysis of prognostic factors of acute lymphoblastic leukemia in infants: report on CCG 1953 from the Children's Oncology Group. *Blood* **108**, 441-451 (2006).
7. Pui, C.H.*, et al.* Childhood Acute Lymphoblastic Leukemia: Progress Through Collaboration. *J Clin Oncol* **33**, 2938-2948 (2015).
8. Tomizawa, D.*, et al.* Outcome of risk-based therapy for infant acute lymphoblastic leukemia with or without an MLL gene rearrangement, with emphasis on late effects: a final report of two consecutive studies, MLL96 and MLL98, of the Japan Infant Leukemia Study Group. *Leukemia* **21**, 2258-2263 (2007).
9. Krivtsov, A.V. & Armstrong, S.A. MLL translocations, histone modifications and leukaemia stem-cell development. *Nat Rev Cancer* **7**, 823-833 (2007).
10. Yokoyama, A., Lin, M., Naresh, A., Kitabayashi, I. & Cleary, M.L. A higher-order complex containing AF4 and ENL family proteins with P-TEFb facilitates oncogenic and physiologic MLL-dependent transcription. *Cancer Cell* **17**, 198-212 (2010).
11. Ernst, P.*, et al.* Definitive hematopoiesis requires the mixed-lineage leukemia gene. *Dev Cell* **6**, 437-443 (2004).
12. Milne, T.A.*, et al.* MLL targets SET domain methyltransferase activity to Hox gene promoters. *Mol Cell* **10**, 1107-1117 (2002).
13. Bernt, K.M.*, et al.* MLL-rearranged leukemia is dependent on aberrant H3K79 methylation by DOT1L. *Cancer Cell* **20**, 66-78 (2011).
14. Bitoun, E., Oliver, P.L. & Davies, K.E. The mixed-lineage leukemia fusion partner AF4 stimulates RNA polymerase II transcriptional elongation and mediates coordinated chromatin remodeling. *Hum Mol Genet* **16**, 92-106 (2007).

15. Lin, C., *et al.* AFF4, a component of the ELL/P-TEFb elongation complex and a shared subunit of MLL chimeras, can link transcription elongation to leukemia. *Mol Cell* **37**, 429-437 (2010).
16. Stumpel, D.J., *et al.* Specific promoter methylation identifies different subgroups of MLL-rearranged infant acute lymphoblastic leukemia, influences clinical outcome, and provides therapeutic options. *Blood* **114**, 5490-5498 (2009).
17. Armstrong, S.A., *et al.* MLL translocations specify a distinct gene expression profile that distinguishes a unique leukemia. *Nat Genet* **30**, 41-47 (2002).
18. Gale, K.B., *et al.* Backtracking leukemia to birth: identification of clonotypic gene fusion sequences in neonatal blood spots. *Proc Natl Acad Sci U S A* **94**, 13950-13954 (1997).
19. Greaves, M.F., Maia, A.T., Wiemels, J.L. & Ford, A.M. Leukemia in twins: lessons in natural history. *Blood* **102**, 2321-2333 (2003).
20. Andersson, A.K., *et al.* The landscape of somatic mutations in infant MLL-rearranged acute lymphoblastic leukemias. *Nat Genet* **47**, 330-337 (2015).
21. Driessen, E.M., *et al.* Frequencies and prognostic impact of RAS mutations in MLL-rearranged acute lymphoblastic leukemia in infants. *Haematologica* **98**, 937-944 (2013).
22. Emerenciano, M., *et al.* Subclonality and prenatal origin of RAS mutations in KMT2A (MLL)-rearranged infant acute lymphoblastic leukaemia. *Br J Haematol* **170**, 268-271 (2015).
23. Stam, R.W., *et al.* Targeting FLT3 in primary MLL-gene-rearranged infant acute lymphoblastic leukemia. *Blood* **106**, 2484-2490 (2005).
24. Chillon, M.C., *et al.* Prognostic significance of FLT3 mutational status and expression levels in MLL-AF4+ and MLL-germline acute lymphoblastic leukemia. *Leukemia* **26**, 2360-2366 (2012).
25. Basso, G., *et al.* The immunophenotype in infant acute lymphoblastic leukaemia: correlation with clinical outcome. An Italian multicentre study (AIEOP). *Br J Haematol* **81**, 184-191 (1992).
26. Dinndorf, P.A. & Reaman, G.H. Acute lymphoblastic leukemia in infants: evidence for B cell origin of disease by use of monoclonal antibody phenotyping. *Blood* **68**, 975-978 (1986).
27. Pieters, R., *et al.* Relation between age, immunophenotype and in vitro drug resistance in 395 children with acute lymphoblastic leukemia--implications for treatment of infants. *Leukemia* **12**, 1344-1348 (1998).
28. Stam, R.W., *et al.* Gene expression profiling-based dissection of MLL translocated and MLL germline acute lymphoblastic leukemia in infants. *Blood* **115**, 2835-2844 (2010).

29. Van der Velden, V.H., *et al.* Prognostic significance of minimal residual disease in infants with acute lymphoblastic leukemia treated within the Interfant-99 protocol. *Leukemia* **23**, 1073-1079 (2009).
30. Guenther, M.G., *et al.* Aberrant chromatin at genes encoding stem cell regulators in human mixed-lineage leukemia. *Genes Dev* **22**, 3403-3408 (2008).
31. Krivtsov, A.V., *et al.* H3K79 methylation profiles define murine and human MLL-AF4 leukemias. *Cancer Cell* **14**, 355-368 (2008).
32. Daigle, S.R., *et al.* Potent inhibition of DOT1L as treatment of MLL-fusion leukemia. *Blood* **122**, 1017-1025 (2013).
33. Daigle, S.R., *et al.* Selective killing of mixed lineage leukemia cells by a potent small-molecule DOT1L inhibitor. *Cancer Cell* **20**, 53-65 (2011).
34. Stumpel, D.J., *et al.* Connectivity mapping identifies HDAC inhibitors for the treatment of t(4;11)-positive infant acute lymphoblastic leukemia. *Leukemia* **26**, 682-692 (2012).
35. Garrido Castro, P., *et al.* The HDAC inhibitor panobinostat (LBH589) exerts in vivo anti-leukaemic activity against MLL-rearranged acute lymphoblastic leukaemia and involves the RNF20/RNF40/WAC-H2B ubiquitination axis. *Leukemia* (2017).
36. Zuber, J., *et al.* RNAi screen identifies Brd4 as a therapeutic target in acute myeloid leukaemia. *Nature* **478**, 524-528 (2011).
37. Dawson, M.A., *et al.* Inhibition of BET recruitment to chromatin as an effective treatment for MLL-fusion leukaemia. *Nature* **478**, 529-533 (2011).
38. Schafer, E., *et al.* Promoter hypermethylation in MLL-r infant acute lymphoblastic leukemia: biology and therapeutic targeting. *Blood* **115**, 4798-4809 (2010).
39. Sanjuan-Pla, A., *et al.* Revisiting the biology of infant t(4;11)/MLL-AF4+ B-cell acute lymphoblastic leukemia. *Blood* **126**, 2676-2685 (2015).
40. O'Connor, K.A. & Roth, B.L. Finding new tricks for old drugs: an efficient route for public-sector drug discovery. *Nat Rev Drug Discov* **4**, 1005-1014 (2005).
41. Stam, R.W., *et al.* Differential mRNA expression of Ara-C-metabolizing enzymes explains Ara-C sensitivity in MLL gene-rearranged infant acute lymphoblastic leukemia. *Blood* **101**, 1270-1276 (2003).
42. Pommier, Y. Drugging topoisomerases: lessons and challenges. *ACS Chem Biol* **8**, 82-95 (2013).
43. Hsiang, Y.H., Lihou, M.G. & Liu, L.F. Arrest of replication forks by drug-stabilized topoisomerase I-DNA cleavable complexes as a mechanism of cell killing by camptothecin. *Cancer Res* **49**, 5077-5082 (1989).
44. Furuta, T., *et al.* Phosphorylation of histone H2AX and activation of Mre11, Rad50, and Nbs1 in response to replication-dependent DNA double-strand

breaks induced by mammalian DNA topoisomerase I cleavage complexes. *J Biol Chem* **278**, 20303-20312 (2003).
45. Matsuoka, S., Huang, M. & Elledge, S.J. Linkage of ATM to cell cycle regulation by the Chk2 protein kinase. *Science* **282**, 1893-1897 (1998).
46. Slatter, J.G., Su, P., Sams, J.P., Schaaf, L.J. & Wienkers, L.C. Bioactivation of the anticancer agent CPT-11 to SN-38 by human hepatic microsomal carboxylesterases and the in vitro assessment of potential drug interactions. *Drug Metab Dispos* **25**, 1157-1164 (1997).
47. Kaneda, N., Nagata, H., Furuta, T. & Yokokura, T. Metabolism and pharmacokinetics of the camptothecin analogue CPT-11 in the mouse. *Cancer Res* **50**, 1715-1720 (1990).
48. Kotecha, R.S., Gottardo, N.G., Kees, U.R. & Cole, C.H. The evolution of clinical trials for infant acute lymphoblastic leukemia. *Blood Cancer J* **4**, e200 (2014).
49. Lovelace, K., vanGessel, Y., Asher, L.V. & Vogel, P. Spontaneous acute tumor lysis syndrome in a DBA/1J mouse: a case report and review. *Toxicol Pathol* **31**, 486-490 (2003).
50. Corsello, S.M.*, et al.* Identification of AML1-ETO modulators by chemical genomics. *Blood* **113**, 6193-6205 (2009).
51. Roti, G.*, et al.* Complementary genomic screens identify SERCA as a therapeutic target in NOTCH1 mutated cancer. *Cancer Cell* **23**, 390-405 (2013).
52. Sakasai, R., Teraoka, H., Takagi, M. & Tibbetts, R.S. Transcription-dependent activation of ataxia telangiectasia mutated prevents DNA-dependent protein kinase-mediated cell death in response to topoisomerase I poison. *J Biol Chem* **285**, 15201-15208 (2010).
53. Houghton, P.J.*, et al.* Efficacy of topoisomerase I inhibitors, topotecan and irinotecan, administered at low dose levels in protracted schedules to mice bearing xenografts of human tumors. *Cancer Chemother Pharmacol* **36**, 393-403 (1995).
54. Armstrong, S.A.*, et al.* Inhibition of FLT3 in MLL. Validation of a therapeutic target identified by gene expression based classification. *Cancer Cell* **3**, 173-183 (2003).
55. Benito, J.M.*, et al.* MLL-Rearranged Acute Lymphoblastic Leukemias Activate BCL-2 through H3K79 Methylation and Are Sensitive to the BCL-2-Specific Antagonist ABT-199. *Cell Rep* **13**, 2715-2727 (2015).
56. Borkin, D.*, et al.* Pharmacologic inhibition of the Menin-MLL interaction blocks progression of MLL leukemia in vivo. *Cancer Cell* **27**, 589-602 (2015).
57. Richmond, J.*, et al.* Effective targeting of the P53-MDM2 axis in preclinical models of infant MLL-rearranged acute lymphoblastic leukemia. *Clin Can-*

cer Res **21**, 1395-1405 (2015).
58. Feng, Z.*, et al.* Pharmacological inhibition of LSD1 for the treatment of MLL-rearranged leukemia. *J Hematol Oncol* **9**, 24 (2016).
59. He, S.*, et al.* Menin-MLL inhibitors block oncogenic transformation by MLL-fusion proteins in a fusion partner-independent manner. *Leukemia* **30**, 508-513 (2016).
60. Jones, L.*, et al.* A review of new agents evaluated against pediatric acute lymphoblastic leukemia by the Pediatric Preclinical Testing Program. *Leukemia* **30**, 2133-2141 (2016).
61. Venditto, V.J. & Simanek, E.E. Cancer therapies utilizing the camptothecins: a review of the in vivo literature. *Mol Pharm* **7**, 307-349 (2010).
62. Marsh Rde, W., Talamonti, M.S., Katz, M.H. & Herman, J.M. Pancreatic cancer and FOLFIRINOX: a new era and new questions. *Cancer Med* **4**, 853-863 (2015).
63. Fujita, K., Kubota, Y., Ishida, H. & Sasaki, Y. Irinotecan, a key chemotherapeutic drug for metastatic colorectal cancer. *World J Gastroenterol* **21**, 12234-12248 (2015).
64. Kantarjian, H.M.*, et al.* Phase I study of Topotecan, a new topoisomerase I inhibitor, in patients with refractory or relapsed acute leukemia. *Blood* **81**, 1146-1151 (1993).
65. Prebet, T.*, et al.* Combination of cytarabine and topotecan in patients treated for acute myeloid leukemia with persistent disease after frontline induction. *Leuk Lymphoma* **53**, 2186-2191 (2012).
66. Wagner, L.M. Fifteen years of irinotecan therapy for pediatric sarcoma: where to next? *Clin Sarcoma Res* **5**, 20 (2015).
67. Thompson, P.A.*, et al.* Pharmacokinetics of irinotecan and its metabolites in pediatric cancer patients: a report from the children's oncology group. *Cancer Chemother Pharmacol* **62**, 1027-1037 (2008).
68. Hijiya, N.*, et al.* Phase II study of topotecan in combination with dexamethasone, asparaginase, and vincristine in pediatric patients with acute lymphoblastic leukemia in first relapse. *Cancer* **112**, 1983-1991 (2008).
69. Trachtenberg, B.H.*, et al.* Anthracycline-associated cardiotoxicity in survivors of childhood cancer. *Pediatr Cardiol* **32**, 342-353 (2011).
70. Na, Y.S.*, et al.* The histone deacetylase inhibitor PXD101 increases the efficacy of irinotecan in in vitro and in vivo colon cancer models. *Cancer Chemother Pharmacol* **68**, 389-398 (2011).
71. Na, Y.S.*, et al.* Effects of the HDAC inhibitor CG2 in combination with irinotecan, 5-fluorouracil, or oxaliplatin on HCT116 colon cancer cells and xenografts. *Oncol Rep* **24**, 1509-1514 (2010).
72. Sarcar, B., Kahali, S. & Chinnaiyan, P. Vorinostat enhances the cytotoxic

effects of the topoisomerase I inhibitor SN38 in glioblastoma cell lines. *J Neurooncol* **99**, 201-207 (2010).
73. Sampson, V.B.*, et al.* Vorinostat Enhances Cytotoxicity of SN-38 and Temozolomide in Ewing Sarcoma Cells and Activates STAT3/AKT/MAPK Pathways. *PLoS One* **10**, e0142704 (2015).
74. Bruzzese, F.*, et al.* Synergistic antitumor effect between vorinostat and topotecan in small cell lung cancer cells is mediated by generation of reactive oxygen species and DNA damage-induced apoptosis. *Mol Cancer Ther* **8**, 3075-3087 (2009).
75. Greaves, M.F. Infant leukaemia biology, aetiology and treatment. *Leukemia* **10**, 372-377 (1996).
76. Kampen, K.R.*, et al.* Insights in dynamic kinome reprogramming as a consequence of MEK inhibition in MLL-rearranged AML. *Leukemia* **28**, 589-599 (2014).
77. Lavallee, V.P.*, et al.* The transcriptomic landscape and directed chemical interrogation of MLL-rearranged acute myeloid leukemias. *Nat Genet* **47**, 1030-1037 (2015).
78. Hartsink-Segers, S.A.*, et al.* Aurora kinases in childhood acute leukemia: the promise of aurora B as therapeutic target. *Leukemia* **27**, 560-568 (2013).
79. Spijkers-Hagelstein, J.A., Pinhancos, S.S., Schneider, P., Pieters, R. & Stam, R.W. Chemical genomic screening identifies LY294002 as a modulator of glucocorticoid resistance in MLL-rearranged infant ALL. *Leukemia* **28**, 761-769 (2014).
80. Berenbaum, M.C. Synergy, additivism and antagonism in immunosuppression. A critical review. *Clin Exp Immunol* **28**, 1-18 (1977).
81. Prior, I.A., Lewis, P.D. & Mattos, C. A comprehensive survey of Ras mutations in cancer. *Cancer Res* **72**, 2457-2467 (2012).
82. Biondi, A., Cimino, G., Pieters, R. & Pui, C.H. Biological and therapeutic aspects of infant leukemia. *Blood* **96**, 24-33 (2000).
83. Irving, J.*, et al.* Ras pathway mutations are prevalent in relapsed childhood acute lymphoblastic leukemia and confer sensitivity to MEK inhibition. *Blood* **124**, 3420-3430 (2014).
84. Burgess, M.R.*, et al.* Preclinical efficacy of MEK inhibition in Nras-mutant AML. *Blood* **124**, 3947-3955 (2014).
85. Kirkwood, J.M.*, et al.* Phase II, open-label, randomized trial of the MEK1/2 inhibitor selumetinib as monotherapy versus temozolomide in patients with advanced melanoma. *Clin Cancer Res* **18**, 555-567 (2012).
86. Flaherty, K.T.*, et al.* Improved survival with MEK inhibition in BRAF-mutated melanoma. *N Engl J Med* **367**, 107-114 (2012).
87. Ascierto, P.A.*, et al.* MEK162 for patients with advanced melanoma har-

bouring NRAS or Val600 BRAF mutations: a non-randomised, open-label phase 2 study. *Lancet Oncol* **14**, 249-256 (2013).
88. Catalanotti, F.*, et al.* Phase II trial of MEK inhibitor selumetinib (AZD6244, ARRY-142886) in patients with BRAFV600E/K-mutated melanoma. *Clin Cancer Res* **19**, 2257-2264 (2013).
89. Janne, P.A.*, et al.* Selumetinib plus docetaxel for KRAS-mutant advanced non-small-cell lung cancer: a randomised, multicentre, placebo-controlled, phase 2 study. *Lancet Oncol* **14**, 38-47 (2013).
90. Minjgee, M., Toulany, M., Kehlbach, R., Giehl, K. & Rodemann, H.P. K-RAS(V12) induces autocrine production of EGFR ligands and mediates radioresistance through EGFR-dependent Akt signaling and activation of DNA-PKcs. *Int J Radiat Oncol Biol Phys* **81**, 1506-1514 (2011).
91. Nakanishi, H., Nakamura, T., Canaani, E. & Croce, C.M. ALL1 fusion proteins induce deregulation of EphA7 and ERK phosphorylation in human acute leukemias. *Proc Natl Acad Sci U S A* **104**, 14442-14447 (2007).
92. Hatzivassiliou, G.*, et al.* Mechanism of MEK inhibition determines efficacy in mutant KRAS- versus BRAF-driven cancers. *Nature* **501**, 232-236 (2013).
93. Jones, C.L.*, et al.* MAPK signaling cascades mediate distinct glucocorticoid resistance mechanisms in pediatric leukemia. *Blood* **126**, 2202-2212 (2015).
94. Aries, I.M.*, et al.* Towards personalized therapy in pediatric acute lymphoblastic leukemia: RAS mutations and prednisolone resistance. *Haematologica* **100**, e132-136 (2015).
95. Rambal, A.A., Panaguiton, Z.L., Kramer, L., Grant, S. & Harada, H. MEK inhibitors potentiate dexamethasone lethality in acute lymphoblastic leukemia cells through the pro-apoptotic molecule BIM. *Leukemia* **23**, 1744-1754 (2009).
96. Iglesias-Serret, D.*, et al.* Regulation of the proapoptotic BH3-only protein BIM by glucocorticoids, survival signals and proteasome in chronic lymphocytic leukemia cells. *Leukemia* **21**, 281-287 (2007).
97. Spijkers-Hagelstein, J.A.*, et al.* Glucocorticoid sensitisation in Mixed Lineage Leukaemia-rearranged acute lymphoblastic leukaemia by the pan-BCL-2 family inhibitors gossypol and AT-101. *Eur J Cancer* **50**, 1665-1674 (2014).
98. Kerstjens, M.*, et al.* MEK inhibition is a promising therapeutic strategy for MLL-rearranged infant acute lymphoblastic leukemia patients carrying RAS mutations. *Oncotarget* (2016).
99. Walters, D.M.*, et al.* Inhibition of the growth of patient-derived pancreatic cancer xenografts with the MEK inhibitor trametinib is augmented by combined treatment with the epidermal growth factor receptor/HER2 inhibitor

lapatinib. *Neoplasia* **15**, 143-155 (2013).
100. Menzies, A.M. & Long, G.V. Dabrafenib and trametinib, alone and in combination for BRAF-mutant metastatic melanoma. *Clin Cancer Res* **20**, 2035-2043 (2014).
101. National-Toxicology-Program. Spleen - Extramedullary Hematopoiesis. (2015).
102. Nordmann, T.M.*, et al.* Trametinib after disease reactivation under dabrafenib in Erdheim-Chester disease with both BRAF and KRAS mutations. *Blood* **129**, 879-882 (2017).
103. Prieto, C.*, et al.* Activated KRAS Cooperates with MLL-AF4 to Promote Extramedullary Engraftment and Migration of Cord Blood CD34+ HSPC But Is Insufficient to Initiate Leukemia. *Cancer Res* **76**, 2478-2489 (2016).
104. Dordelmann, M.*, et al.* Prednisone response is the strongest predictor of treatment outcome in infant acute lymphoblastic leukemia. *Blood* **94**, 1209-1217 (1999).
105. Polak, A.*, et al.* MEK Inhibition Sensitizes Precursor B-Cell Acute Lymphoblastic Leukemia (B-ALL) Cells to Dexamethasone through Modulation of mTOR Activity and Stimulation of Autophagy. *PLoS One* **11**, e0155893 (2016).
106. Stam, R.W.*, et al.* Silencing of the tumor suppressor gene FHIT is highly characteristic for MLL gene rearranged infant acute lymphoblastic leukemia. *Leukemia* **20**, 264-271 (2006).
107. Fiskus, W.*, et al.* Combined epigenetic therapy with the histone methyltransferase EZH2 inhibitor 3-deazaneplanocin A and the histone deacetylase inhibitor panobinostat against human AML cells. *Blood* **114**, 2733-2743 (2009).
108. Fillmore, C.M.*, et al.* EZH2 inhibition sensitizes BRG1 and EGFR mutant lung tumours to TopoII inhibitors. *Nature* **520**, 239-242 (2015).
109. Wee, Z.N.*, et al.* EZH2-mediated inactivation of IFN-gamma-JAK-STAT1 signaling is an effective therapeutic target in MYC-driven prostate cancer. *Cell Rep* **8**, 204-216 (2014).
110. Chiang, P.K. Biological effects of inhibitors of S-adenosylhomocysteine hydrolase. *Pharmacol Ther* **77**, 115-134 (1998).
111. Liteplo, R.G. DNA (cytosine) methylation in murine and human tumor cell lines treated with S-adenosylhomocysteine hydrolase inhibitors. *Cancer Lett* **39**, 319-327 (1988).
112. Kraus, D.*, et al.* Nicotinamide N-methyltransferase knockdown protects against diet-induced obesity. *Nature* **508**, 258-262 (2014).
113. Mentch, S.J.*, et al.* Histone Methylation Dynamics and Gene Regulation Occur through the Sensing of One-Carbon Metabolism. *Cell Metab* **22**, 861-

873 (2015).
114. Caudill, M.A.*, et al.* Intracellular S-adenosylhomocysteine concentrations predict global DNA hypomethylation in tissues of methyl-deficient cystathionine beta-synthase heterozygous mice. *J Nutr* **131**, 2811-2818 (2001).
115. Borchardt, R.T., Keller, B.T. & Patel-Thombre, U. Neplanocin A. A potent inhibitor of S-adenosylhomocysteine hydrolase and of vaccinia virus multiplication in mouse L929 cells. *J Biol Chem* **259**, 4353-4358 (1984).
116. Tan, J.*, et al.* Pharmacologic disruption of Polycomb-repressive complex 2-mediated gene repression selectively induces apoptosis in cancer cells. *Genes Dev* **21**, 1050-1063 (2007).
117. D'Angelo, V.*, et al.* EZH2 is increased in paediatric T-cell acute lymphoblastic leukemia and is a suitable molecular target in combination treatment approaches. *J Exp Clin Cancer Res* **34**, 83 (2015).
118. Ueda, K.*, et al.* Inhibition of histone methyltransferase EZH2 depletes leukemia stem cell of mixed lineage leukemia fusion leukemia through upregulation of p16. *Cancer Sci* **105**, 512-519 (2014).
119. Zhang, L.*, et al.* Inhibition of histone H3K79 methylation selectively inhibits proliferation, self-renewal and metastatic potential of breast cancer. *Oncotarget* **5**, 10665-10677 (2014).
120. Miranda, T.B.*, et al.* DZNep is a global histone methylation inhibitor that reactivates developmental genes not silenced by DNA methylation. *Mol Cancer Ther* **8**, 1579-1588 (2009).
121. Inaba, M., Nagashima, K., Tsukagoshi, S. & Sakurai, Y. Biochemical mode of cytotoxic action of neplanocin A in L1210 leukemic cells. *Cancer Res* **46**, 1063-1067 (1986).
122. Fernandez-Sanchez, M.E., Gonatopoulos-Pournatzis, T., Preston, G., Lawlor, M.A. & Cowling, V.H. S-adenosyl homocysteine hydrolase is required for Myc-induced mRNA cap methylation, protein synthesis, and cell proliferation. *Mol Cell Biol* **29**, 6182-6191 (2009).
123. Gannon, O.M., Merida de Long, L., Endo-Munoz, L., Hazar-Rethinam, M. & Saunders, N.A. Dysregulation of the repressive H3K27 trimethylation mark in head and neck squamous cell carcinoma contributes to dysregulated squamous differentiation. *Clin Cancer Res* **19**, 428-441 (2013).
124. Fiskus, W.*, et al.* Superior efficacy of a combined epigenetic therapy against human mantle cell lymphoma cells. *Clin Cancer Res* **18**, 6227-6238 (2012).
125. Zhou, J.*, et al.* The histone methyltransferase inhibitor, DZNep, up-regulates TXNIP, increases ROS production, and targets leukemia cells in AML. *Blood* **118**, 2830-2839 (2011).
126. Coulombe, R.A., Jr., Sharma, R.P. & Huggins, J.W. Pharmacokinetics of the antiviral agent 3-deazaneplanocin A. *Eur J Drug Metab Pharmacokinet* **20**,

197-202 (1995).
127. Jiang, X.*, et al.* Functional Characterization of D9, a Novel Deazaneplanocin A (DZNep) Analog, in Targeting Acute Myeloid Leukemia (AML). *PLoS One* **10**, e0122983 (2015).
128. Waring, M.J.*, et al.* An analysis of the attrition of drug candidates from four major pharmaceutical companies. *Nat Rev Drug Discov* **14**, 475-486 (2015).
129. Hay, M., Thomas, D.W., Craighead, J.L., Economides, C. & Rosenthal, J. Clinical development success rates for investigational drugs. *Nat Biotechnol* **32**, 40-51 (2014).
130. Lipinski, C.A., Lombardo, F., Dominy, B.W. & Feeney, P.J. Experimental and computational approaches to estimate solubility and permeability in drug discovery and development settings. *Adv Drug Deliv Rev* **46**, 3-26 (2001).
131. Zhang, M.Q. & Wilkinson, B. Drug discovery beyond the 'rule-of-five'. *Curr Opin Biotechnol* **18**, 478-488 (2007).
132. Deng, L.*, et al.* Identification of novel antipoxviral agents: mitoxantrone inhibits vaccinia virus replication by blocking virion assembly. *J Virol* **81**, 13392-13402 (2007).
133. Kinnings, S.L.*, et al.* Drug discovery using chemical systems biology: repositioning the safe medicine Comtan to treat multi-drug and extensively drug resistant tuberculosis. *PLoS Comput Biol* **5**, e1000423 (2009).
134. Brundin, P.*, et al.* Linked clinical trials--the development of new clinical learning studies in Parkinson's disease using screening of multiple prospective new treatments. *J Parkinsons Dis* **3**, 231-239 (2013).
135. Martin, S.A.*, et al.* Methotrexate induces oxidative DNA damage and is selectively lethal to tumour cells with defects in the DNA mismatch repair gene MSH2. *EMBO Mol Med* **1**, 323-337 (2009).
136. Beaulieu, C.L.*, et al.* A generalizable pre-clinical research approach for orphan disease therapy. *Orphanet J Rare Dis* **7**, 39 (2012).
137. Duenas-Gonzalez, A.*, et al.* The prince and the pauper. A tale of anticancer targeted agents. *Mol Cancer* **7**, 82 (2008).
138. Dunkel, M., Gunther, S., Ahmed, J., Wittig, B. & Preissner, R. SuperPred: drug classification and target prediction. *Nucleic Acids Res* **36**, W55-59 (2008).
139. Xie, L., Xie, L. & Bourne, P.E. Structure-based systems biology for analyzing off-target binding. *Curr Opin Struct Biol* **21**, 189-199 (2011).
140. Iorio, F.*, et al.* Discovery of drug mode of action and drug repositioning from transcriptional responses. *Proc Natl Acad Sci U S A* **107**, 14621-14626 (2010).
141. Legehar, A., Xhaard, H. & Ghemtio, L. IDAAPM: integrated database of

ADMET and adverse effects of predictive modeling based on FDA approved drug data. *J Cheminform* **8**, 33 (2016).
142. Moreno, D.A.*, et al.* Differential expression of HDAC3, HDAC7 and HDAC9 is associated with prognosis and survival in childhood acute lymphoblastic leukaemia. *Br J Haematol* **150**, 665-673 (2010).
143. Raedler, L.A. Farydak (Panobinostat): First HDAC Inhibitor Approved for Patients with Relapsed Multiple Myeloma. *Am Health Drug Benefits* **9**, 84-87 (2016).
144. Yun, S.*, et al.* Targeting epigenetic pathways in acute myeloid leukemia and myelodysplastic syndrome: a systematic review of hypomethylating agents trials. *Clin Epigenetics* **8**, 68 (2016).
145. Klaus, C.R.*, et al.* DOT1L inhibitor EPZ-5676 displays synergistic antiproliferative activity in combination with standard of care drugs and hypomethylating agents in MLL-rearranged leukemia cells. *J Pharmacol Exp Ther* **350**, 646-656 (2014).
146. Bardini, M., *et al*. Antileukemic Efficacy of BET Inhibitor in a Preclinical Mouse Model of MLL-AF4(+) Infant ALL. *Mol Cancer Ther* **17**, 1705-1716 (2018).
147. Grembecka, J.*, et al.* Menin-MLL inhibitors reverse oncogenic activity of MLL fusion proteins in leukemia. *Nat Chem Biol* **8**, 277-284 (2012).

About the author

Mark Kerstjens was born on the 26th of February 1988 in Beverwijk. He finished his high school education (Gymnasium) at the Kennemer College Beverwijk in 2006. With a passion for chemistry and biology, and interest in disease and medicine, Mark continued his education with Pharmaceutical Sciences at the Vrije Universiteit in Amsterdam. There he obtained his BSc degree in 2010, having done an internship in the Medicinal Chemistry department, at both the synthesis and pharmacology groups. Based on this experience, he ultimately chose to follow-up with a Master's Drug Discovery & Safety, specializing in molecular pharmacology. As part of his Master's education, he went abroad for a research internship at the oncology site of Boehringer-Ingelheim in Vienna, Austria. He obtained his MSc degree in 2012. After a short period working as a research assistant at the Computational Chemistry group at the Vrije Universiteit in Amsterdam, Mark commenced his PhD research at the Pediatric Oncology/Hematology department of Prof. Dr. Rob Pieters, in the group of Dr. Ronald W. Stam, to work on improved therapeutics against *MLL*-rearranged infant ALL. A drug library screening campaign in the first year of his PhD laid the foundation for different research projects. Through cooperation within the infant ALL group, as well as in collaboration with other researchers, Mark continued to work on the most promising therapeutic candidates until 2016, of which the results have been described in this thesis.

List of publications

M. Kerstjens*, E.M.C. Driessen*, M. Willekes, S. Mimoso Pinhanços, P. Schneider, R. Pieters and R.W. Stam.
MEK inhibition is a promising therapeutic strategy for *MLL*-rearranged infant acute lymphoblastic leukemia patients carrying *RAS* mutations. *Oncotarget, 2016*.

P. Garrido Castro, E.H.J. van Roon, S. Mimoso Pinhanços, L. Trentin, P. Schneider, **M. Kerstjens**, G. Te Kronnie, O. Heidenreich, R. Pieters, and R.W. Stam.
The HDAC inhibitor panobinostat (LBH589) exerts *in vivo* anti-leukaemic activity against *MLL*-rearranged acute lymphoblastic leukaemia and involves the RNF20/RNF40/WAC-H2B ubiquitination axis. *Leukemia, 2017.*

M. Kerstjens, S. Mimoso Pinhanços, P. Garrido Castro, P. Schneider, P. Wander, R. Pieters and R.W. Stam.
Trametinib inhibits *RAS*-mutant *MLL*-rearranged ALL at specific niche sites and reduces ERK phosphorylation *in vivo. Haematologica, 2018.*

M. Kerstjens*, P. Garrido Castro*, S. Mimoso Pinhanços, P. Schneider, P. Wander, R. Pieters and R.W. Stam.
Irinotecan induces complete remission in human *MLL*-rearranged acute lymphoblastic leukemia xenotransplanted mice. *Submitted.*

M. Kerstjens, S. Mimoso Pinhanços, P. Garrido Castro, P. Schneider, B.D. van Zelst, P. Wander, M. Willekes, S.G. Heil, R. Pieters and R.W. Stam.
S-Adenosylhomocysteine hydrolase inhibitor DZNep inhibits *MLL*-rearranged acute lymphoblastic leukemia *in vitro* and splenic engraftment *in vivo. Submitted.*

M. Bardini, L. Trentin, F. Rizzo, M. Vieri, A.M. Savino, P. Garrido Castro, G. Fazio, E.H.J. van Roon, **M. Kerstjens**, N.N. Smithers, R.K. Prinjha, G. Te Kronnie, G. Basso, R.W. Stam, R. Pieters, A. Biondi* and G.Cazzaniga*.
Anti-leukemic efficacy of BET inhibitor in a preclinical mouse model of MLL-AF4+ infant ALL. *Molecular Cancer Therapeutics, 2018.*

L.T. Bate-Eya, N.A. Schubert, B. Koopmans, D. Lelieveld, D.A. Egan, **M. Kerstjens**, R.W. Stam, J. Koster, H.N. Caron, J.J. Molenaar1 and M.E.M. Dolman.
High-throughput screening identifies idasanutlin as a re-sensitizing drug for venetoclax-resistant neuroblastoma cells. *Submitted.*

PhD portfolio

Name PhD candidate:	Mark Kerstjens
Erasmus MC department:	Pediatric Oncology/Hematology
Research school:	Molecular Medicine (MolMed)
PhD period:	October 2012 – October 2016
Promoter:	Prof. dr. R. Pieters
Co-promoter:	Dr. R.W. Stam

Courses	Year	ECTS
Basic human genetics	2012	0.5
Research management for PhD students	2012/2013	1.0
Anatomy	2012/2013	7.0
Laboratory animal science (WOD Art.9)	2013	6.0
Biostatistical methods	2013	5.7
Molecular aspects of hematologic disorders	2014/2015	1.4
Course on R	2016	1.5
Good Laboratory and Manufacturing Practices	2016	0.6
Employability outside academia	2016	1.0
Biobusiness summer school	2016	1.5

Symposia		
Molecular medicine symposium	2013/2014/2015	1.0
56th Annual ASH meeting, San Francisco, USA	2014	1.0
Daniel den Hoed symposium	2015	0.3
20th Congress of EHA, Vienna, Austria	2015	1.0
Princess Máxima Center retreat	2015/2016	1.0
Annual Leukemia meeting of the Kind-Philipp Foundation, Wilsede, Germany	2016	1.0

Presentations		
56th Annual ASH meeting, San Francisco, USA; *poster presentation*	2014	1.5

Daniel den Hoed symposium; *oral presentation*	2015	2.0
20th Congress of EHA, Vienna, Austria; *oral presentation*	2015	2.0
Princess Máxima Center retreat *oral presentation*	2015	2.0
Pediatric Oncology Research meetings *oral presentations*	2012-2016	8.0
Infant ALL Research group meeting *oral presentations*	2012-2016	3.0

Peer reviewing		
Oncotarget (4x)	2016	3.0

Supervising		
Priscilla Wander; MSc research project	2014/2015	10.0

Total		**63.0**

Awards & Grants

EHA Annual Meeting Travel Grant, Vienna, Austria, 2015.

Project grant: "The role of NF-κB signaling in *MLL*-rearranged infant acute lymphoblastic leukemia and glucocorticoid resistance". Stichting KiKa. Project #184. 2015.

Dankwoord

Allereerst ben ik de kinderen met leukemie en hun ouders dankbaar voor het doneren van materiaal ten behoeve van het onderzoek. Deze bijdrage heeft een belangrijke rol gespeeld in het onderzoek wat tot op heden gedaan is, en zal een belangrijke rol blijven spelen zolang deze ziekte nog niet de wereld uit is. Ik wens deze kinderen en hun ouders sterkte in de strijd tegen leukemie.

Prof. Dr. R. Pieters. Beste Rob, jouw ervaring en visie waren tijdens onze meetings voor mij belangrijk om het grote plaatje in het onderzoek in het oog te houden. Rustig en fair gaf je feedback, of het nou om de plannen in het onderzoek ging, of over de door mij geschreven stukken (want, hier en daar mocht het wel wat minder wollig). Bedankt voor alles en ik wens je veel succes met het Prinses Máxima Centrum.

Dr. R.W. Stam. Beste Ronald, bedankt dat je me de mogelijkheid gegeven hebt om binnen jouw groep 4 jaar onderzoek te doen. De aanloop naar mijn aanstelling was denk ik voor ons allebei bijzonder. Toch ben ik blij dat het zo gelopen is, en dat je me de kans hebt gegeven me te bewijzen. De afgelopen jaren zijn voor mij een leuke en ontzettend leerzame periode geweest. Van het samen uitzoeken van de hits uit de drug libraries tot de discussies over de opzet van de *in vivo* studies; bedankt voor je support, vertrouwen en feedback.

Mijn dank gaat uit naar de leescommissie: Prof. Dr. Monique den Boer, Prof. Dr. Josef Vormoor en Prof. Dr. Rene Bernards, bedankt voor het beoordelen van mijn proefschrift. Graag wil ik Dr. Inge van der Sluis, Prof. Dr. Ruud Delwel en Prof. Dr. Michel Zwaan bedanken voor het plaatsnemen in de grote commissie.

Goed onderzoek kun je niet alleen doen. Daarom wil ik iedereen van de Infant groep bedanken voor de prettige samenwerking en leuke momenten. Sandra, your dedication and organization made it a joy to work with you. Memories from the fun but sometimes stressful days in the EDC and labs still make me smile, as does the bit of Portuguese you taught me along the way. Patricia, thank you for all the good advice and sharp reviews during the sometimes tedious writing process. I've always admired your broad scientific knowledge, and enjoyed the dinners and "borrels". Good luck with the next steps in your career. Priscilla, jij begon als mijn student, om daarna ook je PhD te beginnen in de groep. Met jouw inzet en toewijding ga je het ongetwijfeld ver schoppen. Het was fijn om met je samen te werken en af en toe een escape room te doen. Bedankt voor al je hulp en vriendschap; en alvast veel succes met de afronding van jouw PhD. Pauline, jij was voor mijn een belangrijk orakel om gedurende mijn onderzoek mijn weg te vinden op en om het lab. Bedankt en ook jij

veel succes met jouw PhD project. Emma, voor het MEK inhibitor project hebben we fijn samengewerkt. Bedankt voor je support en jij ook succes met de laatste loodjes. Merel, bedankt dat je me de eerste periode op weg hebt geholpen in de groep en op het lab, met name met het opstarten van de drug library screens. Eddy, bedankt voor je gevoel voor humor op het lab en voor de gesprekken over epigenetische drugs en sequencing. Miky, I enjoyed our work and discussions on drug synergism and BET inhibitors. Adrian, I always liked your enthusiasm for the different projects. Verder wil ik de studenten Joshua, Melissa, Patricia en Chantal bedanken voor hun inzet.

Ook de mensen buiten de groep waar ik actief mee heb samengewerkt wil ik graag bedanken. Sandra en Bertrand, bedankt voor jullie input en bijdrage aan hoofdstuk 5. Jullie LC-MS data waren een belangrijk onderdeel voor de DZNep puzzel. Emmy en Jan, mooi om te zien dat jullie drug library screening project ook mooie resultaten heeft opgeleverd. Bedankt dat ik daar een bijdrage aan heb mogen leveren. Dirk en Jules, bedankt voor jullie input en support voor het RAS project en de induceerbare RAS constructen.

Iedereen binnen de afdeling kindergeneeskunde: bedankt voor de fijne tijd. Ik koester warme herinneringen aan de lab-uitjes, kerstfeesten, borrels, spelletjesavonden, mountainbike-weekends, escape rooms, etentjes en coffee-breaks.
Mijn kamergenoten van de “Little Girls room”. Bob, ik heb bewondering voor jouw heldere en pragmatische kijk op PhD’en en jouw onvermoeibare interesse voor wetenschap in het algemeen. Ik heb genoten van de grappen, puzzels en limericks die we konden uitwisselen. Het was een grote eer om je paranimf te mogen zijn. Lieneke, of we het nou hadden over serieuze zaken, of dat de halve kamer weer eens de leukste thuis probeerde te zijn, jij was er altijd graag bij. Je bent altijd een fijne gesprekspartner geweest voor de uitdagingen waar je tijdens en na je PhD tegen aanloopt. Bedankt voor je vriendschap en support. Roel, jij staat voor mij te boek als een harde werker. Of het nou om je onderzoek ging, of om het “ophalen” van de achterblijvers tijdens het mountainbiken: jij gaf altijd gas. Ook heb ik mooie herinneringen aan de avonturen met jou en Bob in San Francisco. Bedankt daarvoor. Isabel, discussions with you were always interesting. I think you’re a terrific scientist. Thanks for being good company at the mountainbike weekends and the conference in Wilsede (where I remember almost getting lost). Alex, of het nou om videogames, bordspellen, boogschieten of onderzoek ging, het was altijd leuk om met jou te praten. Judith, ik heb jouw kundigheid met R altijd bewonderd, naast dat het heel gezellig was om je erbij te hebben bij het mountainbiken. Joao, you always were a lot of fun to have around, whether it was having a buzz in the office, during soccer games or on a bike.
Dirk, bedankt voor alle goede adviezen en tips, naast alle humor die we konden de-

len. Rui, I remember our fun soccer matches, biking and a game of pool that earned you a nickname. Cesca, bedankt voor de coffee-breaks, het paintballen en de lol tijdens borrels en etentjes. Aurélie, bedankt voor je vrolijkheid op het lab, bij het mountainbiken en het badmintontoernooi. Femke, bedankt voor de goede gesprekken bij de koffie en de gezelligheid tijdens het fietsen. Marcel, het was altijd fijn om met jou te praten over poker, en te genieten van bier en lekker eten.
Mijn eerste kamergenoten: Dicky, Rolien, Silvia, Lilian, Malou, Lisette, Arian en Ytje; bedankt voor de warme ontvangst.
De analisten van de patiëntendienst wil ik graag bedanken voor hun bijdrage om onderzoek met primair materiaal binnen de afdeling mogelijk te maken: Jessica, Wilco, Susan, Lonneke, Pauline, Merel, Patty.
Eric, Iris, Marjolein, Myrte, Ellen, Clarissa, Cees, Yvette, Jordy, Ruben, Willemieke, Joris, Lieke, Rosanna, Ingrid, Farhad, Linda, Lea, Theo, Cynthia, Kirsten, Yun-Lei, Diana, Ad, Sharon, Nicole, Noorie, Askar, Patrick, Sanne, Jasmijn, Eva, Eva, Jenny, Daria, Magban, Elnaz; het was fijn om jullie als collega te hebben.

Ook wil ik de groepsleiders van lab kindergeneeskunde bedanken. Monique, bedankt dat je de secretaris van mijn leescommissie wilde zijn. Ook dank voor al je vragen en suggesties tijden de vele werkbesprekingen. Jules, Maarten, Janneke en Wendy, bedankt voor de prettige discussies en feedback tijdens alle meetings. Ik wens jullie allen het beste.

Mijn collega's bij Janssen Vaccines wil ik bedanken voor de warme ontvangst; de Molecular Bioassays en Viral & Microbial Safety teams in het bijzonder. Graag wil ik Michelle, Femke en Mark bedanken voor het vertrouwen en de kansen die ze me hebben geboden, terwijl dit proefschrift nog in voorbereiding was. Azra, bedankt voor je support in aanloop naar en tijdens mijn begin bij Janssen. Fellow Geeks and vikings: Martijn, Saskia, Michelle, Ewoud, Gerard, Mark and Harold, I hope we can conquer many more obstacles together.

Mitchell, Vincent en Bas. Ik heb altijd ontzettend veel voldoening gehaald uit de momenten wanneer wij als Stoelendans met muziek bezig waren, of het nou oefenen in Amsterdam of Alkmaar was, bij de optredens of gewoon onder het genot van lekker eten. Bas, ik heb jouw kennis en plezier voor alles wat met muziek te maken heeft altijd bewonderd. Vince, jouw doorzettingsvermogen bij alles wat je doet en meemaakt heb ik veel respect voor. Je bent een topgozer. Mitch, jouw relativeringsvermogen kan ik af en toe een voorbeeld aan nemen. Of het nou ging met een goed gesprek, een middagje jammen of tot in de kleine uurtjes gamen, je bent voor mij een belangrijke steunpilaar geweest. Ik ben blij dat we al zo lang buddies zijn.

Sebastiaan, onze etentjes en avondjes stappen waren voor mij een welkome afleiding en een goed moment om ervaringen uit te wisselen, of met veel plezier herinneringen uit Wenen op te halen. Bedankt voor je steun.

Vero, Preya and Vali, Waiman and Lynn, thanks a lot for all the terrific food, parties and trips. Ruud, Patrick en Saori, Anton en Christy, Valentijn, bedankt voor de gezelligheid tijdens (winter)bbq's en verjaardagen. Azra, Sabrina, Raymond en Folkert, het was fijn om af en toe PhD ervaringen uit te kunnen wisselen en herinneringen op te kunnen halen. Maarten, Ismayil en Joeri, onze bordspelavonden waren een welkome afleiding tijdens de laatste periode.

De families Kerstjens, De Graaf en Van Offenbeek wil ik bedanken voor hun steun de afgelopen jaren. Paula en Peter, Jan en Béatrice, Gé en Anita, Roel en Sanne, Ivo en Susan, Norbert en Carmen, Rick en Emma, Jan en Erica, bedankt voor jullie onvermoeibare belangstelling voor mijn onderzoek en de fijne gesprekken en gezelligheid bij verjaardagen en feestjes. Ivo, het was fijn om headbangend alles af en toe even los te laten. Ook dank aan Adri en Annette, Lennaert en Rebecca, Gray en Jamillah, en de families Deij, Bleeker en De Roon.

Het is ontzettend fijn om uit een warm nest te komen. Lieve Jeroen, Bart en Saskia, jullie betekenen heel veel voor me. Jullie hebben me altijd gesteund, met grappen en grollen, een luisterend oor en met het ophalen van herinneringen. Jeroen, samen genieten van lekker eten met een alcoholische versnapering, en met een goed gesprek, is altijd een welkome afleiding. Bart, onze gedeelde interesses zijn fijn om samen even te ontkomen aan de soms stressvolle tijden, of het nou om bordspellen, videogames, lekker koken of Star Wars gaat, samen met jou is het altijd top. Saskia, het is geweldig met jou samen katten te knuffelen, van taco's te genieten en er voor elkaar te kunnen zijn als het soms even niet mee zit. Zonder jullie waren de afgelopen jaren een stuk zwaarder geweest.

Lieve pap en mam. Ik kan moeilijk uitdrukken hoe belangrijk jullie voor me zijn en hoeveel jullie voor me betekend hebben. Jullie hebben me gevormd tot de persoon die ik nu ben. Jullie hebben me bijgestuurd op cruciale momenten om de juiste keuzes te maken en ik ben jullie daar ongelofelijk dankbaar voor. De afgelopen jaren zijn niet makkelijk geweest, maar altijd kon ik rekenen op jullie onvoorwaardelijke steun. Zonder jullie was dit proefschrift er niet geweest.

Lieve Jody, bedankt dat je er al die tijd voor me geweest bent. Er zijn talloze momenten dat je me motiveerde en aan wist te sporen om door te zetten, juist als het even tegen zat. Zeker de laatste loodjes waren pittig, maar je stond daarbij altijd

achter me. Het is voor ons allebei een mooie maar ook pittige periode geweest. Jouw liefde, geduld en pragmatische instelling waren voor mij onmisbaar bij het afronden van dit proefschrift. Ik kijk uit naar onze toekomst samen.